論文 / 著書情報
Article / Book Information

題目(和文)	高選択的二酸化炭素光還元に向けた助触媒の開発
Title(English)	Development of Co-catalyst for Selective Photocatalytic CO2 Reduction.
著者(和文)	殷 鴿
Author(English)	Ge Yin
出典(和文)	学位:博士(学術), 学位授与機関:東京工業大学, 報告番号:甲第10675号, 授与年月日:2017年9月20日, 学位の種別:課程博士, 審査員:宮内 雅浩,中島 章,日野出 洋文,松下 伸広,松下 祥子
Citation(English)	Degree:Doctor (Academic), Conferring organization: Tokyo Institute of Technology, Report number:甲第10675号, Conferred date:2017/9/20, Degree Type:Course doctor, Examiner:,,,,
学位種別(和文)	博士論文
Category(English)	Doctoral Thesis
種別(和文)	要約
Type(English)	Outline

平成 29 年度博士論文
論　文　要　約

Development of Co-catalyst for Selective Photocatalytic CO_2 Reduction.

高選択的二酸化炭素光還元に向けた助触媒の開発

東京工業大学大学院
理工学研究科　材料工学専攻

Ge YIN

Notice: The entire thesis will be not published until 2018/10/01, because it contains reference to unpublished work for which copyright permission cannot be obtained in *Session 5.2.2&5.4, Chapter 6, Session 7.2~7.4.* Thus only the outline of these sessions and chapters is presented instead of the full article.

Contents

Chapter. 1 ..... **7**

Introduction **7**

1.1 CO_2 reduction **7**

1.1.1 The definition of photocatalytic CO_2 reduction. **7**

1.1.2 The mechanism of CO_2 photoreduction. **9**

1.2 Co-catalyst **10**

1.3 Semiconductor light harvesters **11**

1.4 Evaluation parameters **15**

1.5 Previous researches **16**

1.6 Objective and research strategies **18**

References **21**

Chapter. 2 ..... **28**

The development and evaluation of Cu_xO nanocluster. **28**

2.1 Introduction **28**

2.2 Experimental Procedures **29**

2.2.1 Fabrication of copper oxide nanocluster-modified electrode. **29**

2.2.2 Electrochemical evaluation. **30**

2.2.3 Photocatalytic evaluation. **30**

2.3 Results and Discussion **32**

2.3.1 Characterization and Electrochemical evaluation of Cu_xO nanocluster **32**

2.3.2 Characterization and photocatlaytic evaluation **35**

2.4 Mechanism analysis **43**

2.4.1 Isotope tracer experiment **43**

2.4.2 ESR analyses **44**

2.5 Conclusion **46**

References: **48**

Chapter. 3 ..... **51**

The development and evaluation of Cu-Zn alloy **51**

3.1 Introduction **51**

3.2 Experimental procedures **53**

3.2.1 Preparation of Cu-Zn film electrodes **53**

3.2.2 Electrochemical screening **53**

3.2.3 Photoelectrochemical CO_2-reduction performance tests **54**

3.3 Results and Discussion **56**

3.3.1 Characterization **56**

3.3.2 Electrochemical evaluation. **58**

3.3.2 Photoelectrochemical evaluation. **60**

3.4 Conclusion **62**

References **64**

Chapter 4 ..... **66**

The reaction mechanism analyses **66**

4.1 The literature studies about the selectivity of CO_2 reduction on the catalyst surface. **66**

4.2 In-situ FTIR analyses. **69**

4.3 Conclusion **71**

References **72**

Chapter. 5 ..... **74**

The nanoparticlization of the Cu-Zn alloy **74**

5.1 Introduction **74**

5.2 Experimental procedures **74**

5.2.1 Preparation of Cu-Zn nanoparticles using vacuum sealing method. **74**

5.2.2 Preparation of Cu-Zn nanoparticles ink using chemical co-reduction method. (outline) **75**

5.2.3 Photocatalytic CO_2-reduction performance tests **75**

5.3 The Cu-Zn NPs synthesized by vacuum sealing method. **76**

5.3.1 Characterization **76**

5.3.2 Photocatalytic evaluation **78**

5.4 The Cu-Zn NPs synthesized by chemical co-reduction methods. (outline) **81**

5.5 Conclusion **81**

References **82**

Chapter. 6 ..... **83**

Visible-light-driven CO_2 photoreduction. (outline) **83**

References: **84**

Chapter. 7 ..... **86**

Design strategy for highly selective catalyst **86**

7.1 Scientific contribution **86**

7.1.1 the idea of surface adsorption conditions tuning by alloying for highly selective CO_2 reduction catalyst design. **86**

7.1.2 the demonstration and experimental prove of the reaction pathway from CO_2 into HCOOH. **88**

7.1.3. the Cu-Zn alloy was proved to be the active sites of CO_2 reduction. **89**

7.2 Engineering contribution (outline) **90**

7.3 Industry contribution (outline) **90**

7.4 Outlook (outline) **90**

7.5 General design strategy for highly selective catalyst **90**

References **91**

Chapter 8 ..... **94**

Summary **94**

Acknowledgement **98**

Appendix **99**

The preparation and evaluation of Zn-and Sn-based alloys. **99**

Journal Publications **115**

First author: **115**

Contributed works: **115**

International Conferences **116**

Oral: **116**

Poster **116**

Domestic Conferences: **117**

Oral: **117**

Poster: **117**

Awards: **117**

Chapter. 1

Introduction

1.1 CO_2 reduction

1.1.1 The definition of photocatalytic CO_2 reduction.

Recent years, the development of renewable energy, especially solar energy was increasing rapidly because it is unlimited and absolutely clean. In the meanwhile, the over emission of CO_2 began one of the biggest environmental issues in the world, many solutions such as Carbon Capture and Storage (CCS), the development of low-CO_2 emission materials and systems in various of industries have been operated. Among all those solutions, photocatalytic CO_2 reduction have been paid strong attention, due to its outstanding advantages.

Photocatalytic CO_2 reduction was also called artificial photosynthesis, since it was inspired by photosynthesis of the nature plants. Same as nature photosynthesis in which CO_2 and water was converted into O_2 and glucose under the sun light, photocatalytic CO_2 reduction tries to convert CO_2 into organic compounds through photocatalysts by means of solar energy.[1-5] The photo-catalytic CO_2 reduction can not only decrease the CO_2 emission by means of a clean energy source, but also produce useful fuels such as carbon monoxide, methane, methanol, formic acid and formaldehyde, which can be directly used or easily stored.

During photocatalytic CO_2 reduction, the main reactions are shown as below.

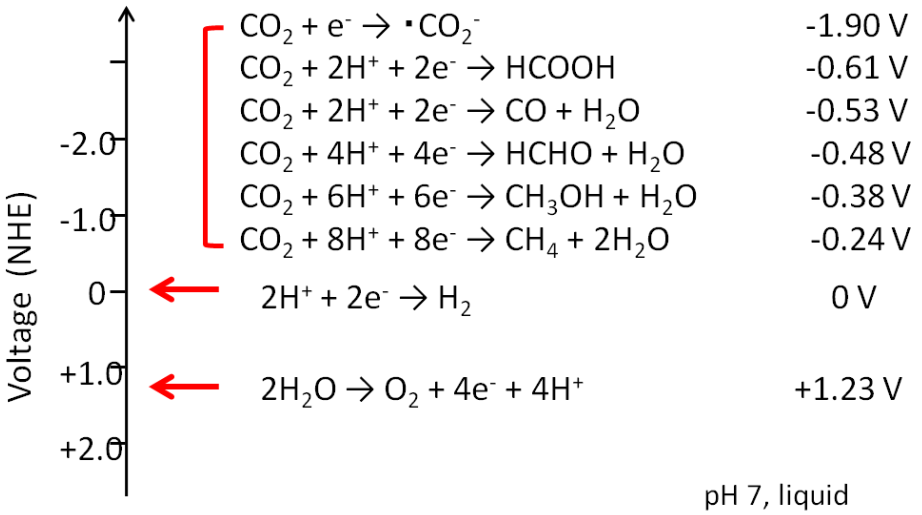

Figure 1.1 *The reactions of CO_2 reduction.*

The research of photocatalytic CO_2 reduction began from last century. In 1972, Prof.

Fujishima and Prof. Honda published their research of water photolysis. They constructed an electrochemical cell in which titanium dioxide electrode connected with a platinum black electrode, as we can see in *Figure 1.2*.[6] When the surface of TiO_2 electrode was irradiated, they observed that oxygen evolution occurred at the TiO_2 electrode and hydrogen evolution occurred at the platinum electrode. This is what we called "Honda-Fujishima Effect", and the process that generate H_2 and O_2 from water was called water splitting.

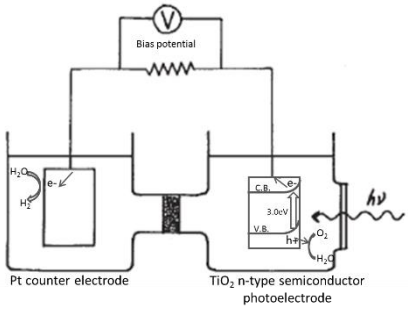

Figure 1.2 *Honda-Fujishima effect.*

In 1978, Prof. Halmann used p-type gallium phosphide (p-GaP) as a photocathode, converted aqueous carbon dioxide to formic acid, formaldehyde and methanol with part or all of the energy being supplied by light irradiation[7]. In the next year, Prof. Inoue and Prof. Fujishima proposed several candidates such as TiO_2, CdS, GaP, ZnO and SiC as photocatalyst powders and explained the correlation between the conduction band energy of the photocatalytic semiconductor materials and their capacity for photocatalyticly convert carbon dioxide into methanol, shown in *Figure 1.3*.[8] And later, Prof. Halmann [9] reported their research using strontium titanate to catalyze CO_2 to HCOOH, HCHO and CH_3OH.

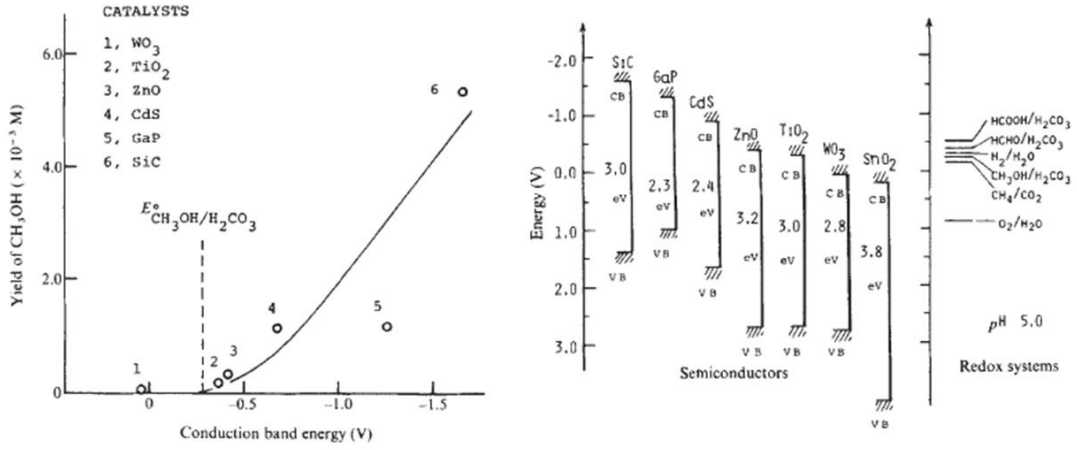

Figure 1.3 *The report from Prof. Inoue and Prof. Fujishima, elaborated the Candidates materials for photocatalytic CO_2 reduction, and the correlation between their conduction band energy and their capacity for photocatalyticly convert carbon dioxide into methanol.*

1.1.2 The mechanism of CO_2 photoreduction.

The most ideal and expected photocatalytic CO_2 reduction system consists of a photocatalytic semiconductor, termed a light harvester, coupled with a co-catalyst. Under light irradiation, excited electrons in the conduction band of the light harvester are injected into the co-catalyst to promote CO_2 reduction, while photogenerated holes in the valence band of the light harvester oxidize reducing agents, such as water molecules to produce oxygen.

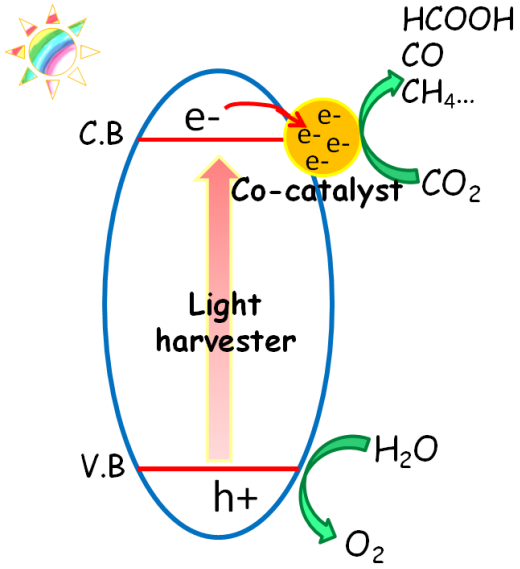

Figure 1.4 *Model of the common construction of photocatalytic CO_2 reduction system.*

To achieve highly efficient photocatalytic CO_2 reduction, hard requirements for the light harvester and co-catalyst are essential. Briefly, for the light harvesters, 1) the conduction band must be high enough to provide high reductivity to reduce CO_2; 2) the valence band must be deep enough so that it can oxidize water into O_2; 3) to achieve high solar conversion efficiency, light harvesters with narrow bandgap which is sensitive to visible light are more desired, since half of the solar energy comes from visible region. However, these requirements are difficult to be achieved at the same time for most of the semiconductor materials. Thus, a Z-scheme system which is combined by two kinds of light harvesters catalyzing reduction and oxidation respectively is used for visible light sensitive photocatalytic CO_2 reduction. This will be introduced in details in *session 1.4*.

As for the co-catalysts, they are commonly used to decrease the recombination of excited electrons, facilitate CO_2 activation, produce reaction sites, accumulate reductive electrons and decide the reaction selectivity. A good co-catalyst for CO_2 reduction should behave below properties, 1) it must be efficient to drive multi-electron reductions, since the generation of all the CO_2 reduction products needs more than 2 electrons; 2) it should achieve selective CO_2 reduction for certain kind of product; 3) it should be stable during the reaction; 4) as a co-catalyst, it should be able to be easily-decorated to the surface of the light harvesters, which means versatility is needed.

At last, from environment-friendly view, the co-catalyst and light harvester materials must be derived from abundant and non-toxic elements, and the synthesis procedure should be safe and clean.

This research focused on the development of an efficient, stable and universal co-catalyst with high product selectivity for CO_2 reduction. The developed co-catalyst will be used to achieve visible-light-driven CO_2 reduction with high products selectivity.

1.2 Co-catalyst

During the photocatalytic CO_2 reduction, co-catalyst is where the CO_2 reduction reactions are actually happening. Co-catalyst plays roles to improve the light harvester surface, to provide the recombination of photoexicited electrons and holes, to increase the local electrons density for multi-electrons reaction catalyzing, to modify the surface CO_2 absorption strength and produce reaction sites.

In a hydrous condition, since the proceeding requirements for water splitting is easier than CO_2 reduction, a good CO_2 reduction co-catalyst need to be able to inhibit the water splitting and promote CO_2 reduction. In the meanwhile, co-catalyst also decides the reduction product, selectively convert CO_2 into one kind of molecular, among all the choices of CH_4, CO, HCOOH and so on.

According to the mechanism of the photocatalytic CO_2 reduction, co-catalyst was applied by the photoexicited electrons and high reduction potential from the light harvester, and this is actually similar to electrochemical CO_2 reduction, in where the CO_2 reduction electrocatalysts was directly supplied by cathodic current and bias-potential. Thus, the co-catalyst in the photocatalytic CO_2 reduction can be the same as CO_2 reduction electrocatalyst. And their catalytic properties can be evaluated by electrochemical methods. Also, their effects to CO_2 reduction can be discussed easier as an electrochemical case.

Nowadays, three kinds of CO_2 reduction catalysts are commonly used, CO_2 fixation enzymes,[10] molecular catalyst especially ruthenium or rhenium organic compounds,[11-12] and metal or alloy catalysts.[13-21] However, even though the former two kinds had shown high performance, their development is limited by the expensive price and complicated synthesis process. Thus, in the present research, metal and alloy based co-catalyst were mainly researched.

The metal catalysts used for electrochemical CO_2 reduction has been studied since last century, for example, Prof. Hashimoto and Prof. Hori had explored and reviewed almost all kinds of metal and metal alloy about their electrocatalytic CO_2 reduction performance,[13-14, 22-24] Figure 1.5 showed parts of the results.

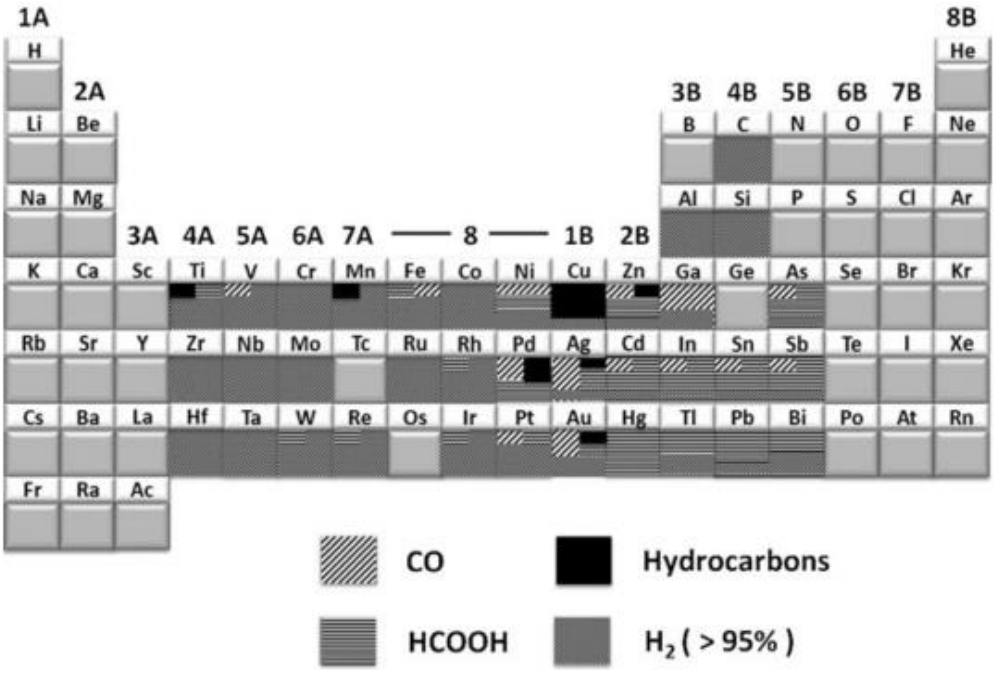

Figure.1.5 *Periodic table showing the electrocatalytic CO_2 reduction products at ambient conditions.*

As we can see, the metal co-catalysts, especially Cu[25-34], Au[35-40], Ag[41-44], Zn[18, 42, 45-48], behave different trends to mainly catalyze water splitting or convert CO_2 into hydrocarbons, CO or HCOOH. However, the selectivity for one certain kind of CO_2 reduction product was not high enough for pure metal or metal oxide. The mechanism of their selectivity has not been completely clear, but it was commonly believed that the products selectivity was influenced by the surface adsorption strength for CO_2 and other intermediate species such as CO* and COOH*. The reaction pathways of CO_2 reduction and their relationship of the products selectivity was discussed in ***Chapter 5*** with comprehensive literature studies.

1.3 Semiconductor light harvesters

As introduced in the primary session, under light irradiation, inside of the light harvester, electrons separate from holes and transfer into the reduction sites to drive CO_2 reduction; on the other side, holes transfer and join in to the oxygen generation. Considering from thermodynamics point, the potential level of the conduction band must be more negative than the reduction potential of possible CO_2 reductive reactions, shown in Figure 1.1. In the similar way, the potential level of the valence band must be more positive than the oxidation potential. Furthermore, from a kinetics view, on each side an overpotential is required to ensure a high rate of reaction. Thus, the band gap of the semiconductor seems to be the wider the better. However, on the other hand, high absorption for visible light is commonly desired in order to

achieve a higher solar efficiency. So the exactly control of the edges position of band gap behaves extremely important.[3]

However, it very difficult to find an ideal light harvester with all these properties above, according to Prof. Scaife's research (Fig 1.6),[49] to most of the n-type oxide semiconductors, such as TiO_2, $SrTiO_3$, ZnO, $BaTiO_3$ and metal niobates, a relationship between flat band potential, $V_{fb}(SHE)$, and bandgap, E_g.

$$V_{fb}(SHE)=2.94- E_g$$

was confirmed, since the valence band position of these oxides was fixed by the O*2p*-orbit and the conduction band position depends to the metal*2p*-orbit. That means the narrower the bandgap is, the lower the conduction band position becomes. But low conduction band position cannot provide enough reduction potential for CO_2 reduction.

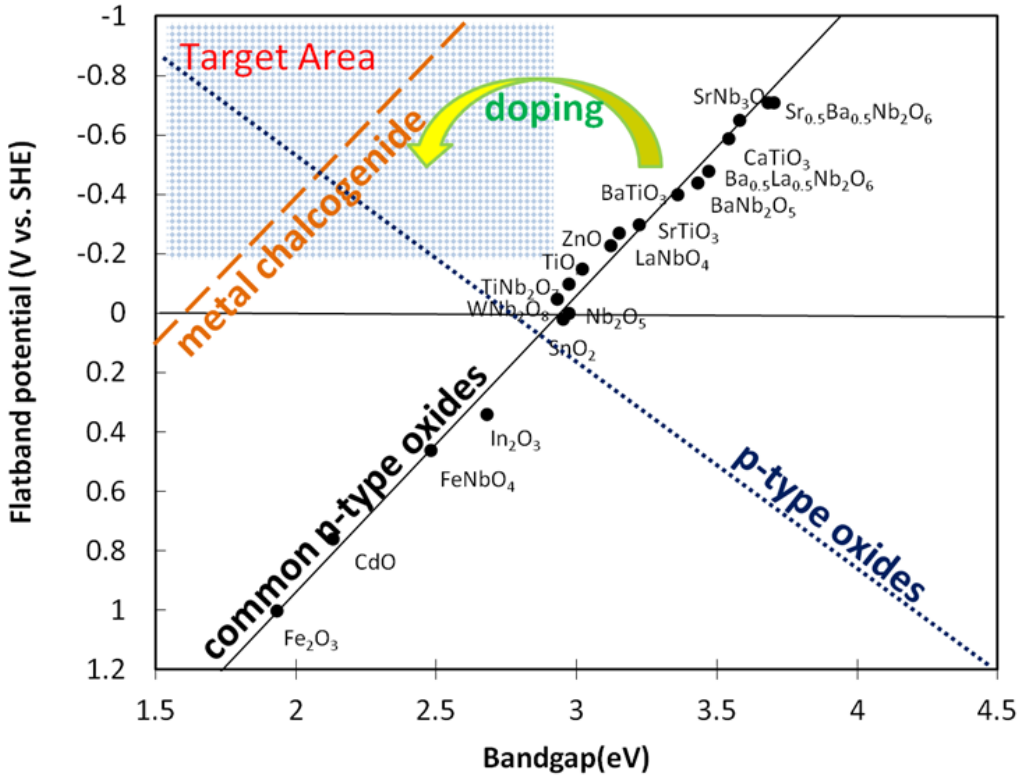

Figure 1.6 *The relationship between the flat band potential and bandgap of most kinds of metal oxide semiconductors and the strategy to develop efficient light harvester materials for photocatalytic CO_2 reduction.*

As we can see from the figure above, "target area" represents the ideal light harvester materials with high conduction band and narrow bandgap. According to the band structure theory, three ways can be used to reach the target area.

The first way is using metal chalcogenide[50] quantum dots such as CdS,[51-52] SnS[53] and ZnS.[54] Since sulfur behaves less electronegativity than oxygen, the valence band position of metal chalcogenide is lighter than metal oxide. Thus, the band structure of metal chalcogenide should follow a relationship shown in the figure and show more possibility to locate in the target area.

Further, according to the quantum size effect, the band structure and the electron mobility can be controlled by the size of the chalcogenide particle. The quantum dots can be prepared by an easy way called successive ionic layer absorption reaction (SILAR), in which the particle size can be controlled by adjusting the reaction times easily.[53] However, most kinds of metal sulfides has low stability in hydrous solution

The second method is developing p-type metal oxides which follow converse relationship with n-type oxides, such as $CaFe_2O_4$.[55-58]

And the third way is doping other element into the semiconductor, by building new energy level under the conduction band to obtain narrower bandgap.[59-61] For example, doping Rh into $SrTiO_3$ shows high possibility to transform $SrTiO_3$ to a visible light active material.[62]

However, it must be notices that even among many kinds of metal sulfides or p-type metal oxides, there were very rare cases which can reach the reaction potential for CO_2 reduction and water oxidation at the same time, as we can see from Fig.1.7.

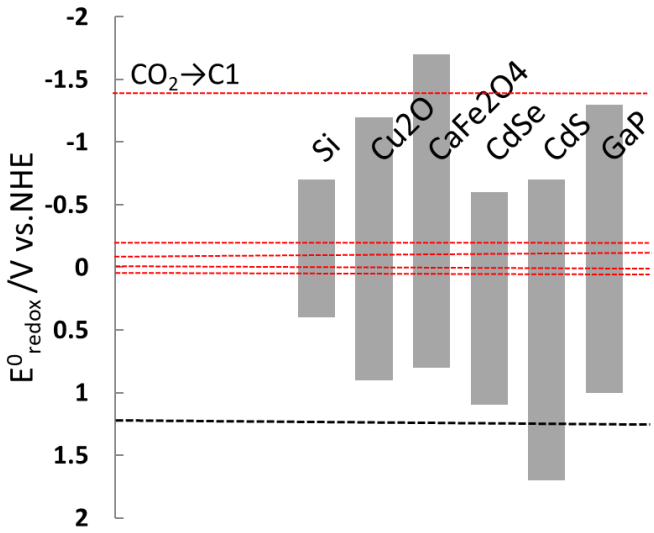

Figure 1.7 *The band structure of some kinds of metal sulfides and metal oxides.*

The trade-off between the requirement for CO_2 photoreduction and the requirement for visible light irradiation was a severe problem making visible-light-driven photocatalytic CO_2 reduction difficult to be achieved. To make up the shortage in the oxidation side, sacrificial agents were used as electron donor instead of water in many previous researches, such as triethanolamine (TEOA)[63-64] or ethylenediaminetetraacetic acid (EDTA)[65]. Besides, the reaction from CO_2 and water into O_2 and CO_2 reduction products is an uphill reaction, while the application of the sacrificial agents can decrease the ΔG of the reaction. Even in some researches, methanol was used as sacrificial agent, and in that case the reaction would become a downhill reaction, while it is meaningless to generate CO or HCOOH using methanol.

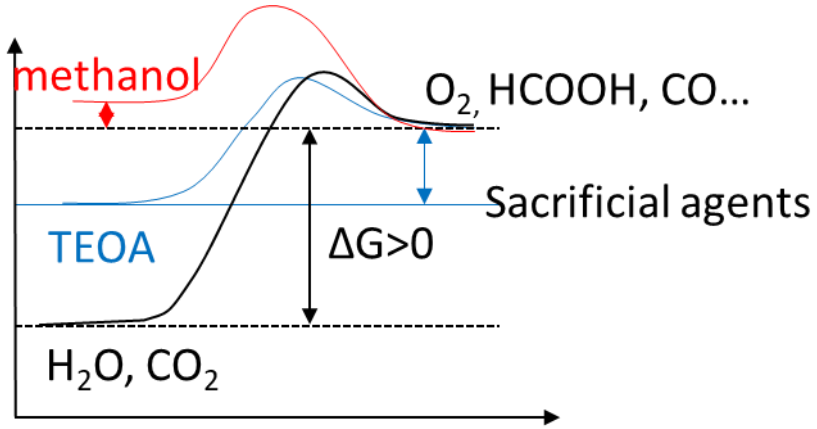

Figure 1.8 *the reaction ΔG for photocatalytic CO_2 reduction with ant without sacrificial agents.*

To overcome the difficulties of using visible light as energy source and using water as electron donor, Z-Scheme system was developed.[58, 66-67] Two kinds of light harvesters are used in this system, as seen in Figure 1.9, one light harvester provides the high conduction band for CO_2 reduction, the other light harvester provides the deep valence band for O_2 generation. The electrons and holes between them combine through the interface or an electron mediator. By using Z-Scheme system, the requirement of light harvesters decreased and many kinds of semiconductors could be used. For example, in the reduction side, visible light sensitive materials such as $CaFe_2O_4$, [55-58] SnS QDs,[53] C_3N_4,[68-70] P-GaP[71-73]… can be used. And WO_3,[56, 74-78] $BiVO_3$,[58] Fe_2O_3[79]… can be used in the oxidation side.

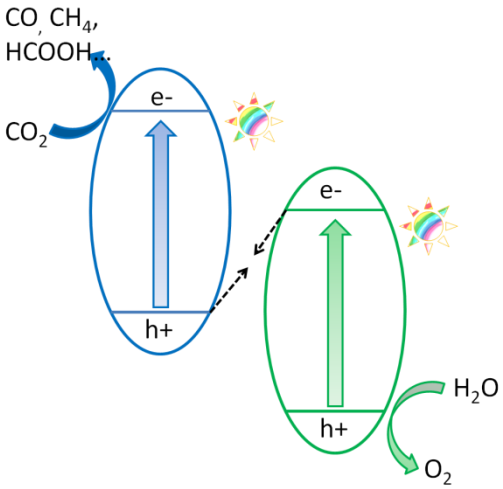

Figure 1.9 *Z-Scheme for visible light sensitive CO_2 photoreduction.*

Except for the methods introduced above, the electrodeization of the light harvester has attracted more and more attention. By using a light harvester electrode in a photoelectochemical cell, as seen in the figure below, bias-potential can be applied to make up the substantial band

energy and supply overpotential for the reduction or oxidation reactions. In this system, not only bias-potential can be applied, also both of the photocathode and photoanode can be improved by using CO_2 reduction co-catalyst and O_2 evolution co-catalyst, respectively. Based on these advantages, this kind of photoelectrochemical cell has been used more and more generally.

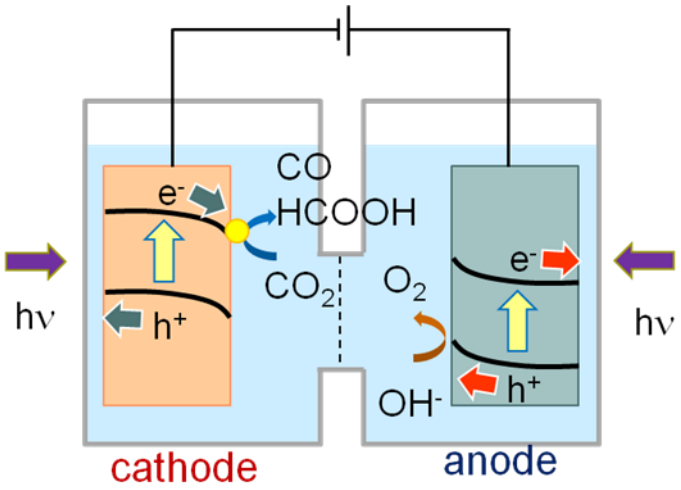

Figure 1.10 *The construction of a photoelectrochemical cell.*

Furthermore, by employing a proton exchange membrane, the products from the reduction side and oxidation side can be easily separated. Different electrolytes can be used in two sides. Also, the reverse reaction can be completely eradicated, which is a big advantage because along with the development of the simple system of dispersed photocatalytic powders in the solution, more and more researchers were aware of that the proceeding of reverse reactions had become a big problem hampering the increasing of the conversion efficiency.

1.4 Evaluation parameters

To judge the performance of a photocatalytic CO_2 reduction system, several parameters are commonly used. Since CO_2 photoreduction is a complex, multistep process that combines various aspects, from light absorption to electron generation, products different reductive products, from CO to CH_4, so the measurement parameters are also based on different aspects. There are some common parameters usually used in research papers to evaluate the efficiency of the CO_2 photoreduction system, from light-based to catalysts-based, or products-based, evaluate the solar energy converting efficiency, activity and stability of catalysts, and the selectivity, respectively.

Quantum yields, or quantum efficiency, protons efficiency, is a light-based parameter. It is typically defined in photocatalysis as the ratio of the rate of photocatalytic events to the absorbed photons flux within the specified wavelength range, as shown with equation.

$$\Phi = {}^{N_{\text{photocat.events}}}\!/_{N_{\text{absorbed photons}}}$$

The photocatalytic events refer to the molar photon amount required to obtain all the products.

Beside of quantum efficiency, solar efficiency (also called light-to-energy conversion efficiency) is another important parameter to evaluate the performance of photocatalytic CO_2 reduction. Different with quantum efficiency, solar efficiency is difined as the ratio of photocatalytic events to the whole irradiated light energy, despite of whether this energy is absorbed or not.

$$\Phi_{solar\ energy} = {}^{N_{\text{photocat.events}}}\!/_{N_{\text{irradiated photons}}}$$

However, the calculation of solar energy in a photoelectrochemical system with outer bias supplies will be different, the details will be introduced in ***Chapter 6***.

The turnover number (TON) is a parameter to judge the activity of catalysts, expresses how many times a site participates in the catalytic cycle during the reaction. TON is commonly defined as the ratio of the mole number of photocatalytic products to the mass of catalysts. Commonly a catalyzing behavior can only be admitted when TON is over 4.

$$\text{TON} = N_{\text{photocata.events}}/N_{\text{catalyst sites}}$$

The turnover frequency (TOF) is a related measure defined as the number of photoinduced transformations per catalytic site per time period. What should be noticed is that, either TON or TOF is independent of photon flux, so it's not reliable when comparing different photocatalyst systems.

To measure the selectivity of a electrocatalytic or photocatalytic system, the definition of faradaic efficiency is introduced as the percentage of electrons needed for one specific products to the moral amount of electrons consumed, as equation below shows.

$$\text{Faradaic efficiency} = {}^{Ni_{\text{products elec}}\ e_0}\!/_{\int \text{Adt}} \times 100\%$$

$\int \text{Adt}$ is the moral electric quantity detected by current meter and $e_0 = 1.6 \times 10^{-19}\text{C}$. Faradaic efficiency is an important argument to evaluate a photoelectrochemical system, shows equally importance with bias-potential.

1.5 Previous researches

Several remarkable studies will be introduced here to help the readers to understand the difficulties of the development for highly selective visible-light-driven photocatalytic CO_2 reduction.

In 2010, Dr. Morikawa published his work converting CO_2 into HCOOH with high produced amount under visible light irradiation.[63] N-doped Ta_2O_5 was used as light harvester and a Ru-complex was used as co-catalyst. The Faradic efficiency for HCOOH generation in this research reached 75%. However, in this research, TEOA was used as sacrificial agent in the oxidation side, since the valence band of N-Ta_2O_5 can't catalyze water oxidation.

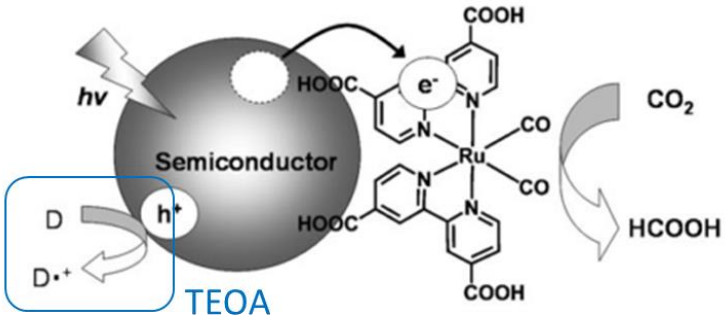

Figure 1.11 *the study of Dr. Morikawa using N- Ta_2O_5 and Ru-complex, converting CO_2 into HCOOH. TEOA was used as sacrificial agent.*

In the next year, their group reported the conversion from CO_2 into HCOOH. The co-catalyst was still Ru-complex, but InP was the light harvester and no sacrificial agent was used.[80] The solar conversion efficiency in this research was 0.04%, which is about one-fifth of 0.2%, the solar conversion efficiency of switchgrass, a promising material for biomass fuel[81] and this value is still the champion data in this area. However, element like In and Ru are so rare and unfriendly to environment that we want to avoid from using in our research.

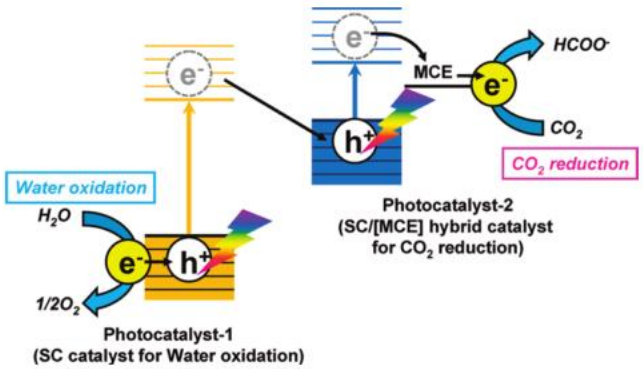

Figure 1.12 *the study using InP and Ru-complex for HCOOH generation from CO_2 under visible light irradiation.*

As introduced before, Z-Scheme system was generally used. In 2016, Prof. Kudo published his work using metal sulfides and BVO to build a Z-Scheme system and successfully converted CO_2 into CO under visible light irradiation.[66] The stoichiometric amount of the produced H_2, CO and O_2 proved that water was used as electron donor during the reaction. However, the produced amount of hydrogen was about hundred times than CO. it means the selectivity for CO_2 reduction was low. Thus, the surface modification by using CO_2 reduction co-catalyst is necessary to increase the selectivity for CO_2 reduction.

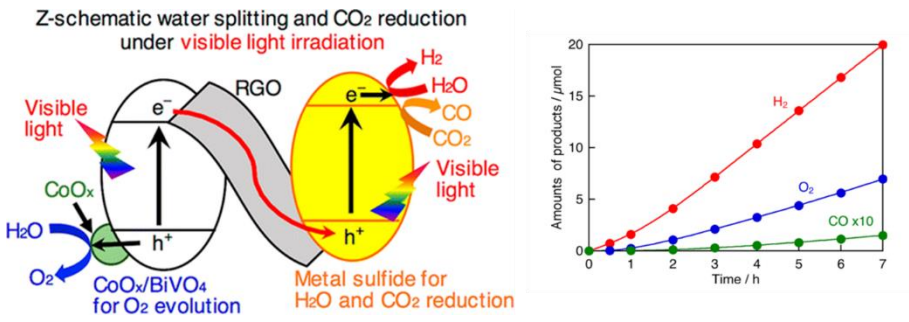

Figure 1.13 *the study of Prof. Kudo using Z-Scheme achieving water splitting and CO_2 reduction under visible light.*

Also in 2016, Prof. Ishitani reported his work, in which a Z-Scheme system consisted of NiO and TaON was used.[82] The surface of NiO was modified with RuRe-complex and the TaON surface was modified with a typical O_2 generation co-catalyst, CoO_x[79, 83]. As result, CO was as main product rather than H_2. However, as seen from Figure 1.14, the produced CO didn't increase linearly, indicating that this system was not stable, even though the TON was calculated to be 12. The conversion efficiency for this work was 0.0016%.

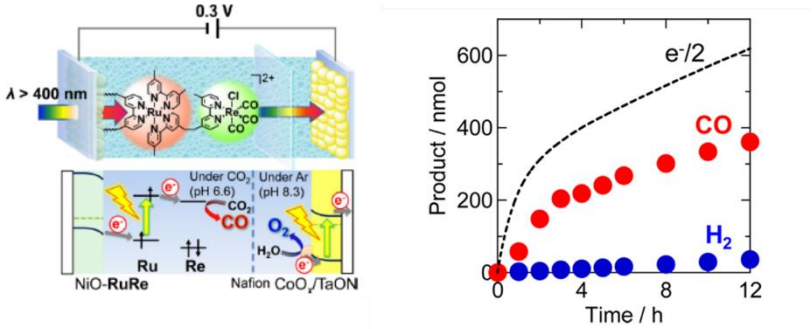

Figure 1.14 *the study of Prof. Ishitani, using RuRe-complex-NiO/TaON for selective generation of CO from CO_2 under visible light irradiation.*

As we can see from these previous researches, the development of light harvesters under visible light irradiation has made great progress, but a robust and economic co-catalyst with high selectivity was still necessary.

1.6 Objective and research strategies

According to the difficulties and previous researches introduce before, the objective of this research was decided.

The objective of this research is to achieve photocatalytic CO_2 reduction 1) under visible light irradiation, 2) using water as electron donor, 3) with high selectivity for HCOOH generation, 4) using robust and economic materials and at last to achieve 5) high solar conversion efficiency.

To accomplish this objective, I focused on the development of an efficient, stable and highly

selective co-catalyst for CO_2 reduction.

The co-catalyst will be developed according to the relationship of the CO_2 reduction pathways and catalyst surface properties. Efficient catalyst compositions were explored by screening their electrocatalytic properties under dark condition by electrochemical evaluation. Then, the photocatalytic evaluation will be operated, after the co-catalyst was combined with light harvesters. At the first stage, I chose wide bandgap light harvesters for the photocatalytic evaluation of the co-catalyst, which are sensitive to UV light, since their potentials of excited charge carriers would be enough strong to drive CO_2 reduction and water oxidation. to acquire reliable and reproducible properties, I have also established the evaluation system, such as chromatographs for gas and liquid sample, isotope trace analysis, and electron spin resonance (ESR). Based on the established system, I firstly confirm the CO_2 reduction under UV irradiation using wide gap semiconductor light harvesters with optimized co-catalysts modification. For more challenging research in the next step, we choose narrower bandgap semiconductors as light harvesters. After an ideal CO_2 reduction co-catalyst was developed, visible light sensitive light harvesters will also be developed and modified by the co-catalyst, further the photocatalytic performance will be evaluated under visible light irradiation. To characterize the materials, especially the alloy co-catalyst with bulk sensitivity, hard-XPS analyses were operated in SPring-8. Also, to analyze the reaction mechanism, in-situ FTIR analysis system was built.

The thesis structure was shown below.

	Chapter 2	Chapter 3 and 5	Chapter 6
Co-catalyst		Higher selectivity and activity →	
	Cu_xO nanoclusters	Cu-Zn alloy electrode and NPs	Cu-Zn alloy NPs
Lighter harvetster		More challenging →	***Goal***
	$Nb_3O_8^-$ nanosheets	$SrTiO_3$ (for photocatalytic evaluation)	$CaFe_2O_4/WO_3$ Z-Scheme
Products	CO	HCOOH	
Publication	*ACS nano, 2014*	*J. Mater. Chem A, 2017*	*Submitted*
	Evaluation system building	***Chapter 4*** Mechanism	***Chapter 7*** Contribution

In ***Chapter 1***, the background, mechanism, difficulties was introduced. Some remarkable

previous researches were also introduced. At last the objective of this thesis is set.

In ***Chapter 2***, a Cu_xO nanocluster material is developed and evaluated. This material was proved to catalyze multi-electron reactions according to the previous reports in the field of photocatalytic environment purification. Electrochemical evaluation was firstly operated to judge its catalytic properties for CO_2 reduction. Then, a $Nb_3O_8^-$ nanosheet material with very high conduction band position was developed and used as the light harvester, on which the Cu_xO nanoclusters were grafted for photocatalytic evaluation. Also, isotope experiment and ESR analysis were operated to clarify the electron injection and element transformation to explain the mechanism during the photocatalytic CO_2 reduction. During this research, a reliable evaluation system was established.

In ***Chapter 3***, higher stability and selectivity were pursued, based on the understanding of CO_2 reduction pathways, and we developed a Cu-Zn alloy electrode as a CO_2 reduction catalyst. The Cu-Zn alloy was expected to achieve high selectivity for HCOOH or CO generation. Its properties were evaluated by electrochemical methods, and photoelectrochemical methods by combining with a $SrTiO_3$ photoanode.

The mechanism of its high selectivity for HCOOH generation was analyzed in ***Chapter 4***, based on plenty of literature studies and in-situ FTIR analyses.

In ***Chapter 5***, to improve the versatility of the Cu-Zn catalyst, make it feasible to combine the Cu-Zn catalyst to any kinds of light harvesters. Two synthesis methods, vacuum sealing method and chemical co-reduction method, were tried and optimized. The Cu-Zn particles were facilely coated onto electrode substrates and/or particulate light harvesters their electrocatalytic and photocatalytic performance were evaluated respectively.

In ***Chapter 6***, the successfully prepared Cu-Zn nanoparticles were loaded onto the surface of visible light sensitive photocathode, $CaFe_2O_4$ electrode, and construct a photoelectrochemical cell with visible light sensitive photoanode of WO_3 nanotree electrode. The CO_2 reduction under visible light irradiation was evaluated. We also prove the water molecule as an electron donor to drive selective CO_2 reduction, similar to natural plants.

Chapter 7 explained the philosophy contribution of this research. The future works and outlook were also introduced.

Chapter 8 is the summary of this work.

References

1. Li, K.; Peng, B.; Peng, T., Recent Advances in Heterogeneous Photocatalytic CO2 Conversion to Solar Fuels. ACS Catalysis ***2016,*** *6, 7485-7527.*

2. Tran, P. D.; Wong, L. H.; Barber, J.; Loo, J. S., Recent advances in hybrid photocatalysts for solar fuel production. Energy & Environmental Science ***2012,*** *5 (3), 5902-5918.*

3. Habisreutinger, S. N.; Schmidt - Mende, L.; Stolarczyk, J. K., Photocatalytic reduction of CO2 on TiO2 and other semiconductors. Angewandte Chemie International Edition ***2013,*** *52 (29), 7372-7408.*

4. Hinogami, R.; Nakamura, Y.; Yae, S.; Nakato, Y., An approach to ideal semiconductor electrodes for efficient photoelectrochemical reduction of carbon dioxide by modification with small metal particles. The Journal of Physical Chemistry B ***1998,*** *102 (6), 974-980.*

5. Jaramillo, T. F.; Nørskov, J. K.; Varley, J.; Grabow, L.; Kuhl, K., The oxidation of water and the reduction of CO2 to fuels.

6. Fujishima, A., Electrochemical photolysis of water at a semiconductor electrode. nature ***1972,*** *238, 37-38.*

7. Halmann, M., Photoelectrochemical reduction of aqueous carbon dioxide on p-type gallium phosphide in liquid junction solar cells. ***1978****.*

8. Inoue, T.; Fujishima, A.; Konishi, S.; Honda, K., Photoelectrocatalytic reduction of carbon dioxide in aqueous suspensions of semiconductor powders. Nature ***1979,*** *277, 637-638.*

9. Halmann, M.; Ulman, M.; Aurian-Blajeni, B., Photochemical solar collector for the photoassisted reduction of aqueous carbon dioxide. Solar Energy ***1983,*** *31 (4), 429-431.*

10. Hansen, H. A.; Varley, J. B.; Peterson, A. A.; Nørskov, J. K., Understanding trends in the electrocatalytic activity of metals and enzymes for CO2 reduction to CO. The journal of physical chemistry letters ***2013,*** *4 (3), 388-392.*

11. Ishida, H.; Tanaka, K.; Tanaka, T., Electrochemical CO2 reduction catalyzed by ruthenium complexes [Ru(bpy)2(CO)2]2+ and [Ru(bpy)2(CO)Cl]+. Effect of pH on the formation of CO and HCOO. Organometallics ***1987,*** *6 (1), 181-186.*

12. Kuriki, R.; Sekizawa, K.; Ishitani, O.; Maeda, K., Visible - Light - Driven CO2 Reduction with Carbon Nitride: Enhancing the Activity of Ruthenium Catalysts. Angewandte Chemie International Edition ***2015,*** *54 (8), 2406-2409.*

13. Hori, Y., Electrochemical CO2 Reduction on Metal Electrodes. In Modern Aspects of Electrochemistry, Vayenas, C.; White, R.; Gamboa-Aldeco, M., Eds. Springer New York: 2008; Vol. 42, pp 89-189.

14. Azuma, M.; Hashimoto, K.; Hiramoto, M.; Watanabe, M.; Sakata, T., Electrochemical Reduction of Carbon Dioxide on Various Metal Electrodes in Low - Temperature Aqueous KHCO 3 Media. Journal of the Electrochemical Society ***1990,*** *137 (6), 1772-1778.*

15. Hara, K.; Kudo, A.; Sakata, T., Electrochemical reduction of carbon dioxide under high pressure on various electrodes in an aqueous electrolyte. Journal of

Electroanalytical Chemistry ***1995,*** *391 (1–2), 141-147.*
16. Ishitani, O.; Inoue, C.; Suzuki, Y.; Ibusuki, T., Photocatalytic reduction of carbon dioxide to methane and acetic acid by an aqueous suspension of metal-deposited TiO2. Journal of photochemistry and photobiology. A, Chemistry ***1993,*** *72 (3), 269-271.*
17. Vassiliev, Y. B.; Bagotsky, V. S.; Osetrova, N. V.; Khazova, O. A.; Mayorova, N. A., Electroreduction of carbon dioxide: Part I. The mechanism and kinetics of electroreduction of CO2 in aqueous solutions on metals with high and moderate hydrogen overvoltages. Journal of Electroanalytical Chemistry and Interfacial Electrochemistry ***1985,*** *189 (2), 271-294.*
18. Watanabe, M.; Shibata, M.; Kato, A.; Azuma, M.; Sakata, T., Design of Alloy Electrocatalysts for CO 2 Reduction: III . The Selective and Reversible Reduction of on Cu Alloy Electrodes. Journal of The Electrochemical Society ***1991,*** *138 (11), 3382-3389.*
19. Varela, A. S.; Ranjbar Sahraie, N.; Steinberg, J.; Ju, W.; Oh, H. S.; Strasser, P., Metal - Doped Nitrogenated Carbon as an Efficient Catalyst for Direct CO2 Electroreduction to CO and Hydrocarbons. Angewandte Chemie International Edition ***2015,*** *54 (37), 10758-10762.*
20. Lim, H.-K.; Shin, H.; Goddard, W. A.; Hwang, Y. J.; Min, B. K.; Kim, H., Embedding Covalency into Metal Catalysts for Efficient Electrochemical Conversion of CO2. Journal of the American Chemical Society ***2014,*** *136 (32), 11355-11361.*
21. Vassiliev, Y. B.; Bagotzky, V. S.; Khazova, O. A.; Mayorova, N. A., Electroreduction of carbon dioxide: Part II. The mechanism of reduction in aprotic solvents. Journal of Electroanalytical Chemistry and Interfacial Electrochemistry ***1985,*** *189 (2), 295-309.*
22. Hori, Y., Modern Aspects of Electrochemistry. 2008; Vol. 42, p 89.
23. Hori, Y.; Wakebe, H.; Tsukamoto, T.; Koga, O., Electrocatalytic process of CO selectivity in electrochemical reduction of CO2 at metal electrodes in aqueous media. Electrochimica Acta ***1994,*** *39 (11), 1833-1839.*
24. Lee, J.; Kwon, Y.; Machunda, R. L.; Lee, H. J., Electrocatalytic Recycling of CO2 and Small Organic Molecules. Chemistry – An Asian Journal ***2009,*** *4 (10), 1516-1523.*
25. Ba, X.; Yan, L.-L.; Huang, S.; Yu, J.; Xia, X.-J.; Yu, Y., New Way for CO2 Reduction under Visible Light by a Combination of a Cu Electrode and Semiconductor Thin Film: Cu2O Conduction Type and Morphology Effect. The Journal of Physical Chemistry C ***2014,*** *118 (42), 24467-24478.*
26. Baturina, O. A.; Lu, Q.; Padilla, M. A.; Xin, L.; Li, W.; Serov, A.; Artyushkova, K.; Atanassov, P.; Xu, F.; Epshteyn, A.; Brintlinger, T.; Schuette, M.; Collins, G. E., CO2 Electroreduction to Hydrocarbons on Carbon-Supported Cu Nanoparticles. ACS Catalysis ***2014,*** *4 (10), 3682-3695.*
27. Calle-Vallejo, F.; Koper, M. T. M., Theoretical Considerations on the Electroreduction of CO to C2 Species on Cu(100) Electrodes. Angewandte Chemie International Edition ***2013,*** *52 (28), 7282-7285.*
28. Chang, X.; Wang, T.; Zhang, P.; Wei, Y.; Zhao, J.; Gong, J., Stable Aqueous Photoelectrochemical CO2 Reduction by a Cu2O Dark Cathode with Improved Selectivity for Carbonaceous Products. Angewandte Chemie ***2016****.*

29. Durand, W. J.; Peterson, A. A.; Studt, F.; Abild-Pedersen, F.; Nørskov, J. K., Structure effects on the energetics of the electrochemical reduction of CO2 by copper surfaces. Surface Science ***2011,*** *605 (15–16), 1354-1359.*

30. Gattrell, M.; Gupta, N.; Co, A., A review of the aqueous electrochemical reduction of CO2 to hydrocarbons at copper. Journal of Electroanalytical Chemistry ***2006,*** *594 (1), 1-19.*

31. Hirunsit, P.; Soodsawang, W.; Limtrakul, J., CO2 Electrochemical Reduction to Methane and Methanol on Copper-Based Alloys: Theoretical Insight. The Journal of Physical Chemistry C ***2015,*** *119 (15), 8238-8249.*

32. Nie, X.; Esopi, M. R.; Janik, M. J.; Asthagiri, A., Selectivity of CO2 Reduction on Copper Electrodes: The Role of the Kinetics of Elementary Steps. Angewandte Chemie International Edition ***2013,*** *52 (9), 2459-2462.*

33. Shoji, S.; Yin, G.; Nishikawa, M.; Atarashi, D.; Sakai, E.; Miyauchi, M., Photocatalytic reduction of CO 2 by CuxO nanocluster loaded SrTiO 3 nanorod thin film. Chemical Physics Letters ***2016,*** *658, 309-314.*

34. Wang, P.; Xia, Y.; Wu, P.; Wang, X.; Yu, H.; Yu, J., Cu(II) as a General Cocatalyst for Improved Visible-Light Photocatalytic Performance of Photosensitive Ag-Based Compounds. The Journal of Physical Chemistry C ***2014,*** *118 (17), 8891-8898.*

35. Chen, Y.; Li, C. W.; Kanan, M. W., Aqueous CO2 reduction at very low overpotential on oxide-derived Au nanoparticles. Journal of the American Chemical Society ***2012,*** *134 (49), 19969-19972.*

36. Friebel, D.; Mbuga, F.; Rajasekaran, S.; Miller, D. J.; Ogasawara, H.; Alonso-Mori, R.; Sokaras, D.; Nordlund, D.; Weng, T.-C.; Nilsson, A., Structure, Redox Chemistry, and Interfacial Alloy Formation in Monolayer and Multilayer Cu/Au(111) Model Catalysts for CO2 Electroreduction. The Journal of Physical Chemistry C ***2014,*** *118 (15), 7954-7961.*

37. Kauffman, D. R.; Alfonso, D.; Matranga, C.; Qian, H.; Jin, R., Experimental and Computational Investigation of Au25 Clusters and CO2: A Unique Interaction and Enhanced Electrocatalytic Activity. Journal of the American Chemical Society ***2012,*** *134 (24), 10237-10243.*

38. Kang, Q.; Wang, T.; Li, P.; Liu, L.; Chang, K.; Li, M.; Ye, J., Photocatalytic Reduction of Carbon Dioxide by Hydrous Hydrazine over Au–Cu Alloy Nanoparticles Supported on SrTiO3/TiO2 Coaxial Nanotube Arrays. Angewandte Chemie International Edition ***2015,*** *54 (3), 841-845.*

39. Zhu, W.; Michalsky, R.; Metin, Ö.; Lv, H.; Guo, S.; Wright, C. J.; Sun, X.; Peterson, A. A.; Sun, S., Monodisperse Au Nanoparticles for Selective Electrocatalytic Reduction of CO2 to CO. Journal of the American Chemical Society ***2013,*** *135 (45), 16833-16836.*

40. Zhu, W.; Zhang, Y.-J.; Zhang, H.; Lv, H.; Li, Q.; Michalsky, R.; Peterson, A. A.; Sun, S., Active and selective conversion of CO2 to CO on ultrathin Au nanowires. Journal of the American Chemical Society ***2014,*** *136 (46), 16132-16135.*

41. Iizuka, K.; Wato, T.; Miseki, Y.; Saito, K.; Kudo, A., Photocatalytic reduction of carbon dioxide over Ag cocatalyst-loaded ALa4Ti4O15 (A= Ca, Sr, and Ba) using water

as a reducing reagent. Journal of the American Chemical Society **2011,** *133 (51), 20863-20868.*

42. Hatsukade, T.; Kuhl, K. P.; Cave, E. R.; Abram, D. N.; Feaster, J. T.; Hahn, C.; Jongerius, A. L.; Jaramillo, T. F. In Influence of Alloying on CO2 Electroreduction on Ag-Zn System, Meeting Abstracts, The Electrochemical Society: 2016; pp 3028-3028.

43. Yamamoto, M.; Yoshida, T.; Yamamoto, N.; Nomoto, T.; Yamamoto, Y.; Yagi, S.; Yoshida, H., Photocatalytic reduction of CO 2 with water promoted by Ag clusters in Ag/Ga 2 O 3 photocatalysts. Journal of Materials Chemistry A **2015,** *3 (32), 16810-16816.*

44. Kim, C.; Jeon, H. S.; Eom, T.; Jee, M. S.; Kim, H.; Friend, C. M.; Min, B. K.; Hwang, Y. J., Achieving Selective and Efficient Electrocatalytic Activity for CO2 Reduction Using Immobilized Silver Nanoparticles. Journal of the American Chemical Society **2015,** *137 (43), 13844-13850.*

45. Grunwaldt, J.-D.; Molenbroek, A.; Topsøe, N.-Y.; Topsøe, H.; Clausen, B., In situ investigations of structural changes in Cu/ZnO catalysts. Journal of Catalysis **2000,** *194 (2), 452-460.*

46. Nakamura, I.; Nakano, H.; Fujitani, T.; Uchijima, T.; Nakamura, J., Evidence for a special formate species adsorbed on the Cu–Zn active site for methanol synthesis. Surface science **1998,** *402, 92-95.*

47. Shirsath, S. E.; Toksha, B. G.; Kadam, R. H.; Patange, S. M.; Mane, D. R.; Jangam, G. S.; Ghasemi, A., Doping effect of Mn2+ on the magnetic behavior in Ni–Zn ferrite nanoparticles prepared by sol–gel auto-combustion. Journal of Physics and Chemistry of Solids **2010,** *71 (12), 1669-1675.*

48. Rosen, J.; Hutchings, G. S.; Lu, Q.; Forest, R. V.; Moore, A.; Jiao, F., Electrodeposited Zn dendrites with enhanced CO selectivity for electrocatalytic CO2 reduction. Acs Catalysis **2015,** *5 (8), 4586-4591.*

49. Scaife, D., Oxide semiconductors in photoelectrochemical conversion of solar energy. Solar Energy **1980,** *25 (1), 41-54.*

50. Kar, P.; Farsinezhad, S.; Zhang, X.; Shankar, K., Anodic Cu2S and CuS nanorod and nanowall arrays: preparation, properties and application in CO2 photoreduction. Nanoscale **2014,** *6 (23), 14305-18.*

51. Wang, C.; Thompson, R. L.; Baltrus, J.; Matranga, C., Visible light photoreduction of CO2 using CdSe/Pt/TiO2 heterostructured catalysts. The Journal of Physical Chemistry Letters **2009,** *1 (1), 48-53.*

52. Srinivasan, N.; Shiga, Y.; Atarashi, D.; Sakai, E.; Miyauchi, M., A PEDOT-coated quantum dot as efficient visible light harvester for photocatalytic hydrogen production. Applied Catalysis B: Environmental **2015,** *179, 113-121.*

53. Shiga, Y.; Umezawa, N.; Srinivasan, N.; Koyasu, S.; Sakai, E.; Miyauchi, M., A metal sulfide photocatalyst composed of ubiquitous elements for solar hydrogen production. Chemical Communications **2016,** *52 (47), 7470-7473.*

54. Zhou, R.; Guzman, M. I., CO2 Reduction under Periodic Illumination of ZnS. The Journal of Physical Chemistry C **2014,** *118 (22), 11649-11656.*

55. Ida, S.; Yamada, K.; Matsunaga, T.; Hagiwara, H.; Matsumoto, Y.; Ishihara, T.,

Preparation of p-Type CaFe2O4 Photocathodes for Producing Hydrogen from Water. Journal of the American Chemical Society **2010,** *132 (49), 17343-17345.*
56. Liu, Z.; Zhao, Z.-G.; Miyauchi, M., Efficient visible light active CaFe2O4/WO3 based composite photocatalysts: effect of interfacial modification. The Journal of Physical Chemistry C **2009,** *113 (39), 17132-17137.*
57. Matsumoto, Y.; Obata, M.; Hombo, J., Photocatalytic reduction of carbon dioxide on p-type CaFe2O4 powder. The Journal of Physical Chemistry **1994,** *98 (11), 2950-2951.*
58. Srinivasan, N.; Sakai, E.; Miyauchi, M., Balanced excitation between two semiconductors in bulk heterojunction Z-scheme system for overall water splitting. ACS Catalysis **2016,** *6 (4), 2197-2200.*
59. Irie, H.; Maruyama, Y.; Hashimoto, K., Ag+-and Pb2+-doped SrTiO3 photocatalysts. A correlation between band structure and photocatalytic activity. The Journal of Physical Chemistry C **2007,** *111 (4), 1847-1852.*
60. Liu, L.; Li, P.; Adisak, B.; Ouyang, S.; Umezawa, N.; Ye, J.; Kodiyath, R.; Tanabe, T.; Ramesh, G. V.; Ueda, S.; Abe, H., Gold photosensitized SrTiO3 for visible-light water oxidation induced by Au interband transitions. Journal of Materials Chemistry A **2014,** *2 (25), 9875-9882.*
61. Nosaka, Y.; Takahashi, S.; Mitani, Y.; Qiu, X.; Miyauchi, M., Reaction mechanism of visible-light responsive Cu(II)-grafted Mo-doped SrTiO3 photocatalyst studied by means of ESR spectroscopy and chemiluminescence photometry. Applied Catalysis B: Environmental **2012,** *111–112 (0), 636-640.*
62. Iwashina, K.; Kudo, A., Rh-doped SrTiO3 photocatalyst electrode showing cathodic photocurrent for water splitting under visible-light irradiation. Journal of the American Chemical Society **2011,** *133 (34), 13272-13275.*
63. Sato, S.; Morikawa, T.; Saeki, S.; Kajino, T.; Motohiro, T., Visible - Light - Induced Selective CO2 Reduction Utilizing a Ruthenium Complex Electrocatalyst Linked to ap - Type Nitrogen - Doped Ta2O5 Semiconductor. Angewandte Chemie International Edition **2010,** *49 (30), 5101-5105.*
64. Suzuki, T. M.; Nakamura, T.; Saeki, S.; Matsuoka, Y.; Tanaka, H.; Yano, K.; Kajino, T.; Morikawa, T., Visible light-sensitive mesoporous N-doped Ta 2 O 5 spheres: synthesis and photocatalytic activity for hydrogen evolution and CO 2 reduction. Journal of Materials Chemistry **2012,** *22 (47), 24584-24590.*
65. Sahara, G.; Kumagai, H.; Maeda, K.; Kaeffer, N.; Artero, V.; Higashi, M.; Abe, R.; Ishitani, O., Photoelectrochemical Reduction of CO2 Coupled to Water Oxidation Using a Photocathode With a Ru(II)-Re(I) Complex Photocatalyst and a CoOx/TaON Photoanode. J Am Chem Soc **2016**.
66. Iwase, A.; Yoshino, S.; Takayama, T.; Ng, Y. H.; Amal, R.; Kudo, A., Water Splitting and CO2 Reduction under Visible Light Irradiation Using Z-Scheme Systems Consisting of Metal Sulfides, CoOx-Loaded BiVO4, and a Reduced Graphene Oxide Electron Mediator. Journal of the American Chemical Society **2016,** *138 (32), 10260-10264.*
67. Sekizawa, K.; Maeda, K.; Domen, K.; Koike, K.; Ishitani, O., Artificial Z-Scheme Constructed with a Supramolecular Metal Complex and Semiconductor for the

Photocatalytic Reduction of CO2. Journal of the American Chemical Society **2013,** *135 (12), 4596-4599.*

68. Cao, S.; Yu, J., g-C3N4-based photocatalysts for hydrogen generation. The journal of physical chemistry letters **2014,** *5 (12), 2101-2107.*

69. Shi, H.; Chen, G.; Zhang, C.; Zou, Z., Polymeric g-C3N4 coupled with NaNbO3 nanowires toward enhanced photocatalytic reduction of CO2 into renewable fuel. Acs Catalysis **2014,** *4 (10), 3637-3643.*

70. Xiang, Q.; Yu, J.; Jaroniec, M., Preparation and enhanced visible-light photocatalytic H2-production activity of graphene/C3N4 composites. The Journal of Physical Chemistry C **2011,** *115 (15), 7355-7363.*

71. Barton, E. E.; Rampulla, D. M.; Bocarsly, A. B., Selective solar-driven reduction of CO2 to methanol using a catalyzed p-GaP based photoelectrochemical cell. Journal of the American Chemical Society **2008,** *130 (20), 6342-6344.*

72. Noda, H.; Yamamoto, A.; Ikeda, S.; Maeda, M.; Ito, K., Influence of light intensity on photoelectroreduction of CO2 at a p-GaP photocathode. Chemistry Letters **1990,** *(9), 1757-1760.*

73. AlOtaibi, B.; Fan, S.; Wang, D.; Ye, J.; Mi, Z., Wafer-level artificial photosynthesis for CO2 reduction into CH4 and CO using GaN nanowires. ACS Catalysis **2015,** *5 (9), 5342-5348.*

74. Arai, T.; Horiguchi, M.; Yanagida, M.; Gunji, T.; Sugihara, H.; Sayama, K., Reaction mechanism and activity of WO3-catalyzed photodegradation of organic substances promoted by a CuO cocatalyst. The Journal of Physical Chemistry C **2009,** *113 (16), 6602-6609.*

75. Nishikawa, M.; Yuto, S.; Hasegawa, T.; Shiroishi, W.; Honghao, H.; Nakabayashi, Y.; Nosaka, Y.; Saito, N., Compositing effects of CuBi2O4 on visible-light responsive photocatalysts. Materials Science in Semiconductor Processing **2017,** *57, 12-17.*

76. Nukui, Y.; Srinivasan, N.; Shoji, S.; Atarashi, D.; Sakai, E.; Miyauchi, M., Vertically aligned hexagonal WO3 nanotree electrode for photoelectrochemical water oxidation. Chemical Physics Letters **2015,** *635, 306-311.*

77. Zhao, Z. G.; Liu, Z. F.; Miyauchi, M., Tailored remote photochromic coloration of in situ synthesized CdS quantum dot loaded WO3 films. Advanced Functional Materials **2010,** *20 (23), 4162-4167.*

78. Chen, S.; Wang, L.-W., Thermodynamic oxidation and reduction potentials of photocatalytic semiconductors in aqueous solution. Chemistry of Materials **2012,** *24 (18), 3659-3666.*

79. Zhong, D. K.; Gamelin, D. R., Photoelectrochemical Water Oxidation by Cobalt Catalyst ("Co–Pi")/α-Fe2O3 Composite Photoanodes: Oxygen Evolution and Resolution of a Kinetic Bottleneck. Journal of the American Chemical Society **2010,** *132 (12), 4202-4207.*

80. Sato, S.; Arai, T.; Morikawa, T.; Uemura, K.; Suzuki, T. M.; Tanaka, H.; Kajino, T., Selective CO2 conversion to formate conjugated with H2O oxidation utilizing semiconductor/complex hybrid photocatalysts. Journal of the American Chemical Society

2011, 133 (39), 15240-15243.
81. Lewandowski, I.; Scurlock, J. M.; Lindvall, E.; Christou, M., The development and current status of perennial rhizomatous grasses as energy crops in the US and Europe. Biomass and bioenergy 2003, 25 (4), 335-361.
82. Sahara, G.; Kumagai, H.; Maeda, K.; Kaeffer, N.; Artero, V.; Higashi, M.; Abe, R.; Ishitani, O., Photoelectrochemical Reduction of CO2 Coupled to Water Oxidation Using a Photocathode with a Ru (II)–Re (I) Complex Photocatalyst and a CoO x/TaON Photoanode. Journal of the American Chemical Society 2016, 138 (42), 14152-14158.
83. Carroll, G. M.; Gamelin, D. R., Kinetic analysis of photoelectrochemical water oxidation by mesostructured Co-Pi/α-Fe 2 O 3 photoanodes. Journal of Materials Chemistry A 2016, 4 (8), 2986-2994.

Chapter. 2

The development and evaluation of Cu_xO nanocluster.

2.1 Introduction

As I introduced in *Session 1.2.2,* Cu is a common catalyst for CO_2 reduction, which can suppress the proceeding of water splitting and improve the CO_2 reduction, especially the generation of hydrocarbonate. [1-20]This is the result of its low adsorption strength for H_+, strong adsorption for CO_2* and appropriate adsorption for CO*.[21] In the meanwhile, Cu is one of the most abundant and cheap element on the earth, which is a big advantage compared to other highly effective CO_2 reduction catalysts such as Au, Rh or Ir.

Until now, a lot of researches has be reported using Cu or Cu alloy, especially Cu-Au alloy to catalyze CO_2 reduction in electrochemical or photocatalytic area.

In the present research, a Cu_xO nanocluster was developed, this material was expected to behave an atmosphere nanocluster structure, as shown below.

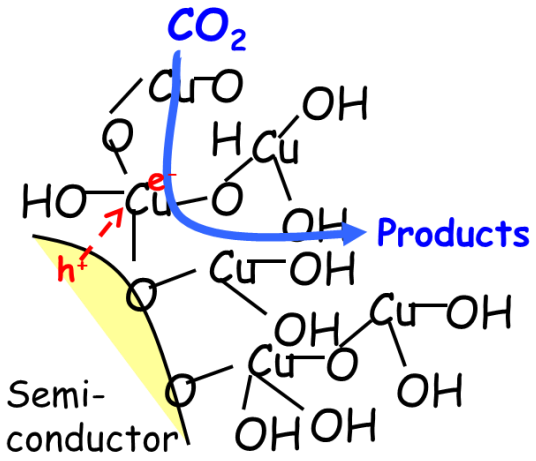

Figure 2.1 *the structure image of the Cu_xO nanocluster.*

This structure if very flexible, the valence number of Cu can change freely, thus when the photoexcited electrons were injected, they can be accumulated inside of the cluster and join multi-electron reactions.

In the previous researches, the Cu_xO nanocluster was proved to be very effective in photodecomposition of organic molecular, bacterial and virus.[22-25] After grafted on the surface of light harvesters, such as TiO_2, the electrons in the valence band of TiO_2 excited into the Cu_xO

nanoclusters through an interfacial charge transfer (IFCT) process under visible light irradiation, and consumed in the multi-electron reduction of oxygen, as shown in Figure 2.2.[25]

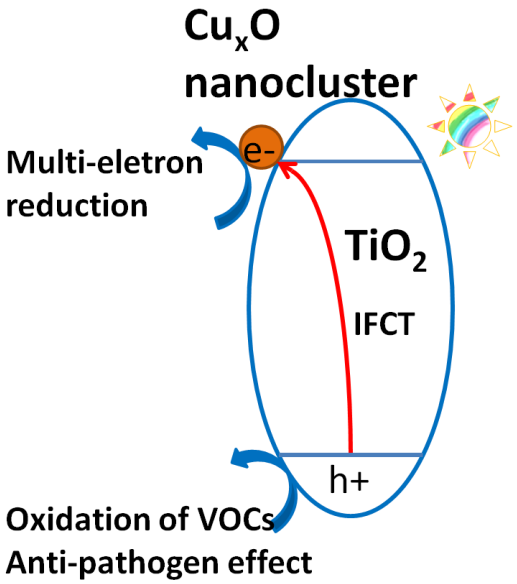

Figure 2.2 *the IFCT transfer in Cu_xO nanoclusters grafted TiO_2 under visible light irradiation.*

However, in the IFCT transfer, the electrons were injected into the Fermi level of Cu(II)/Cu(I),[26] which is not high enough for the CO_2 redcutin, so we expected that different electron transfer occur during the photocatalytic CO_2 reduction.

Besides the Cu_xO nanocluster, Fe(III) and Ti(II) nanoclusters were also studied for photodecomposition, however the expect for their performance for CO_2 reduction is lower than Cu_xO nanocluster the poor activity Fe and Ti showed for CO_2 reduction.

To be noticed, the decomposition and antibacterial are both spontaneous reactions ($\Delta G<0$), while the photocatalytic CO_2 reduction is non-spontaneous process($\Delta G>0$), which is more difficult to achieve. Thus, the development of utilizing the Cu_xO nanocluster as the co-catalyst for photocatalytic CO_2 reduction is obviously challenging and more complicated than the former research.

2.2 Experimental Procedures

2.2.1 Fabrication of copper oxide nanocluster-modified electrode.

The grafting of copper oxide nanoclusters onto titanium (Ti) metal sheets used as the electrode was performed by an impregnation method, as previously described. [22-23, 27] Briefly, Ti sheets (0.10×200×200 mm; Nirako Corp.) were cleaned by ultrasonication sequentially in non-phosphate detergent, distilled water (3 times), and ethanol, and were then immediately

dried using a nitrogen gas gun. Heat-resistant insulating tape was affixed to the entire reverse surfaces of the Ti sheet and was used to surround a 1×1 cm square area on the front side of the sheet. For the grafting of Cu(II) nanoclusters, two Ti sheets were placed into 47.9 mL distilled water heated to 90 °C in a vial reactor. A total of 1.6 mL of a 0.01 M $CuCl_2$ solution, which was prepared from $CuCl_2$•$2H_2O$ as the source of Cu(II), was immediately added to the vial and 0.5 mL 1 M NaOH was then added to adjust the pH to 12. The temperature of the solution was kept at 90 °C with stirring for 1 h. The grafted Ti sheets were then removed from the vials and immediately dried using a nitrogen gas gun.

2.2.2 Electrochemical evaluation.

For electrochemical evaluation, Cu(II) nanoclusters were grafted on the surface of the Ti sheets used as working electrodes. The electrodes were placed in electrolyte solution (0.5 M $KHCO_3$ for CO_2 bubbling and 0.5 M KCl for Ar bubbling; both adjusted to pH 12 with NaOH) inside a closed glass cell and the electrolyte was then bubbled with CO_2 or Ar gas to create different atmospheres. The electrocatalytic properties of the grafted electrodes were evaluated by comparing the cyclic voltammogram curves obtained under CO_2 or Ar bubbling. To confirm that the observed differences were due to the reduction of CO_2 rather than water splitting, cyclic voltammogram curves were also measured for electrodes place in an anhydrous organic electrolyte (acetonitrile containing 0.1 M tetraethylammonium tetrafluoroborate). Ti sheets sputtered with platinum (~50 nm) were used as a control to demonstrate the selectivity for CO_2 reduction, as platinum is a well-known electrocatalyst for water splitting.

2.2.3 Photocatalytic evaluation.

For photocatalytic evaluation, Cu(II) nanoclusters were grafted on the surface of a semiconductor light harvester material, in the present research, $Nb_3O_8^-$ nanosheets was used as a UV light harvester.

Synthesis of $Nb_3O_8^-$ nanosheets. Niobate nanosheets were prepared by delaminating bulk niobate with tetrabutylammonium hydroxide (TBAOH) using a soft-chemical procedure, as previously described.[28-29] Briefly, 1.01 g (0.01 mol) KNO_3 and 3.987 g (0.015 mol) Nb_2O_5 (molar ratio of 2:3) were mixed and ground with an agate mortar into a fine powder, which was then heated to 900 °C over a 3-h period, and was then held at 900 °C for 20 h. Approximately 0.001 mol (0.45g) of the obtained KNb_3O_8 was placed into centrifuge tubes and mixed with 40 mL 2.0 M HNO_3 aqueous solution for acid exchange. KNb_3O_8 was converted into HNb_3O_8•$2H_2O$ by repeating the acid exchange three times. The centrifuge tubes were then centrifuged to remove the acid solution, and the obtained pellet was washed with distilled water until the supernatant reached neutral pH. The protonic oxide was delaminated into colloidal $Nb_3O_8^-$ nanosheets by reaction with an aqueous solution of TBAOH) at a molar ratio 1:1 for

about 10 days with continous shaking. The suspension of $Nb_3O_8^-$ nanosheets was gently washed with sufficient amounts of weak HNO_3 solution during vacuum filtration using a membrane filter (0.025 μm; Millipore), and the filter containing the $Nb_3O_8^-$ nanosheets was then irradiated with black light in humid air to decompose the organic residue into $Nb_3O_8^-$ nanosheet powder.

Grafting copper oxide nanoclusters onto the surface of $Nb_3O_8^-$ nanosheets. The grafting method for semiconductor powders is similar to the method for producing electrodes, but the amount of Cu(II) used for loading was increased from 0.5 to 10 wt%.

The photocatalytic experiments. As shown in Figure 2.1, the prepared powders were dispersed in 20 mL electrolyte (0.5 M $KHCO_3$ aqueous solution, adjusted to pH 12 with NaOH) in a petri dish, which was then placed into a sealed glass reactor (500 mL) covered with a quartz glass cap. CO_2 or Ar gas was bubbled inside of the reactor through silica tubes at a flow rate of 100 mL/min for 30 min to create a saturated atmosphere of CO_2 or Ar. The reactor was irradiated by UV light (Hg-Xe lamp (240~300 nm), LA-410UV, Hayashi. The light spectrum is shown in Figure 2.2), and products in the headspace were collected by a syringe and then injected into gas chromatograph (flame ionization detector [FID] equipped with a methanizer apparatus) to detect CO and methane.

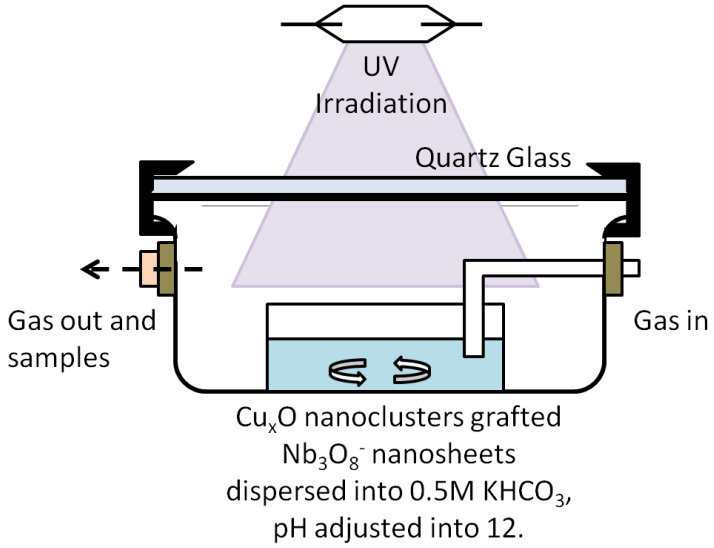

Figure 2.1 *The graphical representation of the evaluation system for photocatalytic CO_2 reduction.*

Isotope experiments. Isotope experiments were performed in a rectangle quartz glass cell (1×1×5 cm). The cells were irradiated with the same UV lamp used in the photocatalytic evaluations, and products in the headspace of the quartz glass cells were detected by gas chromatography (GC)-mass spectrometry (MS) (Shimadzu). All isotope chemicals were purchased from Isotec-Sigma Aldrich.

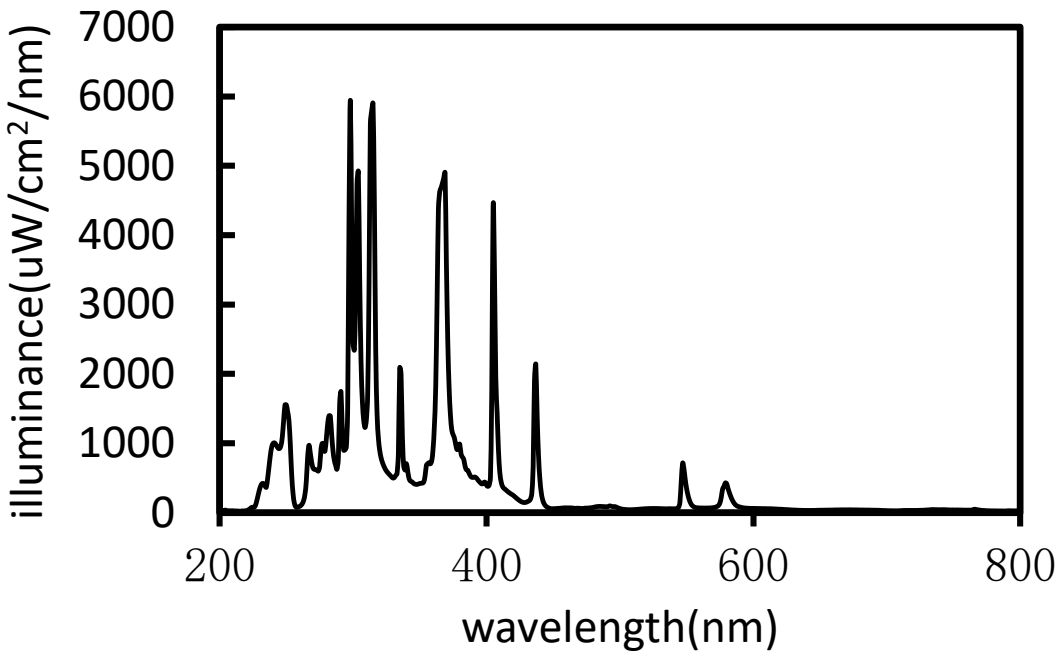

Figure 2.2. *The light spectrum of the UV light used in the PEC cell and photocatalytic evaluation.*

2.3 Results and Discussion

2.3.1 Characterization and Electrochemical evaluation of Cu_xO nanocluster

Cu_xO nanoclusters were grafted onto a metal titanium substrate using an impregnation method and their electrocatalytic properties were then examined under CO_2 or Ar purging in aqueous electrolyte (Fig 2.3). As a comparison an unmodified platinum plate was also examined as a representative conventional cathodic electrode. In an aqueous electrolyte, the platinum cathode exhibited a clear current generated from the water-splitting reaction, and no significant differences were observed between the CO_2 and Ar bubbling conditions. In contrast, the current density of the electrode grafted with Cu_xO nanoclusters under a CO_2 atmosphere was higher than that under Ar bubbling. This current difference was assigned to the cathodic current generation of the reduction of CO_2 molecules and/or carbonic acid in water induced by the Cu_xO nanoclusters, as bare titanium substrate did not generate significant current differences under CO_2 or Ar bubbling.

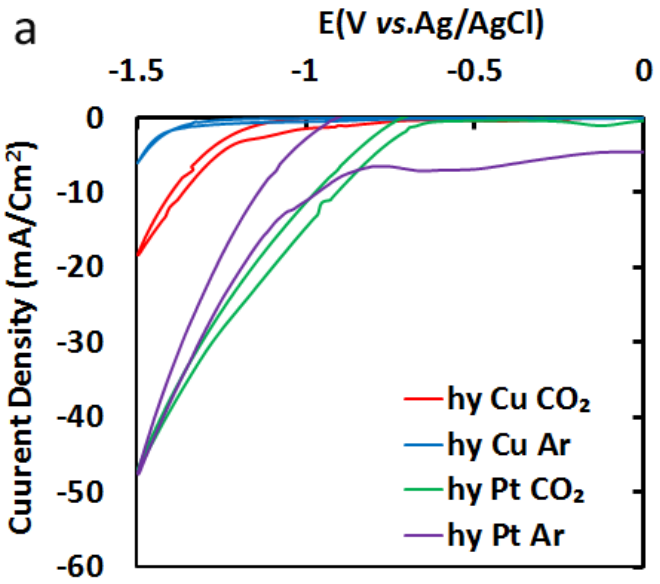

Figure 2.3 *(a) Cyclic voltammograms of Ti sheets grafted with copper oxide nanoclusters or sputtered with platinum in aqueous electrolyte (0.5 M $KHCO_3$ for CO_2 bubbling, 0.5 M KCl for Ar bubbling; pH adjusted to 12 with NaOH).*

Under anhydrous electrolyte conditions, a similar trend was observed, indicating that the Cu_xO nanoclusters act as an effective electrocatalyst for CO_2 reduction.

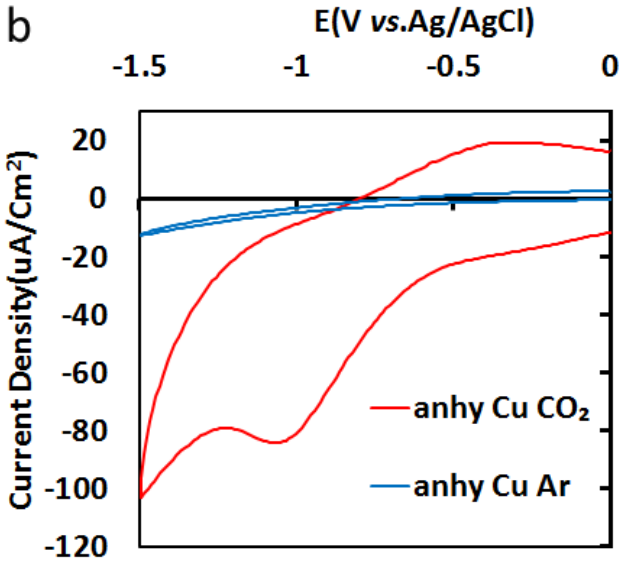

Figure 2.4 *Cyclic voltammograms of Ti sheets grafted with copper oxide nanoclusters in anhydrous organic electrolyte (acetonitrile containing 0.1 M tetraethylammonium tetrafluoroborate) under CO_2 or Ar bubbling.*

X-ray photoelectron spectroscopy (XPS) analysis was conducted under electrochemical

cathodic polarization to determine the valency of copper in each reduction peak (*Fig. 2.5*). Without the application of bias potential (0 V), Cu(II) was detected, as indicated by the presence of high-intensity shake-up satellites at higher binding energy than the main $2p_{3/2}$ and $2p_{1/2}$ peaks, which are not assigned to the spectra of Cu(0) and Cu(I). The satellite peaks of Cu(I) are similar to Cu(II) species, but the presence of Cu(I) was distinguished by the positive shift of the binding energy. Under a bias potential of -0.5 V (*vs*. Ag/AgCl), Cu(II) ions were reduced to Cu(I). Under the bias potential of -1.2 V for several minutes, there is no XPS signal, indicating that the Cu(I) species are reduced to Cu(0) states, which are unstable and detached from the surface of a Ti electrode.

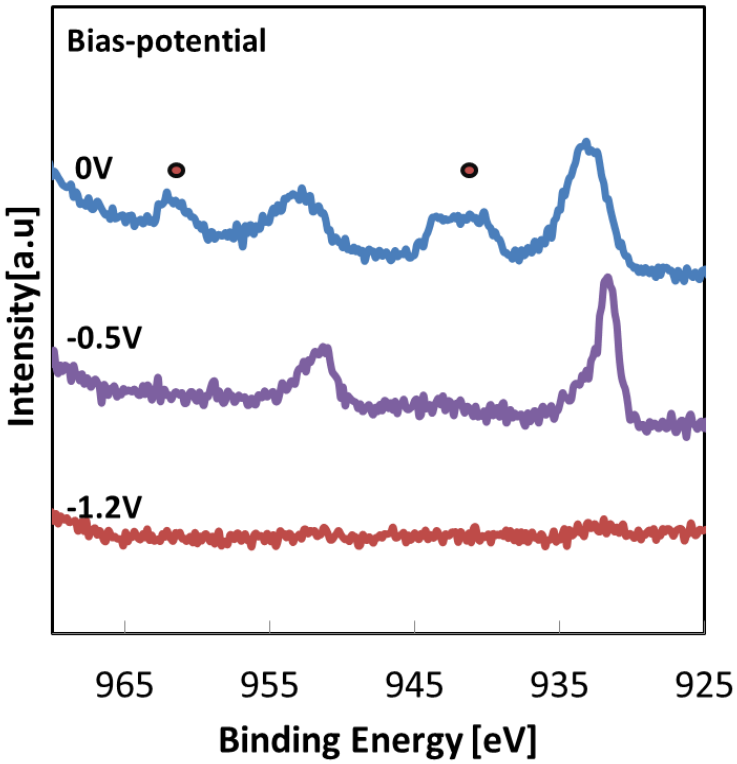

Figure 2.5 *XPS spectra of Cu in copper oxide nanoclusters grafted Ti metal electrode after applied the bias-potential of 0V, -0.5V and -1.2V(vs. Ag/AgCl) respectively. Shape-up satellites of Cu(II) are marked with yellow stars. The intensity was the integrated value. Measurement condition: 10 cycles, 3 repeats, one step = 0.15eV, 40ms.*

The gas composition in the headspace of our electrochemical cell was also detected by gas chromatograph (Figure 2.6), then CO was detected under bias-potential at -0.5 V as well as -1.2 V. These results indicate that the both Cu(II) and Cu(I) species act as catalytic sites for the reduction of CO_2 into CO.

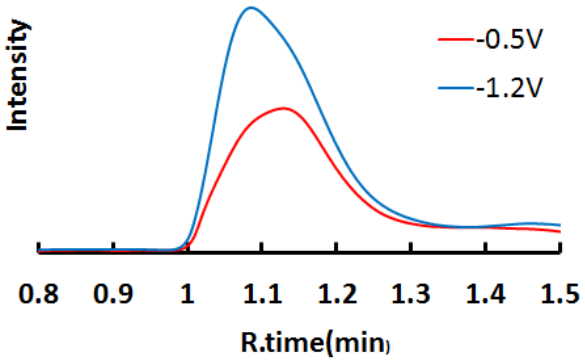

Figure 2.6 *The gas chromatograph of the headspace gas under bias-potential of -0.5V and -1.2V.*

2.3.2 Characterization and photocatlaytic evaluation

To evaluate how Cu_xO nanoclusters works as CO_2 photoreduction co-catalyst, a $Nb_3O_8^-$ nanosheet material was prepared as light harvester.

As revealed by atomic force microscopy (AFM), the prepared $Nb_3O_8^-$ nanosheets had monodispersed sheet morphology with a thickness below 2 nm, and length and widths of hundreds of nanometers (Fig 2.7).

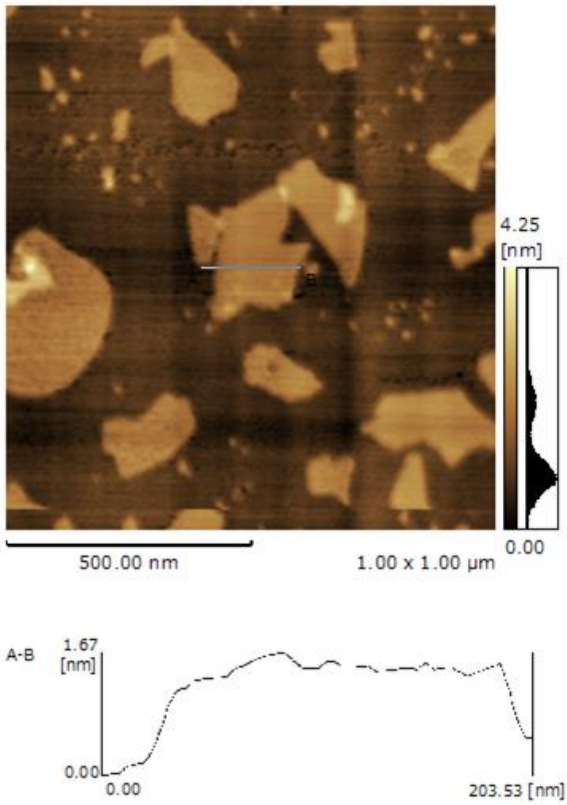

Figure 2.7 *The AFM image of the prepared $Nb_3O_8^-$ nanosheets*

The same nanosheet morphologies were also observed by TEM analysis (Fig 2.8). The obtained TEM diffraction pattern revealed that the $Nb_3O_8^-$ nanosheets had single crystal structure and that the exposed plane was oriented in the [010] direction.

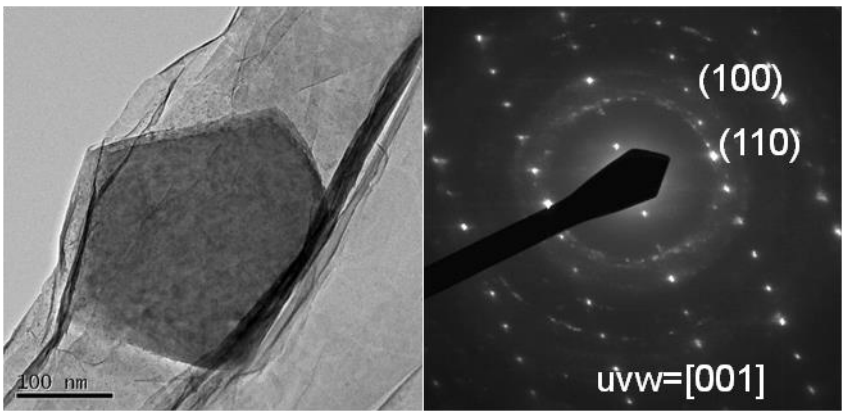

Figure 2.8 *The TEM image and electron diffraction pattern of $Nb_3O_8^-$ nanosheets (L=50 cm)*

The X-ray diffraction pattern of a thin film of $Nb_3O_8^-$ nanosheets clearly indicated that the crystals were oriented in the b-axis direction (Fig 2.9), as the exposed faces of the $Nb_3O_8^-$ nanosheets were attached and stacked on each other.

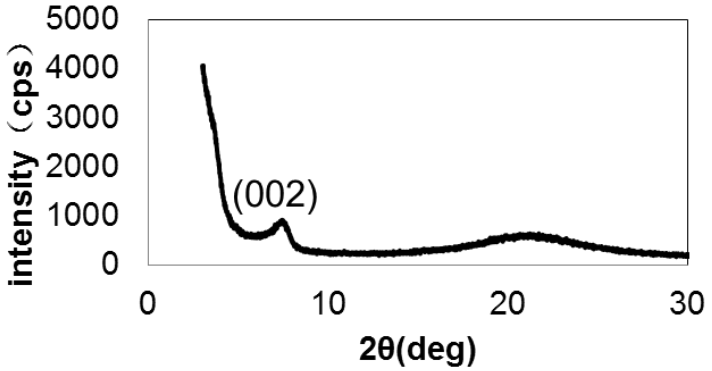

Figure 2.9 *The XRD of the $Nb_3O_8^-$ nanosheets thin film*

After loading Cu_xO nanoclusters onto the surface of $Nb_3O_8^-$ nanosheets, TEM image was observed (Fig 2.10). Nanoclusters of 2~3 nm in size. The results of energy dispersive x-ray spectroscopy (EDS, Fig. 2.11), also confirmed that the Cu_xO nanoclusters were highly dispersed on the surface of the $Nb_3O_8^-$ nanosheets.

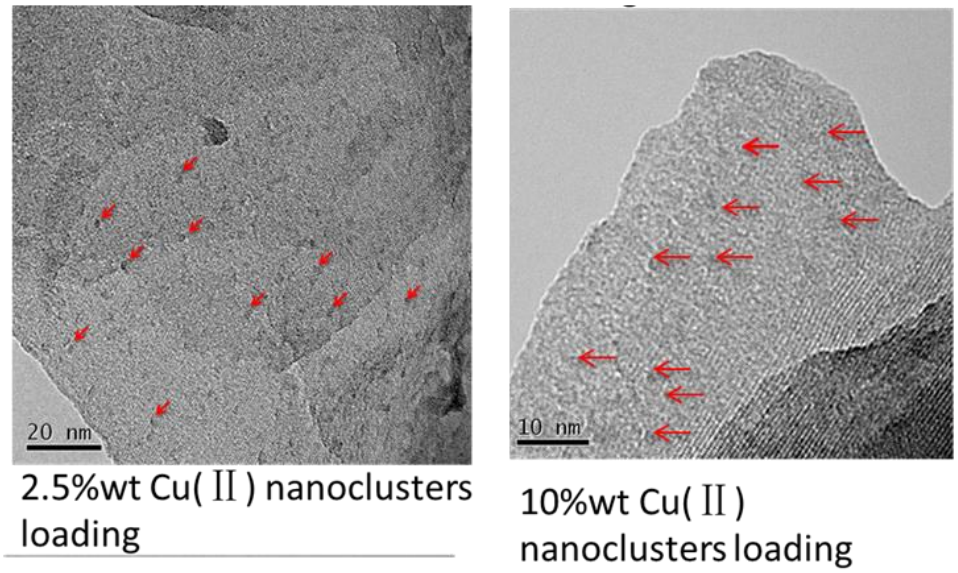

Figure 2.10 *the TEM image of the Cu_xO nanoclusters loaded $Nb_3O_8^-$ nanosheets*

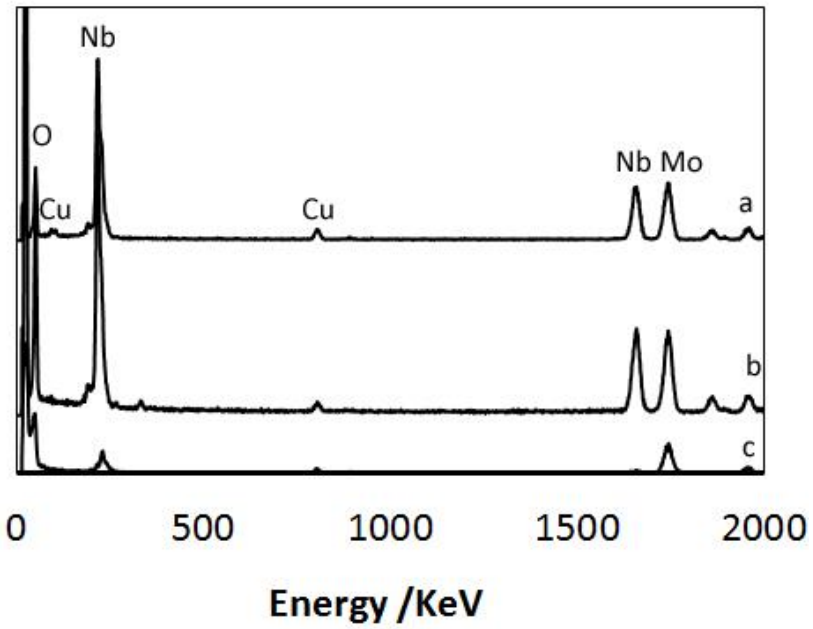

Figure 2.11 *The energy dispersive x-ray spectroscopy (EDS) of 2.5%wt copper oxide nanoclusters grafted $Nb_3O_8^-$ nanosheets (a). For comparison, the spectroscopy of bare $Nb_3O_8^-$ nanosheets (b) and bare sample stage (c).*

For the detailed structural characterization of the Cu_xO nanoclusters, we performed X-ray absorption near edge structure (XANES) and extended X-ray absorption fine structure (EXAFS) analyses using synchrotron apparatus (Fig 2.12). The X-ray absorption analyses revealed that the local structures of the nanoclusters resembled copper monoxide (CuO) and/or copper hydroxide ($Cu(OH)_2$). Previous studies have demonstrated that these amorphous copper oxides are highly stable under photoexcitation conditions and are critical for driving multi-electron reduction reactions.

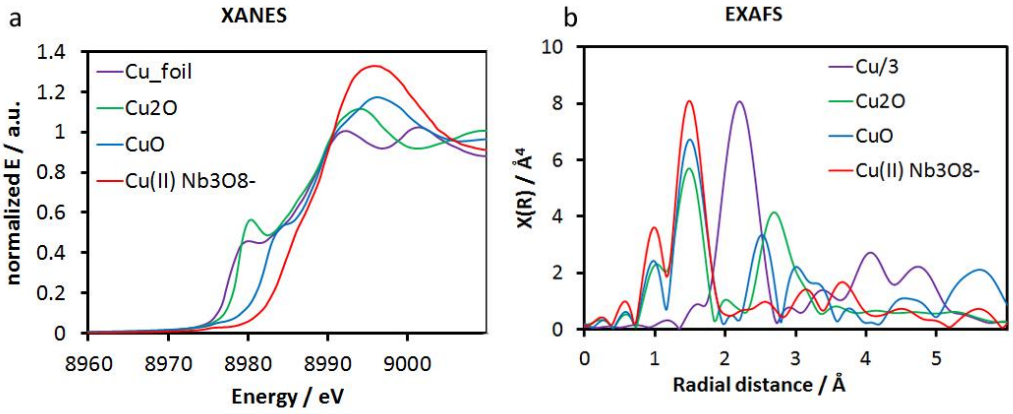

Figure 2.12 *Cu K-edge XANES spectra (a) and EXAFS (b) of 0.5%wt copper oxide nanoclusters grafted $Nb_3O_8^-$ nanosheets. For comparison, the spectra of Cu metal, Cu_2O and CuO were also included.*

UV-visible absorption spectra were obtained for $Nb_3O_8^-$ nanosheets grafted with and without

copper oxide nanoclusters (Fig 2.13). The band-to-band transition of the $Nb_3O_8^-$ nanosheets appeared at 300 nm, whereas the absorption at 430 nm is attributable to interfacial charge transfer (IFCT). The broad absorption in the range of 600-800 nm is attributable to the d-d transition of the Cu(II) species. A plot of the square root of absorption efficiency (α) multiplied by the photon energy ($(\alpha h\nu)^{1/2}$) versus the photon energy showed a linear relationship, indicating that the $Nb_3O_8^-$ nanosheet is an indirect transition-type semiconductor. The bandgap of the $Nb_3O_8^-$ nanosheets was estimated to be 3.56 eV, as calculated from the intersection of the plotted line of $(\alpha h\nu)^{1/2}$ versus photon energy with the abscissa axis.

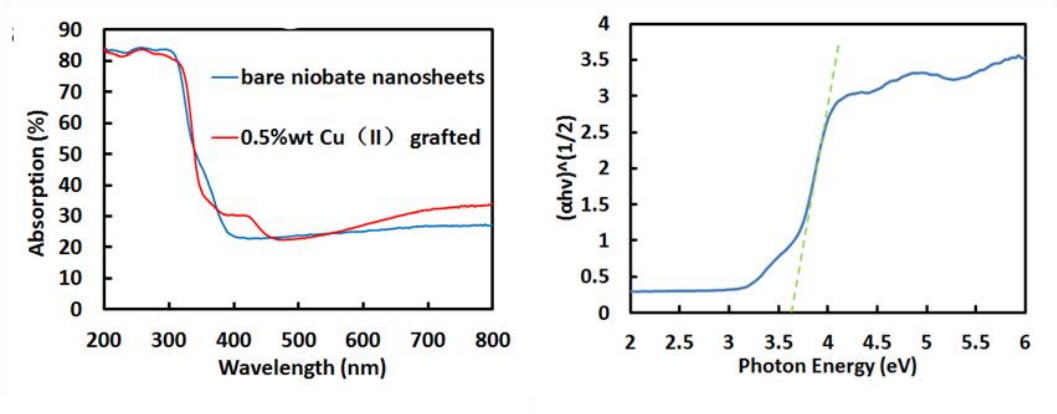

Figure 2.13 *UV-Vis spectra of bare and 0.5 wt% copper oxide nanocluster-grafted $Nb_3O_8^-$ nanosheets. Plot of $(\alpha h\nu)^{1/2}$ versus photon energy for $Nb_3O_8^-$ nanosheets.*

During the photocatalytic evaluation, bare $Nb_3O_8^-$ nanosheets was dispersed into gas-purged solution (0.5 M $KHCO_3$ for CO_2 atmosphere and 0.5 M KCl for Ar atmosphere, adjusted to pH 12 with NaOH) and irradiated with UV light from a Xe-Hg lamp, there was no obvious difference between CO_2 and Ar cases. The detected CO molecules were considered to be a result of the oxidation of surface contaminants on the niobate nanosheets. The reason for this lack of activity was considered to be the lack of reaction sites, as the negatively charged surfaces of $Nb_3O_8^-$ nanosheets limit CO_2 absorption.

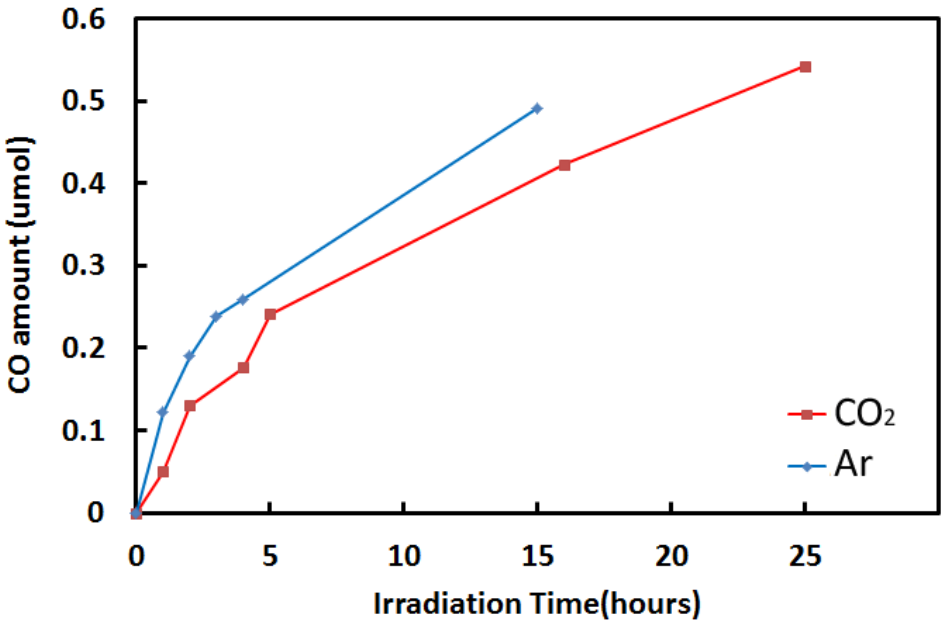

Figure 2.14 *Photocatalytic CO_2 reduction evaluation of $Nb_3O_8^-$ nanosheets powders without any co-catalysts grafted under CO_2 or Ar purging.*

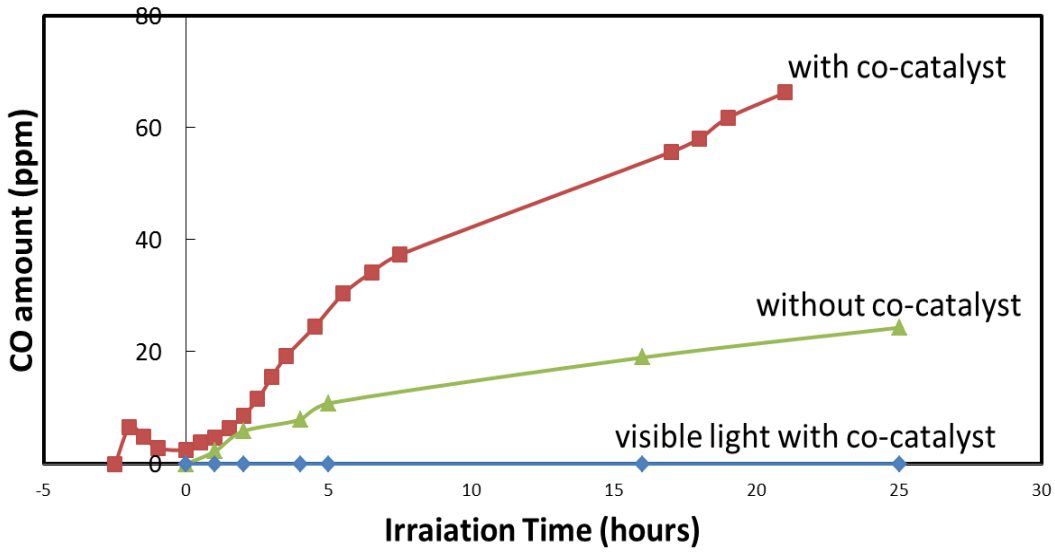

Figure 2.15 *Photocatalytic CO_2 reduction evaluation of $Nb_3O_8^-$ nanosheets powders with and without Cu_xO nanoclusters grafted under CO_2 purging.*

After coating Cu_xO nanoclusters onto the surface of $Nb_3O_8^-$ nanosheets, the produced CO amount increased, as we can see from Figure 2.15. This proved that the Cu_xO nanoclusters increase the CO_2 conversion efficiency as co-catalyst. We also evaluated the photocatalytic activity of the Cu_xO nanoclusters -grafted $Nb_3O_8^-$ nanosheet under visible-light irradiation using an UV cutoff filter. However, negligible activity was detected under visible light, even though the Cu(II)-grafted $Nb_3O_8^-$ nanosheet absorbs visible light by d-d transition and IFCT. These results indicate that the excitation of electrons to a sufficiently high conduction band

level and the modification of the $Nb_3O_8^-$ nanosheet with co-catalysts are indispensable to drive photocatalytic CO_2 reduction.

Also, as we can see from the figure, the CO amount didn't increased linearly, this was considered to be the result of the valence change during the reaction. During the photocatalytic evaluation, color change of the Cu_xO nanoclusters-grafted $Nb_3O_8^-$ nanosheets was observed. As we can see from Figure 2.16, under UV-light irradiation, the material changed from a light blue to musty green color within 1 hour, indicating a change in the valency of copper.

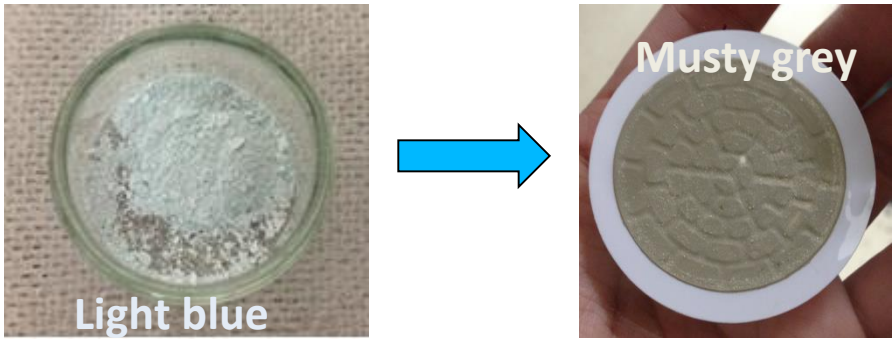

Figure 2.16 *The color change of Cu_xO nanoclusters-grafted $Nb_3O_8^-$ nanosheets before and after the UV irraidiation.*

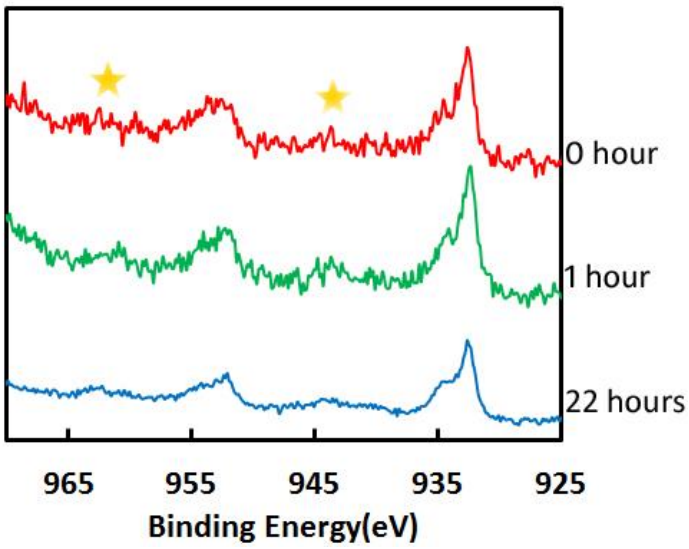

Figure 2.17 *XPS spectra of Cu in the 10%wt copper oxide nanoclusters grafted niobate nanosheets after the UV irradiation of 0 hour, 1 hour and 22 hours. Shape-up satellites of Cu(II) are marked with yellow stars. The intensity was the integrated value. Measurement condition: 10 cycles, 3 repeats, one step = 0.15 eV, 40ms.*

The results of XPS analysis (Fig 2.17) indicated that a proportion of the Cu(II) ions were reduced to Cu(I) in response to UV-light irradiation. Thus, the reaction rate of the Cu(II) nanocluster-grafted $Nb_3O_8^-$ nanosheets was not linear with respect to UV irradiation time, but rather, accelerated under light irradiation. This phenomenon was associated with the color

change of the material. In the initial phase of UV irradiation, a portion of the Cu(II) ions in the nanoclusters are reduced to Cu(I), resulting in a mixture of Cu(II)/Cu(I) ions. The present experimental results suggest that the mixture of Cu(II)/Cu(I) species leads to efficient reduction of CO_2.

The redox potential of Cu(II)/Cu(I) ions is +0.16 V (*versus* NHE at pH=0), which is more positive than that of the two electrons reduction of CO_2/CO. However, the conduction band of the $Nb_3O_8^-$ nanosheet synthesized in the present study is -1.32 V *vs.* Ag/AgCl, which is much more negative than the redox potential of CO_2/CO in the liquid phase (-0.52 V *vs.* NHE at 25 °C, pH 7.0). During UV-light irradiation, excited electrons in the conduction band of $Nb_3O_8^-$ nanosheet are injected into the Cu_xO nanoclusters, leading to a negative shift of the Fermi level of the nanoclusters. This shift allows for the reduction of CO_2 into CO in response to UV irradiation. We attempted to optimize the photocatalytic activity of the Cu_xO nanoclusters-grafted $Nb_3O_8^-$ nanosheet by modifying the loading amount of the copper catalyst and the pH of the electrolyte. The optimal photocatalytic activity for CO_2 reduction was observed for $Nb_3O_8^-$ nanosheets grafted with 0.5wt% copper oxide nanoclusters and dispersed in 0.5 M $KHCO_3$ solution (pH 12), as shown in Fig 2.18.

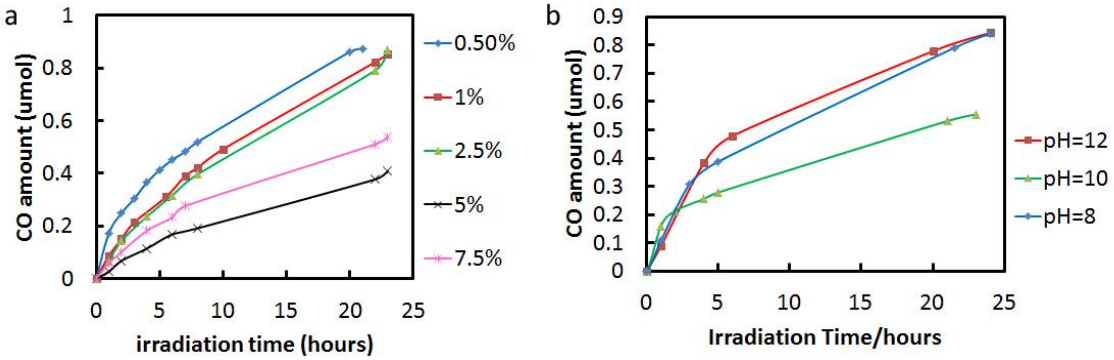

Figure 2.18 *(a) The produced CO amount on terms of copper oxide nanoclusters loading amount. Each group used 900 mg photocatalysts respectively. (b) The produced CO amount on terms of electrolyte pH for 0.5%wt copper oxide nanoclusters grafted niobate nanosheets.*

As supplement, the effect of the nanosheet structure was also evaluated, as we can see from figure 2.19, the raw material, Nb_2O_5 bulk and the HNb_3O_8 bulk were both grafted by Cu_xO nanoclusters, however, compared to the Cu_xO nanoclusters-grafted $Nb_3O_8^-$ nanosheets, less CO was detected under UV irradiation, suggesting that the high conduction band level resulting from the quantum confinement effect is critical for driving CO_2 photo-reduction.

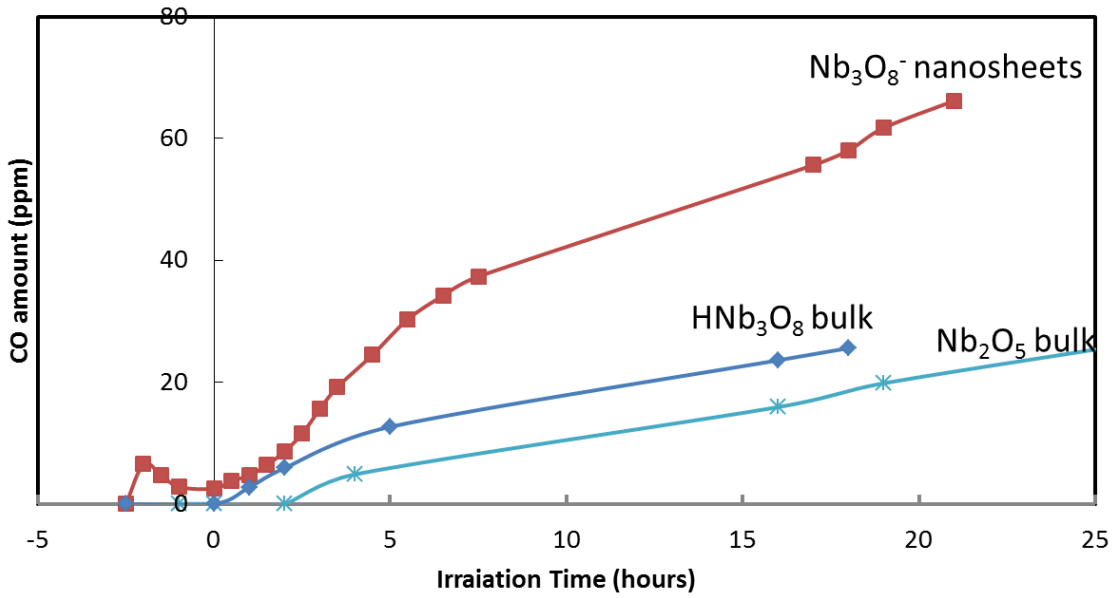

Figure 2.19 *The produced CO amount from the Cu_xO nanoclusters-grafted $Nb_3O_8^-$ nanosheets, Cu_xO nanoclusters-grafted Nb_2O_5 bulk and Cu_xO nanoclusters-grafted HNb_3O_8 bulk under UV irradiation, respectively.*

2.4 Mechanism analysis

2.4.1 Isotope tracer experiment

To verify oxygen generation and CO formation resulting from CO_2 reduction, isotope tracer analyses involving $H_2{}^{18}O$ and $^{13}CO_2$ were conducted for the optimized Cu_xO nanoclusters-$Nb_3O_8^-$ nanosheet photocatalyst. Figure 2.20 shows the mass chromatography spectra for UV-irradiated $Nb_3O_8^-$ nanosheets grafted with 0.5 wt% Cu_xO nanoclusters in 0.5 M $KHCO_3$/ $H_2{}^{18}O$ solution purged with $^{12}CO_2$. A clear peak for $^{18}O_2$ (m/z=36) was observed and continued to increase in size with increasing irradiation time. Figure 2.20(b) shows the mass chromatography spectra for UV-irradiated c Cu_xO nanoclusters-grafted $Nb_3O_8^-$ nanosheets in 0.01 M NaOH/ $H_2{}^{16}O$ solution purged with $^{13}CO_2$, in which a peak corresponding to ^{13}CO (m/z=29) was also detected. Together, these results confirmed that the CO detected during these photocatalytic reactions above was produced from CO_2 reduction and that the oxygen was generated from the oxidation of water.

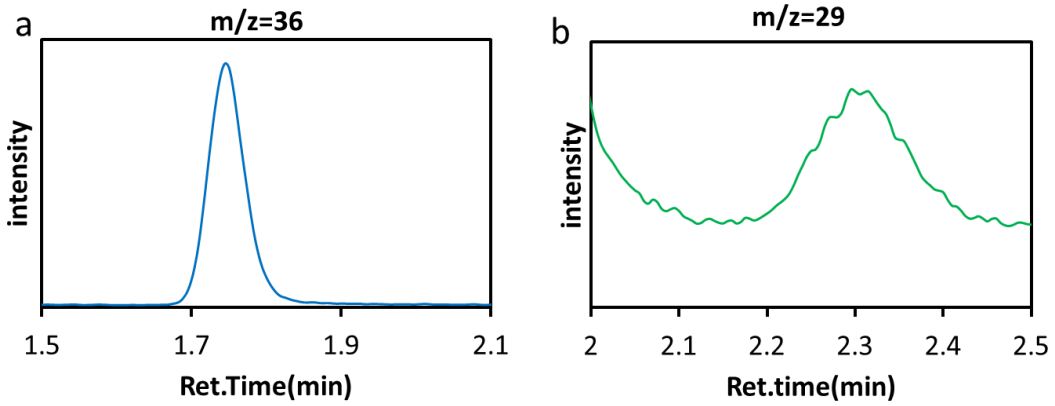

Figure 2.20 *(a) the mass chromatography spectra of $^{18}O_2$ (m/z=36) generated from UV-irradiated Nb_3O_8 nanosheets grafted with 0.5 wt% copper oxide nanoclusters in 0.5 M $KHCO_3$/ $H_2{}^{18}O$ solution purged with $^{12}CO_2$; (b) the peak of ^{13}CO (m/z=29) generated from UV-irradiated copper oxide nanocluster-grafted Nb_3O_8 nanosheets in 0.01 M NaOH/ $H_2{}^{16}O$ solution purged with $^{13}CO_2$.*

2.4.2 ESR analyses

Next, electron spin resonance (ESR) spectra[31] measured under CO_2 atmosphere and vacuum conditions were used to determine the reaction route of the photoelectrons and holes generated during the UV-light irradiation of the Cu_xO nanoclusters-grafted $Nb_3O_8^-$ nanosheets (Fig 2.21). The ESR spectra of bare $Nb_3O_8^-$ nanosheets before and after UV-light irradiation under vacuum or CO_2 atmosphere are shown in Fig 2.21(a) and Fig 2.21(b), respectively. The broad signal appeared around 295 mT, which was assigned to surface Nb^{4+} ions that were generated by reaction with photoelectrons after UV irradiation, decreased in CO_2 atmosphere as compared to vacuum conditions, indicating that the photoelectrons in the conduction band of niobate nanosheets have sufficiently high potential to reduce CO_2, which would thus regenerate Nb^{5+} ions. Even though these ESR results indicate that the conduction band of $Nb_3O_8^-$ nanosheet has enough high potential to reduce CO_2 to some anion radical species, our experimental results revealed that bare $Nb_3O_8^-$ nanosheets did not generate CO molecules. These results also suggest that modification of Cu(II) nanoclusters onto niobate nanosheets light harvester is necessary to promote chemical reactions, including CO production.

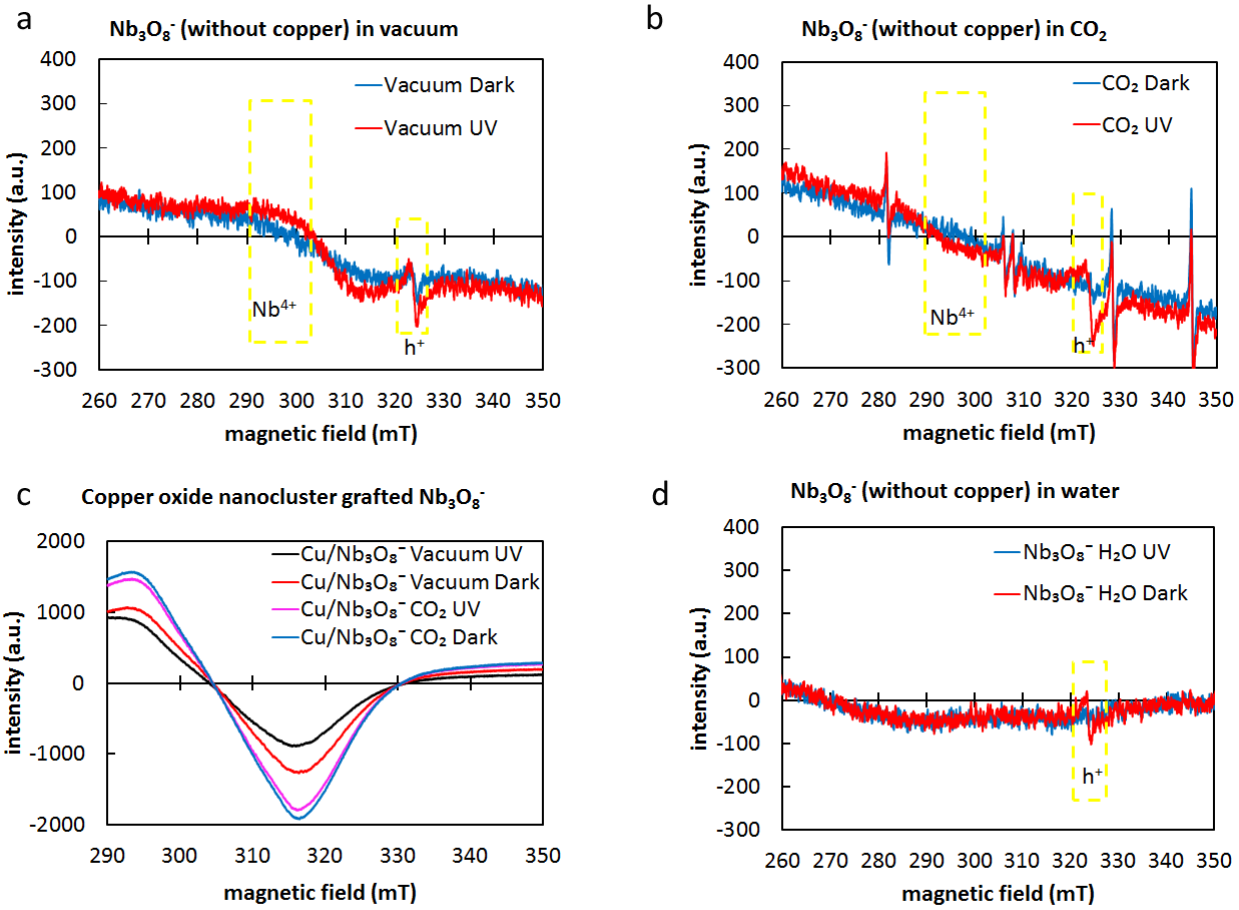

Figure 2.21 *ESR spectra of bare niobate nanosheets in vacuum (a), CO_2 (b) and in water (d). And the ESR spectrum of copper ion nanocluster-grafted niobate nanosheets in the gas phase (b).*

In addition to the ESR analysis under gaseous conditions, we measured difference ESR spectra before and after UV-light irradiation in pure water (Fig 2.21(d)). Under vacuum conditions, photogenerated holes were detected as O^- species around 325 mT, which were assigned to the excited holes in the valence band of the O-*2p* orbital. In CO_2 atmosphere, the intensity of the excited holes increased because the consumption of the photoelectrons kept the existence of holes more stable. However, the intensity of the excited holes decreased under aqueous conditions, suggesting that the photogenerated holes in the valence band of $Nb_3O_8^-$ nanosheets are able to oxidize water to produce oxygen molecules. These results are consistent with the results of the isotope tracing experiment. To examine the role of the Cu_xO nanoclusters, Fig 2.21(c) shows ESR difference spectra before and after UV-light irradiation of the Cu_xO nanoclusters-grafted $Nb_3O_8^-$ nanosheets. The *d*-orbital of Cu(II) species contains nine electrons; thus, a lone pair of electrons that contribute to ESR signal. In contrast, Cu(I) is inactive for ESR. After UV-light irradiation of the Cu(II)-grafted $Nb_3O_8^-$ nanosheet in a vacuum, the ESR signal of Cu(II) decreased, indicating that the excited electrons of the $Nb_3O_8^-$ nanosheet were

injected into the Cu_xO nanoclusters. Notably, however, the ESR signal kept stable, as the excited electrons in the Cu(II) nanoclusters were trapped by CO_2 molecules. The ESR analysis results strongly indicates that electrons are extracted from water molecules, excited by photon energy, and then injected into the Cu_xO nanoclusters, which are highly active sites for the production of CO molecules.

A proposed scheme of the photocatalytic process that occurs on the Cu_xO nanoclusters-grafted $Nb_3O_8^-$ nanosheet is shown in Figure 2.22 Under UV-light irradiation, electrons in the valence band of the $Nb_3O_8^-$ nanosheet are excited to the conduction band and then injected into the Cu_xO nanoclusters, as demonstrated by the ESR and XPS analyses, and the observed color change during the light irradiation. Photogenerated holes in the valence band of the $Nb_3O_8^-$ nanosheet then react with water to produce oxygen molecules, as was confirmed by the results of the isotope trace analysis. The injected electrons reduce CO_2 to produce CO in a chemical reaction that was confirmed by the ESR spectral and isotope CO generation analyses.

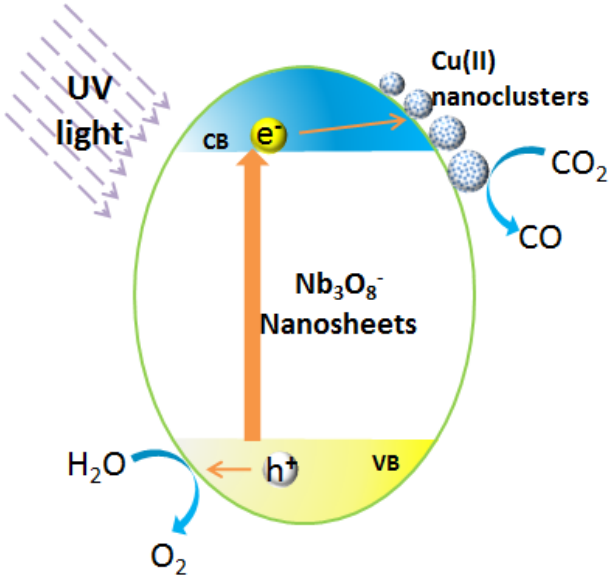

Figure 2.22 *Schematic electric structure of copper ion nanocluster-grafted niobate nanosheets*

2.5 Conclusion

Using an elemental strategy and electrochemical-based investigation, we identified that amorphous Cu_xO nanoclusters function as efficient co-catalysts for the electrocatalytic reduction of CO_2 to CO. Using a wet chemical method, we synthesized $Nb_3O_8^-$ nanosheets as a light harvesting material, which was found to have high conduction band potential because of the quantum confinement effect. The grafting of Cu_xO nanoclusters co-catalysts onto the

$Nb_3O_8^-$ nanosheets led to the efficient reduction of CO_2 molecules to CO under UV-light irradiation. Detailed ESR spectroscopic analysis and isotope labeling experiments demonstrated that electrons are extracted from water molecules and then excited by photon energy, which promotes their injection into Cu_xO nanoclusters, which are highly active sites for producing CO molecules.

This is the first work to demonstrate that Cu_xO nanoclusters act as efficient co-catalysts for the multi-electron reduction of CO_2, and it was published in *ACS Nano*. Notably, Cu_xO nanoclusters are composed of resource abundant and non-toxic elements, and can be easily deposited onto various metal oxide and/or metal chalcogenide light harvesters in mild aqueous media. Although the photocatalyst constructed here functions under UV-light irradiation, it is expected that the present approach for the grafting of co-catalysts onto semiconductors can be applied towards the generation of visible-light harvesting material.

References:

1. Baturina, O. A.; Lu, Q.; Padilla, M. A.; Xin, L.; Li, W.; Serov, A.; Artyushkova, K.; Atanassov, P.; Xu, F.; Epshteyn, A.; Brintlinger, T.; Schuette, M.; Collins, G. E., CO2 Electroreduction to Hydrocarbons on Carbon-Supported Cu Nanoparticles. ACS Catalysis **2014,** *4 (10), 3682-3695.*

2. Gattrell, M.; Gupta, N.; Co, A., A review of the aqueous electrochemical reduction of CO2 to hydrocarbons at copper. Journal of Electroanalytical Chemistry **2006,** *594 (1), 1-19.*

3. Graciani, J.; Mudiyanselage, K.; Xu, F.; Baber, A. E.; Evans, J.; Senanayake, S. D.; Stacchiola, D. J.; Liu, P.; Hrbek, J.; Sanz, J. F., Highly active copper-ceria and copper-ceria-titania catalysts for methanol synthesis from CO2. Science **2014,** *345 (6196), 546-550.*

4. Hinogami, R.; Yotsuhashi, S.; Deguchi, M.; Zenitani, Y.; Hashiba, H.; Yamada, Y., Electrochemical reduction of carbon dioxide using a copper rubeanate metal organic framework. ECS Electrochemistry Letters **2012,** *1 (4), H17-H19.*

5. Hirunsit, P.; Soodsawang, W.; Limtrakul, J., CO2 Electrochemical Reduction to Methane and Methanol on Copper-Based Alloys: Theoretical Insight. The Journal of Physical Chemistry C **2015,** *119 (15), 8238-8249.*

6. Kim, D.; Resasco, J.; Yu, Y.; Asiri, A. M.; Yang, P., Synergistic geometric and electronic effects for electrochemical reduction of carbon dioxide using gold–copper bimetallic nanoparticles. Nat Commun **2014,** *5.*

7. Lunkenbein, T.; Girgsdies, F.; Kandemir, T.; Thomas, N.; Behrens, M.; Schlögl, R.; Frei, E., Bridging the Time Gap: A Copper/Zinc Oxide/Aluminum Oxide Catalyst for Methanol Synthesis Studied under Industrially Relevant Conditions and Time Scales. Angewandte Chemie **2016,** *128 (41), 12900-12904.*

8. Neaţu, Ş.; Maciá-Agulló, J. A.; Concepción, P.; Garcia, H., Gold–Copper Nanoalloys Supported on TiO2 as Photocatalysts for CO2 Reduction by Water. Journal of the American Chemical Society **2014***.*

9. Marc, T., Electrochemical CO 2 reduction on Cu 2 O-derived copper nanoparticles: controlling the catalytic selectivity of hydrocarbons. Physical Chemistry Chemical Physics **2014,** *16 (24), 12194-12201.*

10. Nie, X.; Esopi, M. R.; Janik, M. J.; Asthagiri, A., Selectivity of CO2 Reduction on Copper Electrodes: The Role of the Kinetics of Elementary Steps. Angewandte Chemie International Edition **2013,** *52 (9), 2459-2462.*

11. Male, K. B.; Hrapovic, S.; Liu, Y.; Wang, D.; Luong, J. H. T., Electrochemical detection of carbohydrates using copper nanoparticles and carbon nanotubes. Analytica Chimica Acta **2004,** *516 (1–2), 35-41.*

12. Manthiram, K.; Beberwyck, B. J.; Alivisatos, A. P., Enhanced Electrochemical Methanation of Carbon Dioxide with a Dispersible Nanoscale Copper Catalyst. Journal

of the American Chemical Society **2014,** *136 (38), 13319-13325.*
13. Satoshi Kaneco, K. I. K. O. T. M., Electrochemical CO2 Reduction on a Copper Wire Electrode in Tetraethylammonium Perchlorate Methanol at Extremely Low Temperature. Energy Sources **1999,** *21 (7), 643-648.*
14. Schouten, K. J. P.; Pérez Gallent, E.; Koper, M. T. M., Structure Sensitivity of the Electrochemical Reduction of Carbon Monoxide on Copper Single Crystals. ACS Catalysis **2013,** *3 (6), 1292-1295.*
15. Schouten, K. J. P.; Pérez Gallent, E.; Koper, M. T. M., The influence of pH on the reduction of CO and to hydrocarbons on copper electrodes. Journal of Electroanalytical Chemistry **2014,** *716 (0), 53-57.*
16. Ba, X.; Yan, L.-L.; Huang, S.; Yu, J.; Xia, X.-J.; Yu, Y., New Way for CO2 Reduction under Visible Light by a Combination of a Cu Electrode and Semiconductor Thin Film: Cu2O Conduction Type and Morphology Effect. The Journal of Physical Chemistry C **2014,** *118 (42), 24467-24478.*
17. Calle-Vallejo, F.; Koper, M. T. M., Theoretical Considerations on the Electroreduction of CO to C2 Species on Cu(100) Electrodes. Angewandte Chemie International Edition **2013,** *52 (28), 7282-7285.*
18. Chang, X.; Wang, T.; Zhang, P.; Wei, Y.; Zhao, J.; Gong, J., Stable Aqueous Photoelectrochemical CO2 Reduction by a Cu2O Dark Cathode with Improved Selectivity for Carbonaceous Products. Angewandte Chemie **2016**.
19. Durand, W. J.; Peterson, A. A.; Studt, F.; Abild-Pedersen, F.; Nørskov, J. K., Structure effects on the energetics of the electrochemical reduction of CO2 by copper surfaces. Surface Science **2011,** *605 (15–16), 1354-1359.*
20. Li, C. W.; Kanan, M. W., CO2 reduction at low overpotential on Cu electrodes resulting from the reduction of thick Cu2O films. Journal of the American Chemical Society **2012,** *134 (17), 7231-7234.*
21. Copperthwaite, R. G.; Davies, P. R.; Morris, M. A.; Roberts, M. W.; Ryder, R. A., The reactive chemisorption of carbon dioxide at magnesium and copper surfaces at low temperature. Catal Lett **1988,** *1 (1-3), 11-19.*
22. Liu, M.; Qiu, X.; Hashimoto, K.; Miyauchi, M., Cu (II) nanocluster-grafted, Nb-doped TiO2 as an efficient visible-light-sensitive photocatalysts based on energy-level matching between surface and bulk states. Journal of Materials Chemistry A **2014,** *2, 13571-13579.*
23. Qiu, X.; Miyauchi, M.; Sunada, K.; Minoshima, M.; Liu, M.; Lu, Y.; Li, D.; Shimodaira, Y.; Hosogi, Y.; Kuroda, Y., Hybrid Cu x O/TiO2 Nanocomposites As Risk-Reduction Materials in Indoor Environments. ACS nano **2012,** *6 (2), 1609-1618.*
24. Qiu, X.; Miyauchi, M.; Yu, H.; Irie, H.; Hashimoto, K., Visible-Light-Driven Cu (II)−(Sr1− y Na y)(Ti1− x Mo x) O3 Photocatalysts Based on Conduction Band Control and Surface Ion Modification. Journal of the American Chemical Society **2010,** *132 (43), 15259-15267.*
25. Liu, M.; Inde, R.; Nishikawa, M.; Qiu, X.; Atarashi, D.; Sakai, E.; Nosaka, Y.; Hashimoto, K.; Miyauchi, M., Enhanced Photoactivity with Nanocluster-Grafted Titanium Dioxide Photocatalysts. ACS Nano **2014,** *8 (7), 7229-7238.*

26. Nosaka, Y.; Takahashi, S.; Mitani, Y.; Qiu, X.; Miyauchi, M., Reaction mechanism of visible-light responsive Cu(II)-grafted Mo-doped SrTiO3 photocatalyst studied by means of ESR spectroscopy and chemiluminescence photometry. Applied Catalysis B: Environmental **2012,** *111–112 (0), 636-640.*

27. Liu, M.; Qiu, X.; Miyauchi, M.; Hashimoto, K., Cu (II) oxide amorphous nanoclusters grafted Ti3+ self-doped TiO2: an efficient visible light photocatalyst. Chemistry of Materials **2011,** *23 (23), 5282-5286.*

28. Akatsuka, K.; Takanashi, G.; Ebina, Y.; Sakai, N.; Haga, M.-a.; Sasaki, T., Electrochemical and photoelectrochemical study on exfoliated Nb< sub> 3</sub> O< sub> 8</sub> nanosheet. Journal of Physics and Chemistry of Solids **2008,** *69 (5), 1288-1291.*

29. Katsumata, K.-i.; Okazaki, S.; Cordonier, C. E.; Shichi, T.; Sasaki, T.; Fujishima, A., Preparation and characterization of self-cleaning glass for vehicle with niobia nanosheets. ACS applied materials & interfaces **2010,** *2 (4), 1236-1241.*

30. Hori, Y., Electrochemical CO2 Reduction on Metal Electrodes. In Modern Aspects of Electrochemistry, Vayenas, C.; White, R.; Gamboa-Aldeco, M., Eds. Springer New York: 2008; Vol. 42, pp 89-189.

31. Hirakawa, T.; Kominami, H.; Ohtani, B.; Nosaka, Y., Mechanism of photocatalytic production of active oxygens on highly crystalline TiO2 particles by means of chemiluminescent probing and ESR spectroscopy. The Journal of Physical Chemistry B **2001,** *105 (29), 6993-6999.*

Chapter. 3

The development and evaluation of Cu-Zn alloy

3.1 Introduction

In *Chapter 2*, a Cu_xO nanocluster material was developed as an effective CO_2 reduction catalyst, by combining with light harvester, CO_2 was successfully converted into CO under UV irradiation. However, the activity and stability of Cu_xO nanocluster was questioned, also the selectivity of CO_2 reduction products is limited in CO. Thus, I decided to develop a better CO_2 reduction catalyst with not only high efficiency, but also high selectivity, activity and stability.

First the desired product was determined, The main products of CO_2 reduction in aqueous media are formic acid (HCOOH), carbon monoxide (CO), formaldehyde (HCHO), and methane (CH_4). Among the possible CO_2 reduction products, HCOOH is highly desirable as it is widely used in the energy and chemical industries as a fuel and as a raw material for H_2 generation.[1] HCOOH is also important for the production of various organic agents through thermal treatments or catalytic reactions,[2] and can be used in agricultural and animal husbandry as a silage additive.[3] At the industrial scale, HCOOH is mainly produced from methyl formate, which is synthesised from CH_3OH and CO in the presence of a strong salt base. However, this method requires a large excess of water and the disposal of accumulated by-products. [4] As the market for formic acid is estimated to exceed $600 million by 2019,[5] it is highly desirable to develop clean and renewable HCOOH production processes based on CO_2 conversion with solar-, wind- and/or hydropower.

As introduced in *Chapter 1*, in previous studies, Ru, Re and their complex catalysts were used for selective CO_2 reduction to HCOOH.[2, 6] Although high efficiency (Faradic efficiency over 70%) was achieved, the Ru-complex was precluded from broad use due to its high cost and complicated synthesis. To achieve low-cost and easy preparation, numerous types of metals and alloys were proposed as CO_2-reduction catalysts, such as Zn, Cu, Ag, Au, Cu-Au, etc. These materials can catalyse CO_2 reduction owing to their *d*-electron availability[7] and appropriate surface CO_2 adsorption strengths[8]. However, only a few metals can achieve selective CO_2 to HCOOH conversion with low efficiency and high overpotential. It is known that different CO_2 reduction products are generated via different pathways depending on the balance of the adsorption strengths of reduction intermediates (CO_2^* anion radicals and CO^* radicals) on the catalyst surface. [9-19] While, a lot of researches have proved that combining two different kind of metal into alloy can change the electronic properties and geometric effect.[18] Thus we predicted that the selective conversion of CO_2 to HCOOH can be realized by tuning the surface adsorption conditions of the active reaction intermediates on the catalyst surface through

rational alloying of elemental metals with different adsorption abilities.

As we can see from a figure showing the distribution of various metals showing different products selectivity and their surface adsorption strength for CO radicals, [16] Zn located very near with the HCOOH generation area. And according to the previous electrocatalytic evaluation, Zn does behave good selectivity for HCOOH generation. Because Zn has weak adsorption strength for CO_2^* which is ideal for selective HCOOH generation, but it also leads to that water splitting will competes with CO_2 reduction in the aqueous electrolyte. By combining with other kinds of metals at atomic scale, the surface adsorption strength can be changed. And obviously to get appropriate surface adsorption strength for HCOOH generation, Zn has to be combined with metals in the other side. So, we choose Ni, Cu, Au and Ag to prepare alloy with Zn and evaluate the catalytic property for CO_2 reduction

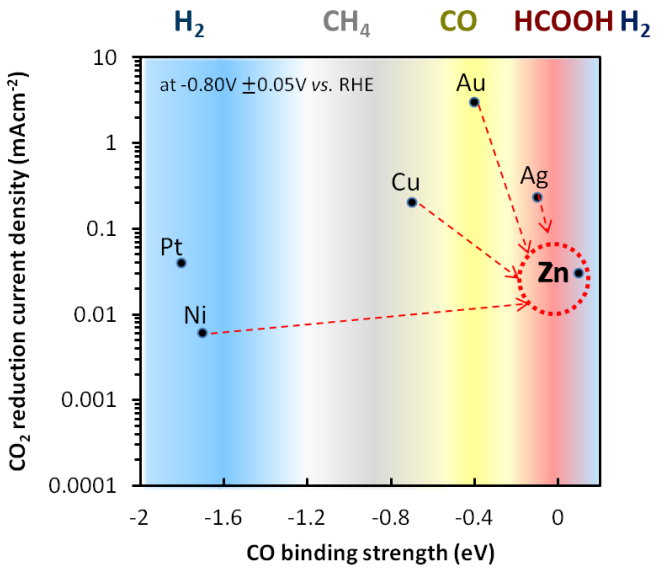

Figure 3.1 *the distribution of various metals of their selectivity and their surface binding strength for CO radicals.*

According to electrochemical screening, Cu-Zn alloy was proved to be active for CO_2 reduction. Other kinds of alloy such as Zn-Au, Zn-Ag, Zn-Ni were also prepared and evaluated. The studies of these alloys were recorded in ***Appendix.1***, also Sn-Cu, Sn-Au, Sn-Ni and Sn-Ag were also evaluated based on same idea.

Cu-Zn alloy are abundant and safe materials thus was also called "poorman's gold", with several desirable catalytic properties. For example, in a Cu/ZnO catalyst, Cu-Zn alloy provides active sites for the hydrogenation of CO_2 from $CO/CO_2/H_2$ gas.[20-22] A Cu/ZnO material was also reported to function as a CO_2 hydrogenation catalyst under high-temperature conditions.[23] A Cu-Zn alloy electrode prepared by an electroplating method on a gold substrate using metal cyanides was proved to be able to catalyze CO_2 reduction into CO and HCOOH by electrochemical way. [24] In the present research, a Cu-Zn alloy prepared by simple synthesis

method behaving high performance for CO_2 reduction under moderate conditions such as room temperature and low bias-potential will be developed.

3.2 Experimental procedures

3.2.1 Preparation of Cu-Zn film electrodes

Titanium (Ti) metal sheets (99.5%, Nilaco Co.) were used as the substrate to fabricate electrodes. Pure Cu films with a thickness of 50 nm were sputtered onto the surface of the Ti sheets. These Cu-coated Ti sheets served as pure Cu electrodes in the control group. The prepared Cu-coated Ti sheets were placed in vacuum-sealed quartz ampoules with pure zinc (Zn) metal grains, as shown in Figure 3.2.

Figure 3.2 *the picture of the sealed glass tube with Zn metal grains and annealed Cu-Zn film inside.*

The vacuum-sealed ampoules were then heated in an electric oven to temperatures higher than the melting point of Zn (> 419 °C at ambient pressure) such that the Cu-coated Ti sheets were annealed in Zn vapour for 1 h to yield the Cu-Zn film electrodes. The Zn concentration of the Cu-Zn film electrode was controlled by tuning the Zn vapour pressure, which was dependent on the heating temperature. In the present research, four kinds of Cu-Zn electrodes were prepared under annealing temperature of 400°C ,450°C, 500°C and 520°C, respectively.

3.2.2 Electrochemical screening

The prepared Cu-Zn film electrodes, pure Pt plates, and Ag/AgCl electrodes were used as working, counter, and reference electrodes, respectively. Air-tight electrochemical cells were half filled with a 0.1 M aqueous solution of $KHCO_3$. The Cu-Zn film electrodes were cleaned

by 10 cycles of repeated cyclic voltammetry in the electrolyte solution: starting bias (E_0)= -0.9 V, 1st operating bias (E_1) = -1.8 V, and 2nd operating bias (E_2)= -0.1 V, with slope 90 mV/sec. Either CO_2 or Ar gas was purged into this electrolyte solution prior to the performance test.

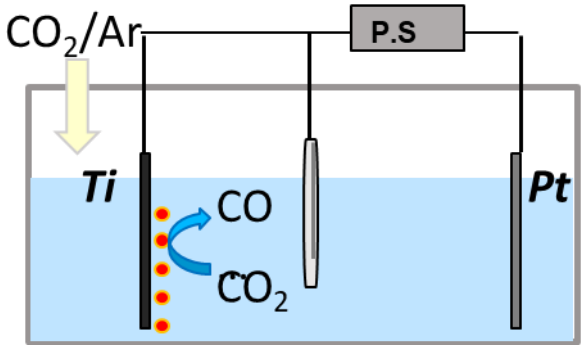

Figure 3.3 *the construction of the electrochemical cell used for electrochemical screening.*

3.2.3 Photoelectrochemical CO_2-reduction performance tests

A H-type glass cell was used for the photoelectrochemical CO_2 reduction over the Cu-Zn film electrodes. The Cu-Zn film electrodes were used as the cathode, while the prepared mesoporous $SrTiO_3$ electrodes were used as the photoanode Figure 3.4. The cathodic- and anodic sides of the glass cell were separated by a Nafion membrane. The electrolyte on the cathodic side was a CO_2-purged 0.1 M $KHCO_3$ solution and that on the anodic side was a 0.01 M NaOH solution containing 0.1 M KCl. During the performance tests, the anodic side was irradiated with UV light (Hg-Xe lamp (240-300nm), LA-410UV, Hayashi Ltd.), illuminance spectra shown below. The gaseous products in the headspace such as CH_4, CO, and H_2 were quantified with a gas chromatograph (BID, SHIMADZU). The liquid products in the electrolyte solution such as HCOOH were quantified with an Ion chromatograph (SHIMADZU).

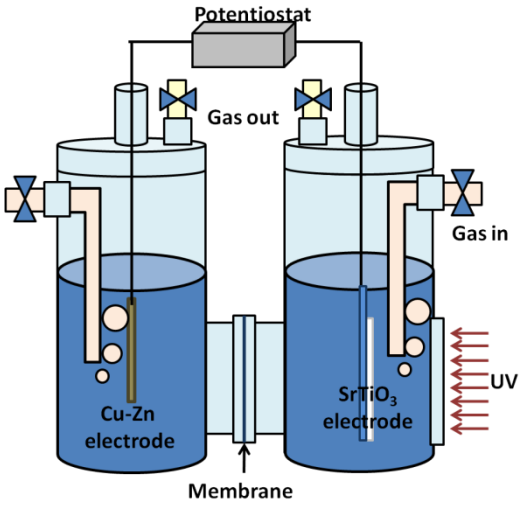

Figure 3.4. *The Photoelectrochemical (PEC) cell construction.*

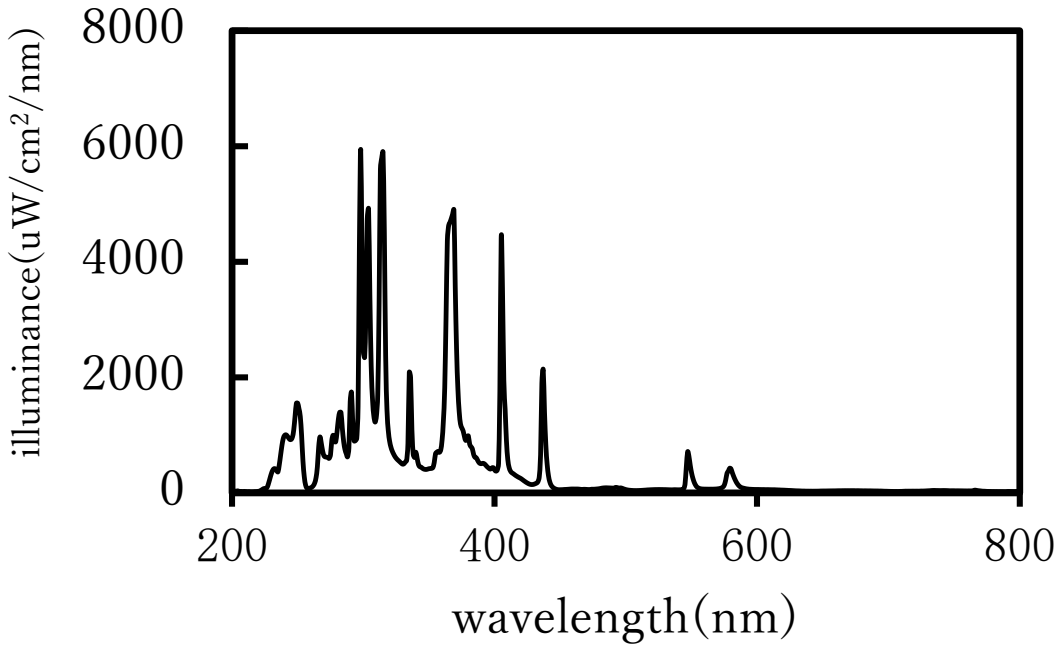

Figure 3.5*The light spectrum of the UV light used in the PEC cell and photocatalytic evaluation.*

Preparation of $SrTiO_3$ photoanodes. $SrTiO_3$ paste was prepared from commercial $SrTiO_3$ powder (ALDRICH, nanopowder, < 100 nm particle size, > 99.5% trace metal basis). Mesoporous $SrTiO_3$ films 8 μm thick were prepared on FTO glass substrates by screen-printing the $SrTiO_3$ paste over the surface, which were further annealed at 450 ˚C for 1 h to yield mesoporous $SrTiO_3$ electrodes. Exposed surface of the FTO substrate was covered with heat-resistant insulating tapes for an electrochemical measurement. The picture of the prepared $SrTiO_3$ electrode was shown below.

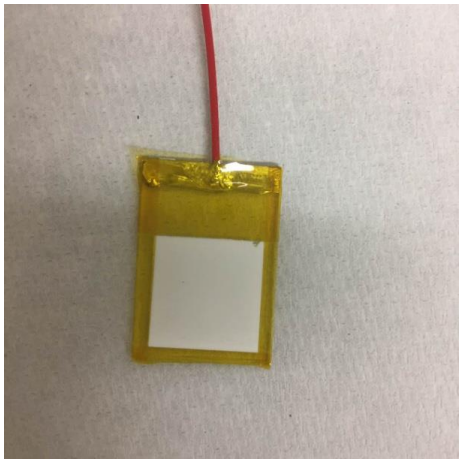

Figure 3.6 *the picture of the prepared $SrTiO_3$ electrode*

3.3 Results and Discussion

3.3.1 Characterization

In this research, several kinds of Cu-Zn electrodes with different element composition were prepared and evaluated, turns out that the electrode exhibit best catalytic properties when the Cu-Zn electrode was prepared under 500°C, with Cu:Zn molar ratio of 5:8. This part will be introduced in 3.3.2 in details, which in this session, the characterization of Cu_5Zn_8 will only be introduced.

The prepared Cu-Zn electrode was mainly analyzed by XPS, XRF and XRD. As seen in Table 3.1, the Zn concentration under 500 ˚C annealing was about 52.19 mass%. The hard X-ray photoelectron spectroscopy (HAXPES; $h\nu$ = 5.95 keV) was analyzed at the undulator beamline BL15XU[52] of SPring-8,[25] as shown in Figure 3.6, The Cu 2*p* and Zn 2*p* peak positions for the Cu-Zn film electrode (Cu:Zn=5:8,) were different from those for pure Cu and Zn metals, indicating that the Cu-Zn film was neither pure Cu nor Zn, but an alloy of Cu and Zn. And in the XRD pattern in Figure 3.7, The reflection peaks at 35.97, 37.89, 43.23, and 62.96° correspond to the (222), (321), (330), and (600) reflections of the atomically ordered Cu_5Zn_8 alloy (cubic),[24, 26] which is consistent with the XRF results. The crystallic structure of Cu_5Zn_8 alloy and the picture of the prepared Cu_5Zn_8 electrode were shown in Figure 3.8.

Table 3.1 *The XRF results (mass%) of the composition analysis of Cu-Zn alloy electrodes prepared under different heating temperature.*

Heating temperature (˚C)	Cu	Zn	Ti
400	97.32	2.68	-
450	76.73	23.27	-
500	47.81	52.19	-
520*	0.86	4.21	94.9-

*The sample under 520˚C was measured at different time with others. In this case Ti composition was also measured. The Zn concentration used in Fig 2d was calculated as 4.21/(4.21+0.86)*100%=83.04%.

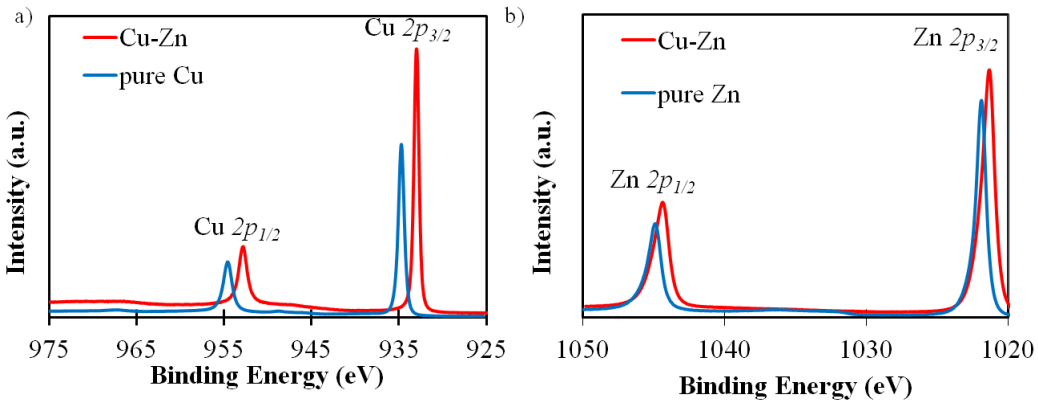

Figure 3.6*The HAXPES spectra of a) Cu 2p and b) Zn 2p core-levels in the Cu-Zn electrode, those of pure Cu and pure Zn were also shown as control groups.*

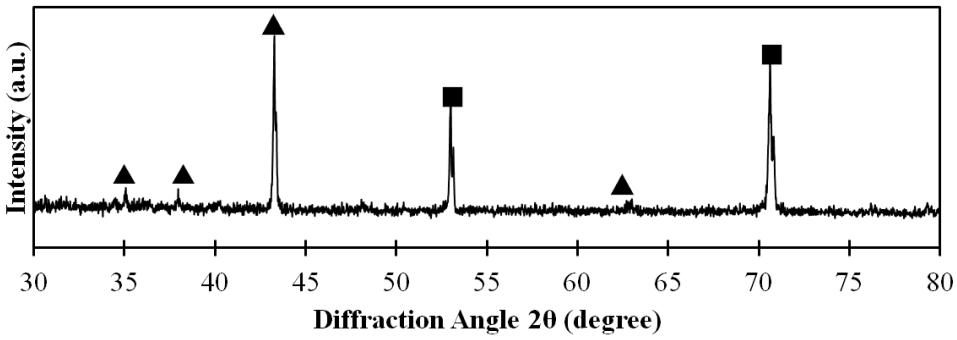

Figure 3.7 *The XRD pattern of the Cu-Zn electrode, Ti metal was used as substrate, ▲, Cu_5Zn_8 (cubic); ■, pure Ti*

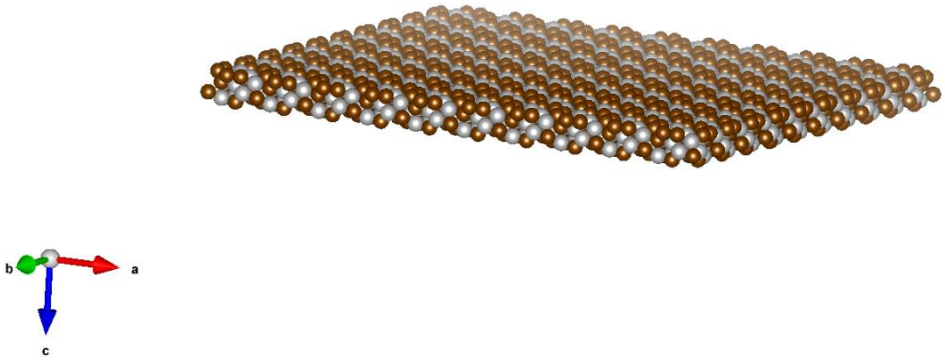

Figure 3.8 *the crystal structure of the Cu_5Zn_8 alloy, simulated.*

3.3.2 Electrochemical evaluation.

The electrocatalytic properties of the prepared Cu-Zn electrodes for CO_2 reduction was evaluated by the Linear sweep voltammetry (LSV) curves under CO_2 and Ar purging. The onset potential of four kinds of Cu-Zn electrode and pure Cu, pure Zn electrodes were compared. As described in the experimental procedures 3.2.1, the atomic ratio of Cu-Zn in the alloys was controlled by varying the annealing temperature under vacuum. Specifically, with increasing heating temperature, the Zn concentration in the Cu-Zn electrode also increased. Figure 3.9 shows the influence of the Zn concentration in the Cu-Zn alloy electrode on the onset potential for CO_2 reduction. The onset potential was lowest, −0.65 V *vs.* Ag/AgCl, at a Zn concentration of ~60 atom%. This onset potential was markedly lower than those of pure Cu (-1.0 V *vs.* Ag/AgCl) and Zn (−1.2 V *vs.* Ag/AgCl). This Zn concentration of ~60% was consistent with the crystal structure (Cu_5Zn_8) determined by XRD.

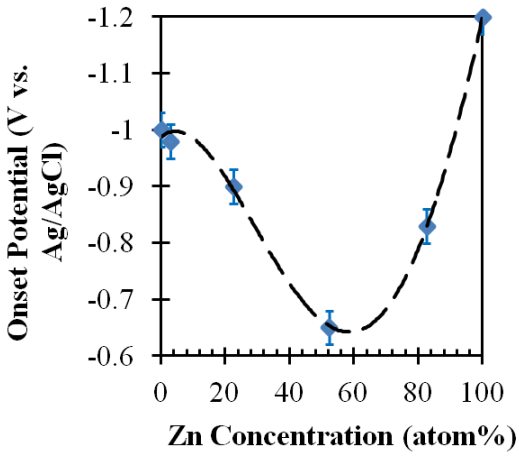

Figure 3.9 *The onset potential for CO_2 reduction at the Cu-Zn electrode as a function of Zn atomic ratio.*

Also, as shown in Figure 3.10, compared to pure Cu and pure Zn, the current density under CO_2 was higher than that of Ar, indicating that Cu_5Zn_8 electrode exhibit good CO_2 reduction electrocatalytic property in the electrochemical sight.

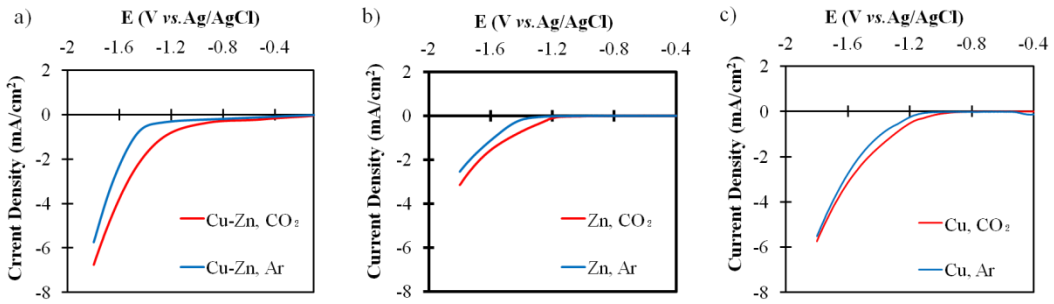

Figure 3.10 *Linear sweep voltammetry (LSV) curves of a) Cu_5Zn_8 alloy electrode, b) pure Cu, and c) pure Zn.*

The reaction products generated by the Cu_5Zn_8 electrode, pure Cu electrode, and pure Zn electrode under different bias potentials are also shown in Figure 3.11, Notably, the scales of the vertical axis for the Cu_5Zn_8 electrode and pure Zn electrode are about 10 times larger than that for the pure Cu electrode. The amount of HCOOH generated at the Cu_5Zn_8 alloy electrode was markedly higher than that produced at the pure Cu electrode (< 0.03 μmol), which generated CH_4 and CO as the main reaction products. The Cu_5Zn_8 alloy electrode also generated more HCOOH than the pure Zn electrode (< 1 μmol). Specifically, under −1.0 V vs. Ag/AgCl, the selectivity of the Cu_5Zn_8 alloy for HCOOH generation was obviously better than pure Cu or pure Zn, as shown in Fig. 3.11d. It is noted that the Faradaic efficiency of the Cu_5Zn_8 alloy for HCOOH generation was 71.11% at a bias application of −1.0 V vs. Ag/AgCl. The CO_2 to HCOOH conversion efficiency of the Cu_5Zn_8 alloy catalyst was higher than that of the previously reported Cu-Zn alloy electrocatalysts.[24]

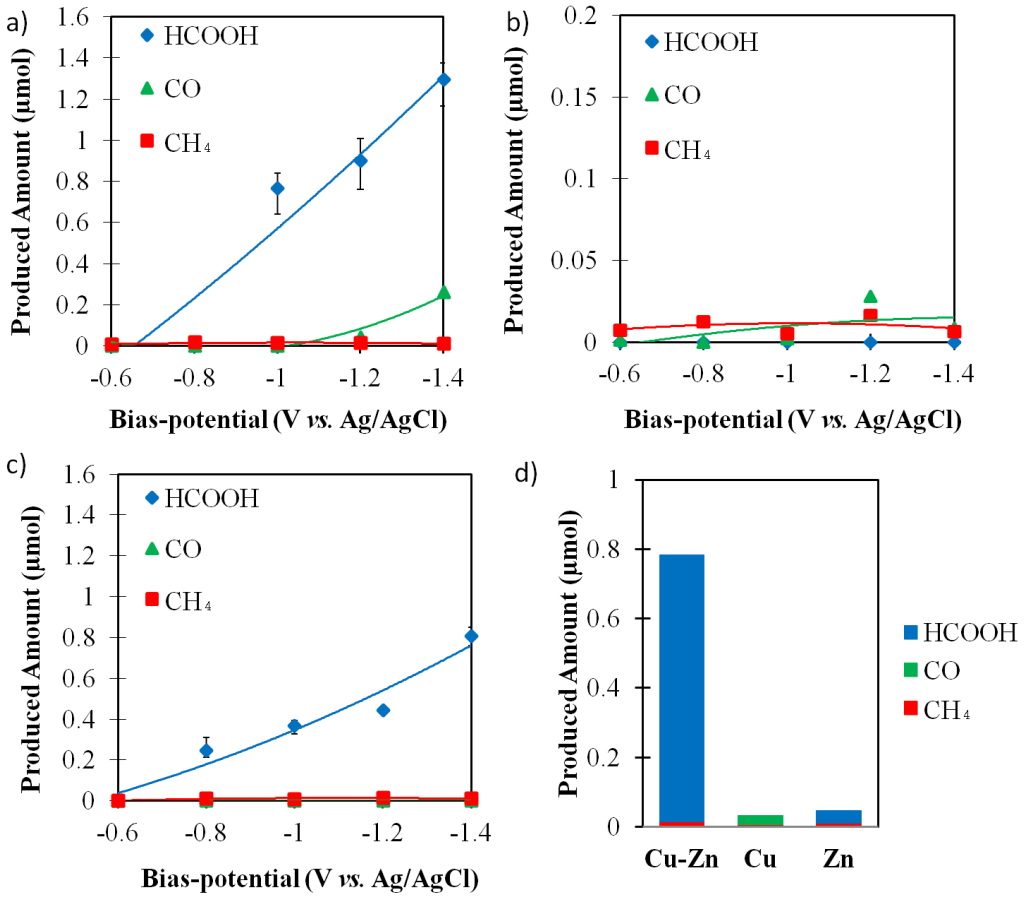

Figure 3.11 *Products generated by a) Cu_5Zn_8 electrode, b) pure Cu electrode, and c) pure Zn electrode in electrochemical cells under different applied bias potentials for 1 h. Bias potentials were applied from -0.6 to -1.4 V vs. Ag/AgCl. d) The CO_2 reduction product distribution generated at Cu_5Zn_8 electrode, pure Cu electrode, and pure Zn electrode under -1.0 V vs. Ag/AgCl.*

The Cu_xO nanoclusters developed in ***Chapter.2*** was also evaluated to compare with Cu-Zn

electrode, using the same method with above, Figure 3.12 shows that Cu-Zn clearly behaved higher selectivity for HCOOH generation than Cu_xO nanocluster, which also generated CO as second main product. Also, since the Cu-Zn alloy was often compared with pure Au, the products from the pure Au electrode were also evaluated, the results shows that the main product for Au was CO.

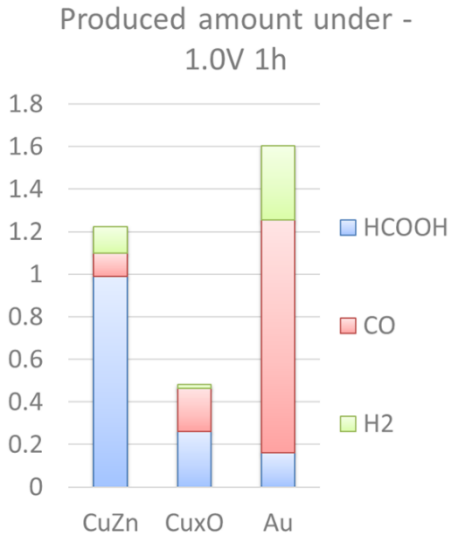

Figure 3.12 *The produced amount from Cu-Zn electrode and Cu_xO nanocluster electrode, hold under -1.2V vs. Ag/AgCl for 10mins.*

3.3.2 Photoelectrochemical evaluation.

The photoelectrochemical evaluation was operated in a H-type glass cell. The Cu-Zn alloy film served as the cathode for CO_2 reduction and a $SrTiO_3$ (STO) film was used as a photo-anode for oxygen production from water. When the STO photoanode was irradiated by UV light, water was oxidized at the anodic side by the photogenerated holes in the valence band of STO, whereas the excited electrons were transferred to the cathodic Cu-Zn film used for CO_2 reduction. The reaction products generated at the cathodic side without any bias application are shown in Figure 3.13. As control experiments, Ar gas was purged into the cathodic side of the PEC. The amount of HCOOH, CO and CH_4 produced under CO_2 purging was markedly higher than that under Ar purging, indicating that CO_2 was reduced by the Cu-Zn electrode.

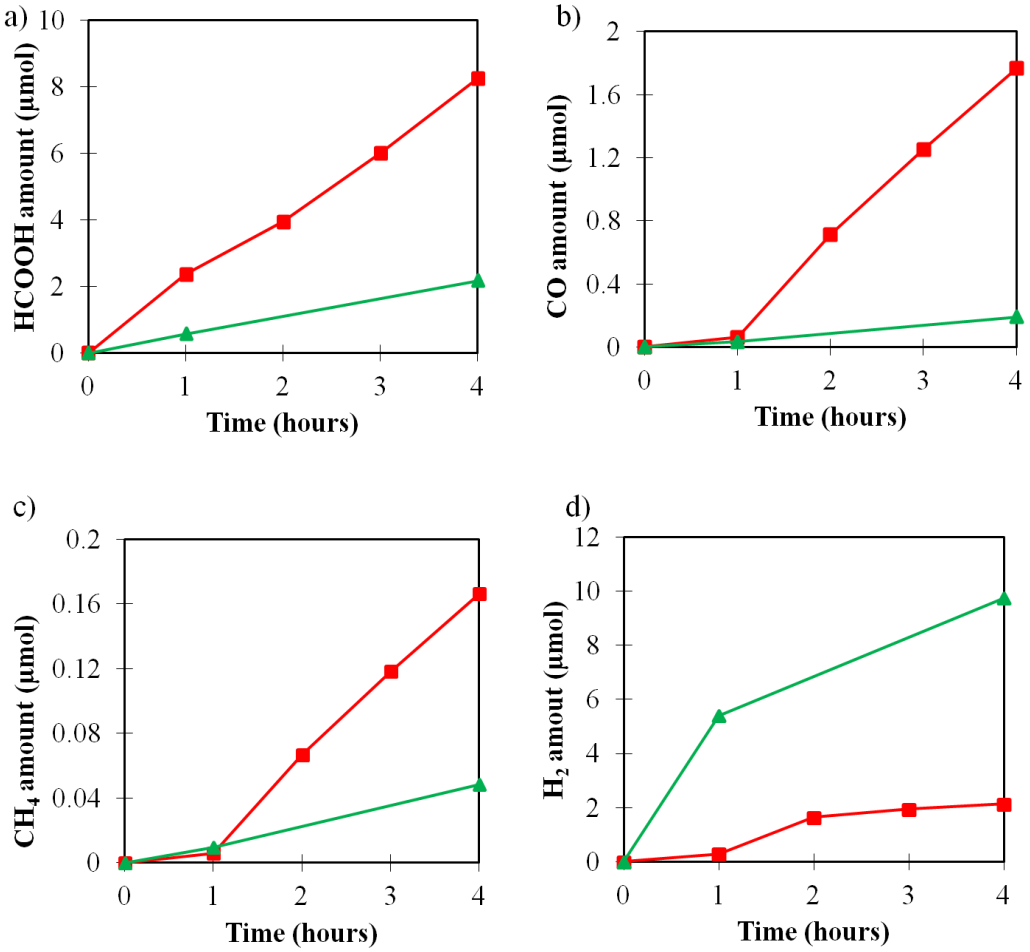

***Figure 3.13**. The produced amounts of Cu-Zn electrode from the PEC cell at rest potential. under CO_2 purging (■), under Ar purging (▲). a) HCOOH, b) CO, c) CH_4, d) H_2.*

Pure Cu and pure Zn were also evaluated as cathodes as control groups, as shown in Figure 3.14, the amount of CO_2 reduction products generated by the Cu-Zn electrode was 2 times higher than those of the pure Cu or Zn electrodes, as was observed in the electrochemical CO_2 reduction experiments. We also calculated the ratio of electrons used for CO_2 reduction product generation verses the total number of electrons used for all products, φ, and found that φ(Cu-Zn) was 75.43%, which markedly higher than φ(Cu) or φ(Zn), which were only 42.26% or 32.66%, respectively. Although the pure Cu film reduced CO_2, HCOOH was not selectively generated. For the pure Zn film, hydrogen was mainly produced through water splitting and only limited CO_2 reduction activity was observed. In contrast, the Cu-Zn electrode exhibited high selectivity for both CO_2 reduction and HCOOH generation. The Faradaic efficiency of HCOOH production was as high as 79.72%. The Cu-Zn electrode also had excellent stability, with the turnover number (TON) for CO_2 reduction reaching 1458.9, which was twice of that of pure Cu (731.3). The quantum efficiency of the photoelectrochemical CO_2 reduction by the

Cu-Zn electrode was 0.13%.

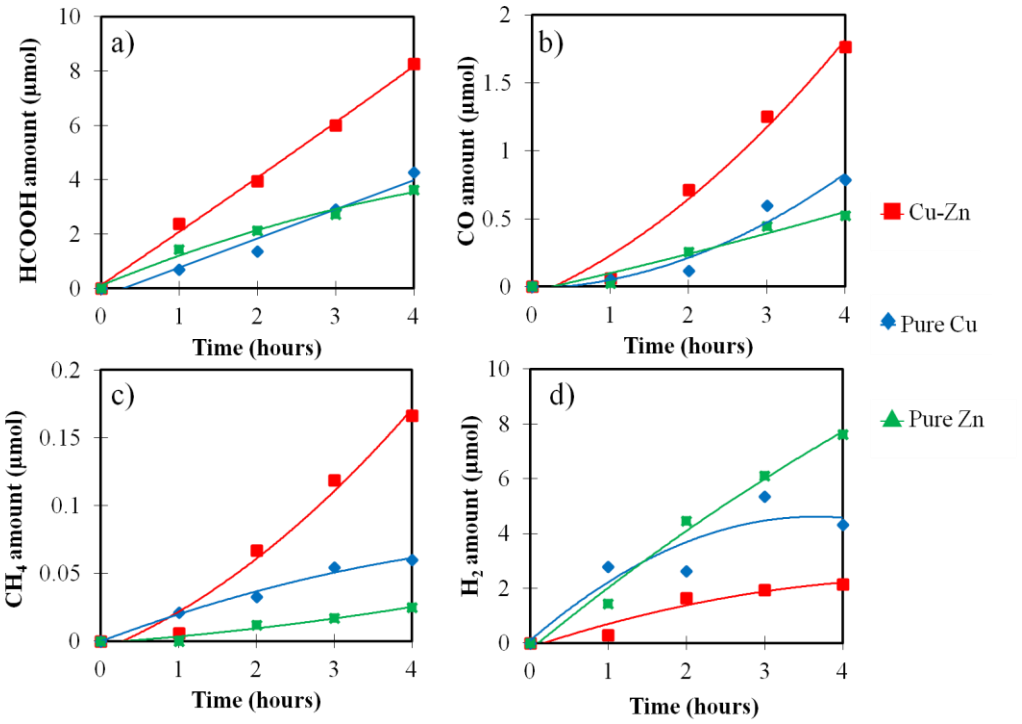

***Figure 3.14**. Amount of a) HCOOH, b) CO, c) CH_4, and d) H_2 produced by a PEC cell equipped with a Cu-Zn electrode as the cathode and CO_2-purged 0.1 M $KHCO_3$ as the electrolyte. PEC cells equipped with a pure Cu cathode and a pure Zn cathode in CO_2-purged 0.1 M $KHCO_3$ as the electrolyte were used as controls.*

3.4 Conclusion

The Cu-Zn alloy catalyst developed in the present research was prepared from abundant and environmental-friendly materials, and exhibited a high conversion efficiency for the reduction of CO_2 into organic molecules, particularly HCOOH. The Faradaic efficiency of converting CO_2 into HCOOH was above 70%, demonstrating that the catalyst has high selectivity for HCOOH generation.

The Cu-Zn alloy catalyst can be used as an electrode for electrochemical CO_2 reduction, or combined with a photoanode for photoelectrochemical reactions. By combining with $SrTiO_3$ electrode in a photoelectrochmical cell as working electrode, the Cu-Zn alloy electrode catalyzed CO_2 into HCOOH with Faradic efficiency above 79.72% under UV irradiation, without applied bias-potential. Also, the TON of the Cu-Zn alloy for CO_2 reduction reached 1458, proving its high stability.

The ability to selectivity regulate CO_2 reduction using the Cu-Zn alloy catalyst described

here may prompt the development of new types of alloy catalysts with high selectivity for CO_2 reduction.

References

1. Johnson, T. C.; Morris, D. J.; Wills, M., Hydrogen generation from formic acid and alcohols using homogeneous catalysts. Chemical Society Reviews **2010,** 39 (1), 81-88.
2. Sato, S.; Morikawa, T.; Saeki, S.; Kajino, T.; Motohiro, T., Visible - Light - Induced Selective CO2 Reduction Utilizing a Ruthenium Complex Electrocatalyst Linked to ap - Type Nitrogen - Doped Ta2O5 Semiconductor. Angewandte Chemie International Edition **2010,** 49 (30), 5101-5105.
3. Baytok, E.; AKSU, T.; KARSLI, M. A.; MURUZ, H., The effects of formic acid, molasses and inoculant as silage additives on corn silage composition and ruminal fermentation characteristics in sheep. Turkish Journal of Veterinary and Animal Sciences **2005,** 29 (2), 469-474.
4. Reutemann, W.; Kieczka, H., Formic Acid. In Ullmann's Encyclopedia of Industrial Chemistry, Wiley-VCH Verlag GmbH & Co. KGaA: 2000.
5. N.p., M. c. Formic Acid Market Worth $618,808.7 Thousand By 2019. http://www.marketsandmarkets.com/PressReleases/formic-acid.asp (accessed 9th Aug).
6. Sato, S.; Arai, T.; Morikawa, T.; Uemura, K.; Suzuki, T. M.; Tanaka, H.; Kajino, T., Selective CO2 conversion to formate conjugated with H2O oxidation utilizing semiconductor/complex hybrid photocatalysts. Journal of the American Chemical Society **2011,** 133 (39), 15240-15243.
7. Hori, Y., Electrochemical CO2 Reduction on Metal Electrodes. In Modern Aspects of Electrochemistry, Vayenas, C.; White, R.; Gamboa-Aldeco, M., Eds. Springer New York: 2008; Vol. 42, pp 89-189.
8. Toyoshima, I.; Somorjai, G., Heats of chemisorption of O2, H2, CO, CO2, and N2 on polycrystalline and single crystal transition metal surfaces. Catalysis Reviews Science and Engineering **1979,** 19 (1), 105-159.
9. Norskov, J. K.; Bligaard, T.; Rossmeisl, J.; Christensen, C. H., Towards the computational design of solid catalysts. Nat Chem **2009,** 1 (1), 37-46.
10. Peterson, A. A.; Abild-Pedersen, F.; Studt, F.; Rossmeisl, J.; Norskov, J. K., How copper catalyzes the electroreduction of carbon dioxide into hydrocarbon fuels. Energy & Environmental Science **2010,** 3 (9), 1311-1315.
11. Hansen, H. A.; Varley, J. B.; Peterson, A. A.; Nørskov, J. K., Understanding trends in the electrocatalytic activity of metals and enzymes for CO2 reduction to CO. The journal of physical chemistry letters **2013,** 4 (3), 388-392.
12. Kortlever, R.; Shen, J.; Schouten, K. J. P.; Calle-Vallejo, F.; Koper, M. T., Catalysts and reaction pathways for the electrochemical reduction of carbon dioxide. The journal of physical chemistry letters **2015,** 6 (20), 4073-4082.
13. Schouten, K. J. P.; Pérez Gallent, E.; Koper, M. T. M., Structure Sensitivity of the Electrochemical Reduction of Carbon Monoxide on Copper Single Crystals. ACS Catalysis **2013,** 3 (6), 1292-1295.

14. Schouten, K. J. P.; Qin, Z.; Gallent, E. P.; Koper, M. T. M., Two Pathways for the Formation of Ethylene in CO Reduction on Single-Crystal Copper Electrodes. Journal of the American Chemical Society **2012,** *134 (24), 9864-9867.*

15. Rodriguez, J. A.; Liu, P.; Stacchiola, D. J.; Senanayake, S. D.; White, M. G.; Chen, J. G., Hydrogenation of CO2 to methanol: Importance of metal–oxide and metal–carbide interfaces in the activation of CO2. ACS Catalysis **2015,** *5 (11), 6696-6706.*

16. Kuhl, K. P.; Hatsukade, T.; Cave, E. R.; Abram, D. N.; Kibsgaard, J.; Jaramillo, T. F., Electrocatalytic Conversion of Carbon Dioxide to Methane and Methanol on Transition Metal Surfaces. Journal of the American Chemical Society **2014**.

17. Chaplin, R. P. S.; Wragg, A. A., Effects of process conditions and electrode material on reaction pathways for carbon dioxide electroreduction with particular reference to formate formation. Journal of Applied Electrochemistry **2003,** *33 (12), 1107-1123.*

18. Karamad, M.; Tripkovic, V.; Rossmeisl, J., Intermetallic Alloys as CO Electroreduction Catalysts—Role of Isolated Active Sites. ACS Catalysis **2014,** *4 (7), 2268-2273.*

19. Hirunsit, P.; Soodsawang, W.; Limtrakul, J., CO2 Electrochemical Reduction to Methane and Methanol on Copper-Based Alloys: Theoretical Insight. The Journal of Physical Chemistry C **2015,** *119 (15), 8238-8249.*

20. Nakamura, J.; Uchijima, T.; Kanai, Y.; Fujitani, T., The role of ZnO in Cu/ZnO methanol synthesis catalysts. Catalysis today **1996,** *28 (3), 223-230.*

21. Nakamura, J.; Choi, Y.; Fujitani, T., On the Issue of the Active Site and the Role of ZnO in Cu/ZnO Methanol Synthesis Catalysts. Topics in Catalysis **2003,** *22 (3), 277-285.*

22. Chu, S.; Fan, S.; Wang, Y.; Rossouw, D.; Wang, Y.; Botton, G. A.; Mi, Z., Tunable Syngas Production from CO2 and H2O in an Aqueous Photoelectrochemical Cell. Angewandte Chemie International Edition **2016,** *55 (46), 14262-14266.*

23. Guan, G.; Kida, T.; Harada, T.; Isayama, M.; Yoshida, A., Photoreduction of carbon dioxide with water over K 2Ti 6O 13 photocatalyst combined with Cu/ZnO catalyst under concentrated sunlight. Applied catalysis. A, General **2003,** *249 (1), 11-18.*

24. Katoh, A.; Uchida, H.; Shibata, M.; Watanabe, M., Design of Electrocatalyst for CO 2 Reduction V. Effect of the Microcrystalline Structures of Cu - Sn and Cu - Zn Alloys on the Electrocatalysis of Reduction. Journal of the Electrochemical Society **1994,** *141 (8), 2054-2058.*

25. Ueda, S., Application of hard X-ray photoelectron spectroscopy to electronic structure measurements for various functional materials. Journal of Electron Spectroscopy and Related Phenomena **2013,** *190, Part B, 235-241.*

26. Zhou, W.; Liu, L.; Wu, P., Structural, electronic and thermo-elastic properties of Cu6Sn5 and Cu5Zn8 intermetallic compounds: First-principles investigation. Intermetallics **2010,** *18 (5), 922-928.*

Chapter 4

The reaction mechanism analyses

Although in chapter 3, we successfully developed a Cu-Zn alloy material behaving high selectivity for HCOOH generation from CO2 reduction, the reason of its high selectivity was still unclear. Thus, in this chapter, I tried to analyze the reaction mechanism on the Cu-Zn surface and explain the high selectivity based on literature studies and in-situ FTIR analyses.

4.1 The literature studies about the selectivity of CO_2 reduction on the catalyst surface.

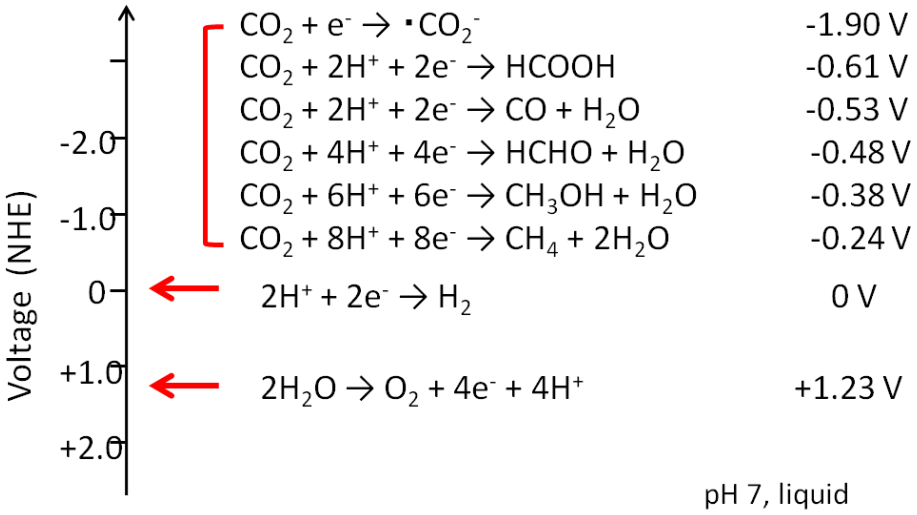

Figure 4.1 *The reactions of CO_2 reduction.*

As we can see from Figure 4.1, in hydrous condition, H_2 generation needs lower reduction potential and less electrons than CO_2 reduction. During the reaction, H^+ and CO_2^* simultaneously approach near to the catalyst surface, when the co-catalyst surface behaves strong H^+ adsorption and poor CO_2 adsorption, then the H_2 generation will take precedence of CO_2 reduction.[1] For example, Figure 4.2 shows the volcano's plots of electrocatalytic water splitting, demonstrating the relationship between the current density for H_2 generation and the surface adsorption strength of H^+.

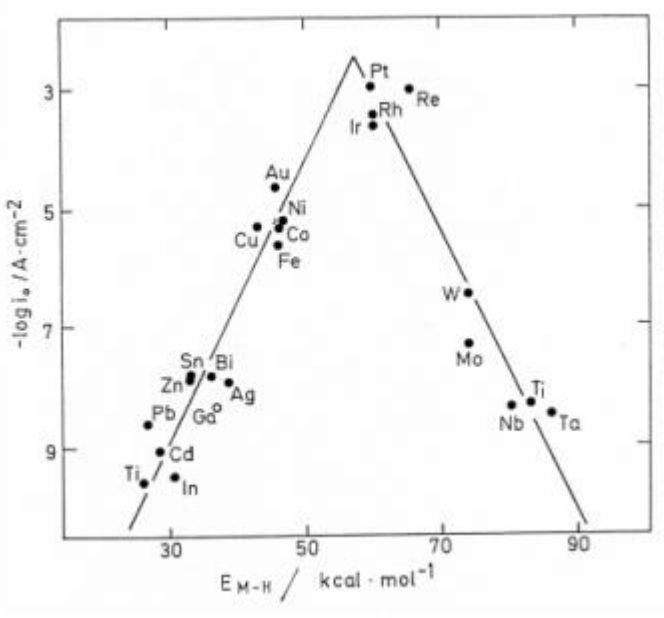

Figure 4.2 *The logarithm of exchange current density (log io) for cathodic hydrogen evolution versus the bonding adsorption strength (ΔEM-H) of intermediate metal-hydrogen (M-H) bond formed during the electrode reaction itself.* [2]

As we can see, compared to Cu, Au, Zn and Ag, Pt has stronger surface adsorption for H^+, thus, the current density of H_2 generation is higher, which indicating H_2 generation has the highest priority than all the CO_2 reductions on the surface of Pt.

On the other side, metals such as Fe and Ti, they behave lower CO_2 adsorption strength than Cu, Au, Zn and Ag, thus compared to CO_2 reduction, H_2 generation will also be the main reaction on their surfaces.

As for the selectivity between different kinds of CO_2 reduction products, lots of researchers had inferred the mechanism based on the theoretical calculation, especially the density functional theory (DFT) and actual products detection results. Especially Prof. Norskov from Stanford University and SLAC Lab, Prof. Koper from Leiden University and Prof Jaramillo from Stanford University have made great contributions to the clarifying of the reaction pathways and selectivity mechanism.[3-13]

During the CO_2 reduction, CO_2 gas is usually bubbled into the hydrous solution, such as $KHCO_3$, $NaHCO_3$and KOH solutions, and dissolved.[14] We use CO_2* to represent the dissolved CO_2 in the solution, which is also the initial active specie of CO_2 reduction. When the catalyst surface has weak adsorption for CO_2* anion radicals, one electron would transfer to CO_2 and CO_2* radicals would be predominantly formed in a state where the C atom is available for hydrogenation, leading to the generation of $HCOO^-$,[6, 11, 15] or just desorption from the surface, as shown in Figure 4.3. Zn trends to HCOOH generation. The Zn surface has very weak adsorption strength for $CO_2^{\bullet-}$ anion radicals; thus, during CO_2 reduction, CO_2 is converted into $HCOO^-$ as the main reaction product. However, due to this weak adsorption strength, proton reduction (water splitting) competes with CO_2 reduction in aqueous electrolytes, and the

selectivity of zinc for CO_2 reduction is quite low.

There is another pathway for HCOOH generation, on the surface of metals that behave stronger H+ adsorption, dissolved CO_2 inserts into the M-H bond and yield HCOOH. The selectivity for HCOOH generation shown from Rh and Ir might come from this pathway.

1. *Free CO_2^* radicals near the catalyst surface.*

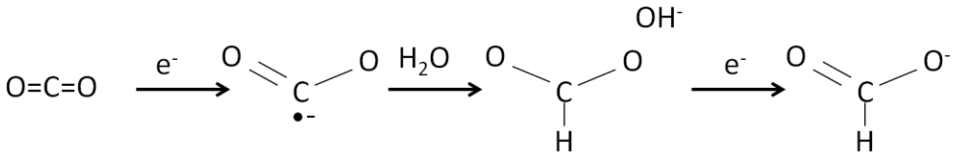

2. *CO_2^* radicals weakly adsorbed on the catalyst surface.*

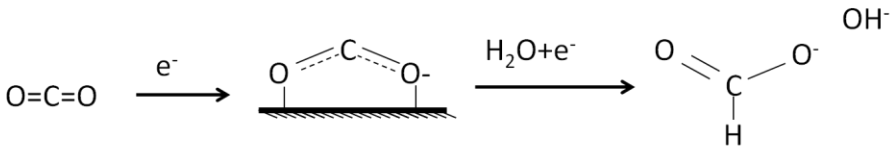

3. *CO_2* inserts into the M-H bond*

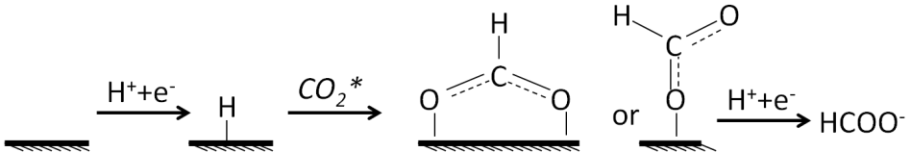

Figure 4.3 *The pathways of HCOOH generation.*

In contrast, when the catalyst surface has high adsorption strength for the CO_2* anion radical, the radical formed on the metal surface is stabilized by *d*-electron back donation and would be subsequently converted to the CO* radical. If the adsorption strength for the CO* radical is weak, the radical would desorb from the metal surface, resulting in the production of CO.Au is a typical metal that shows CO selectivity. If the surface adsorption strength for CO* is stronger, then CO* will to catalyzed into COH* or CHO* species, which convert into CH_4 or CH_3OH respectively. In the case of Cu and Cu oxides, although the CO_2 reduction properties were previously reported, their adsorption and desorption strength with CO_2 was so strong that the CO_2 radicals can be adsorbed on the Cu surface, causing the generation of CH_4 and/or CH_3OH.

Also, when the CO* was attached on the surface, there are also possibility of the CO dimerization, which will lead to the generation of ethylene or ethanol, this will usually happen under a very high reduction potential.

However, if the surface CO* adsorption is too strong, the surface will be poisoned by overcovered CO, thus loss activity for CO_2 reduction. The other reason of the high selectivity for H_2 generation shown by Pt is exactly caused by the surface poisoning.

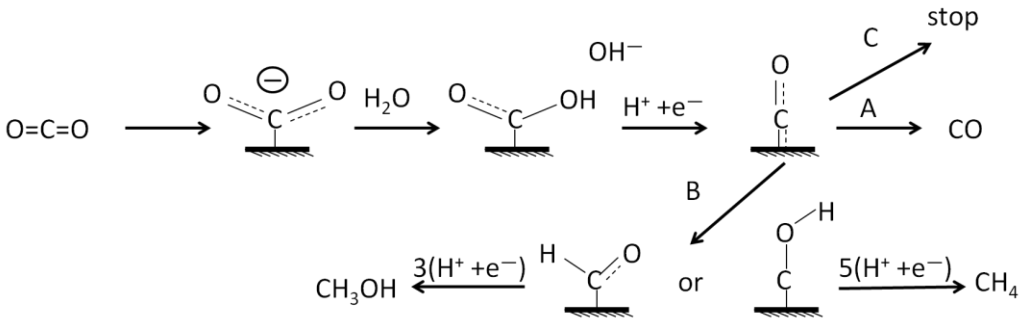

* *A. Weak CO radical adsorption strength*
B. Strong CO radical adsorption strength.
C. the CO radical adsorption strength is too strong

Figure 4.4 *The pathways of CO, CH_4 and CH_3OH generaion.*

4.2 In-situ FTIR analyses.

According to the literature studies, by combining Cu and Zn at the atomic scale in an alloy, high selectivity for HCOOH formation and suppression of hydrogen production were achieved. This proposal is also supported by computational study on the free binding energies of hydrogen and *COOH of intermetallic alloys including Cu-Zn alloy.[12]

To verify our proposal, *in-situ* FT-IR analysis was also operated.

The *in-situ* FT-IR spectra were measured using FTIR6100 (JASCO), the catalytic reaction was conducted in a gas-flow reactor with a quartz window (S.T. Japan), in which Cu-Zn nanoparticle-loaded $SrTiO_3$ powders (prepared by vacuum sealing method, details in ***Chapter 5***) were put in a porous ceramic cup. For pre-treatment, pure Ar gas was introduced to the reactor at the flow rate of 100ml/min at 573K for 1 hour. Heater was only used for pre-treatment.

To simulate the reaction environment during the photocatalytic evaluation, Ar gas or CO_2 gas were introduced into the reactor through bubbling of water to flow humid gas during the analyses. The pH would be a little different, but according to the previous researches, compared to CO_2 bubbled 0.1M $KHCO_3$ which we used in the photocatalytic evaluation, the CO_2 reduction activity in CO_2 bubbled pure water would be weaker since the concentration of the active species was lower.[14] Thus, the reaction operated in the practical photocatalytic evaluation would only be stronger than that in the *in-situ* FTIR analyses below. UV light (Hg-Xe lamp (240-300nm), LA-410UV, Hayashi Ltd, was used as light source. The Cu nanoparticles loaded $SrTiO_3$ was also analyzed as a control group, prepared by chemical reduction method (*Appendix 1.2*). The schematic illustration of the in-situ FT-IR analysis was shown in Figure 4.5.

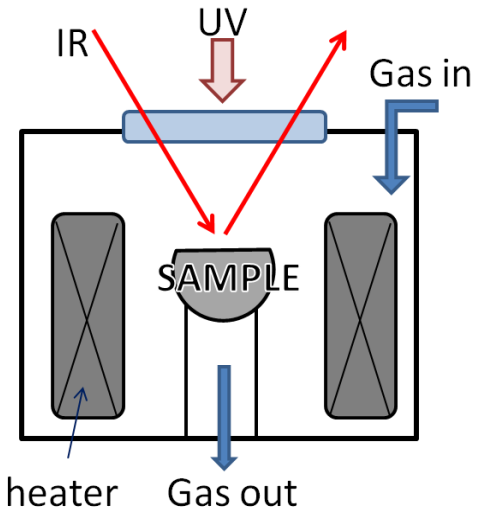

Figure 4.5 *The equipment construction of the gas-flow reactor used in the in situ FTIR analysis.*

as shown in Figure 4.6, When the Cu-Zn nanoparticles loaded $SrTiO_3$ powders was put in humid CO_2 and irradiated by UV light, peak appeared at 1280cm^{-1}, but didn't appear in control groups and the spectra of Cu $SrTiO_3$. According to the FT-IR database and previous studies, this peak assigned to bidentate surface carbonate. This result was consistent with our proposal of the CO_2 to HCOOH reaction route discussed above. As for the Cu nanoparticles loaded $SrTiO_3$, the presence of monodentate surface carbonate, the initiate of the CO and CH_4 routes, was proved by the peak appeared at 1442cm^{-1} These results provide a plausible explanation for the high selectivity of HCOOH generation of Cu-Zn catalyst.

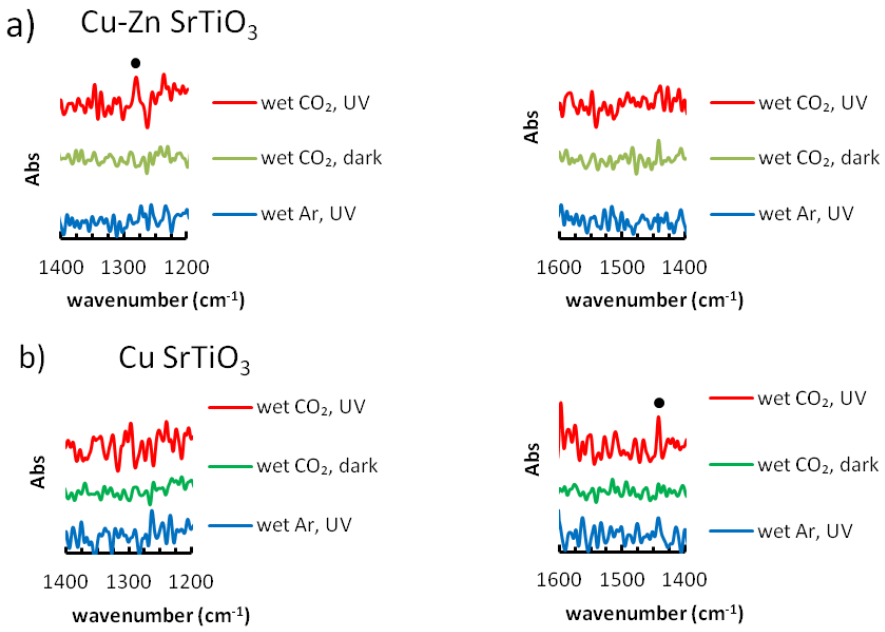

Figure 4.6 *The FT-IR spectra of a) Cu-Zn nanoparticles loaded $SrTiO_3$ powders and b) Cu nanoparticles loaded $SrTiO_3$ powders, measured in wet CO_2 atmosphere under UV irrdiation. Spectra measured in wet CO_2 without UV irradiation and those in wet Ar under UV irradiation were used as control group.*

4.3 Conclusion

As conclusion, our study proved our proposal that the reaction pathways of CO_2 reduction were decided by the surface adsorption strength of CO_2* and CO* radicals on the co-catalyst surface. Weak surface adsorption for CO_2* benefits the HCOOH generation. In the present research, the Cu-Zn alloy promoted the reaction route for HCOOH generation and the adsorbed species was detected by in-situ FTIR.

References

1. Zhang, Y.-J.; Sethuraman, V.; Michalsky, R.; Peterson, A. A., Competition between CO2 Reduction and H2 Evolution on Transition-Metal Electrocatalysts. ACS Catalysis **2014,** 4 (10), 3742-3748.

2. Jaksic, M., Volcano plots along the Periodic table, their causes and consequences on electrocatalysis for hydrogen electrode reactions. Journal of New Materials for Electrochemical Systems **2000,** 3 (2), 153-168.

3. Norskov, J. K.; Bligaard, T.; Rossmeisl, J.; Christensen, C. H., Towards the computational design of solid catalysts. Nat Chem **2009,** 1 (1), 37-46.

4. Peterson, A. A.; Abild-Pedersen, F.; Studt, F.; Rossmeisl, J.; Norskov, J. K., How copper catalyzes the electroreduction of carbon dioxide into hydrocarbon fuels. Energy & Environmental Science **2010,** 3 (9), 1311-1315.

5. Hansen, H. A.; Varley, J. B.; Peterson, A. A.; Nørskov, J. K., Understanding trends in the electrocatalytic activity of metals and enzymes for CO2 reduction to CO. The journal of physical chemistry letters **2013,** 4 (3), 388-392.

6. Kortlever, R.; Shen, J.; Schouten, K. J. P.; Calle-Vallejo, F.; Koper, M. T., Catalysts and reaction pathways for the electrochemical reduction of carbon dioxide. The journal of physical chemistry letters **2015,** 6 (20), 4073-4082.

7. Schouten, K. J. P.; Pérez Gallent, E.; Koper, M. T. M., Structure Sensitivity of the Electrochemical Reduction of Carbon Monoxide on Copper Single Crystals. ACS Catalysis **2013,** 3 (6), 1292-1295.

8. Schouten, K. J. P.; Qin, Z.; Gallent, E. P.; Koper, M. T. M., Two Pathways for the Formation of Ethylene in CO Reduction on Single-Crystal Copper Electrodes. Journal of the American Chemical Society **2012,** 134 (24), 9864-9867.

9. Rodriguez, J. A.; Liu, P.; Stacchiola, D. J.; Senanayake, S. D.; White, M. G.; Chen, J. G., Hydrogenation of CO2 to methanol: Importance of metal–oxide and metal–carbide interfaces in the activation of CO2. ACS Catalysis **2015,** 5 (11), 6696-6706.

10. Kuhl, K. P.; Hatsukade, T.; Cave, E. R.; Abram, D. N.; Kibsgaard, J.; Jaramillo, T. F., Electrocatalytic Conversion of Carbon Dioxide to Methane and Methanol on Transition Metal Surfaces. Journal of the American Chemical Society **2014**.

11. Chaplin, R. P. S.; Wragg, A. A., Effects of process conditions and electrode material on reaction pathways for carbon dioxide electroreduction with particular reference to formate formation. Journal of Applied Electrochemistry **2003,** 33 (12), 1107-1123.

12. Karamad, M.; Tripkovic, V.; Rossmeisl, J., Intermetallic Alloys as CO Electroreduction Catalysts—Role of Isolated Active Sites. ACS Catalysis **2014,** 4 (7), 2268-2273.

13. Hirunsit, P.; Soodsawang, W.; Limtrakul, J., CO2 Electrochemical Reduction to Methane and Methanol on Copper-Based Alloys: Theoretical Insight. The Journal of Physical Chemistry C **2015,** 119 (15), 8238-8249.

14. Zhong, H.; Fujii, K.; Nakano, Y.; Jin, F., Effect of CO2 Bubbling into Aqueous

Solutions Used for Electrochemical Reduction of CO2 for Energy Conversion and Storage. The Journal of Physical Chemistry C **2014**.
15. Hori, Y., Electrochemical CO2 Reduction on Metal Electrodes. In Modern Aspects of Electrochemistry, Vayenas, C.; White, R.; Gamboa-Aldeco, M., Eds. Springer New York: 2008; Vol. 42, pp 89-189.

Chapter. 5

The nanoparticlization of the Cu-Zn alloy

5.1 Introduction

In *Chapter* 3, Cu_5Zn_8 alloy electrode is prepared and proved to be able to catalyze CO_2 reduction selectively into HCOOH in electro- or photo-catalytic CO_2 reduction. However, as a co-catalyst for photocatalytic CO_2 reduction, its utilization was limited by its film form and preparation method.

As we introduced in *Session 1.3*, a lot of light harvesters are used as dispersed powders, to utilize in the powder system, the co-catalyst should also be particlized. In the case of Z-Scheme system, the co-catalyst also should be easily decorated to the surface of the photocathode. Obviously, nanoparticlization of the co-catalyst will broad its versatility.

On the other hand, the vacuum sealing method used for the Cu-Zn alloy electrode preparation needed annealing process under high temperature. For many kinds of light harvester, such as metal chalcogenides, high temperature will destroy their composition or structure, thus make them inactive. Thus, other kinds of synthesis method which can decorate the co-catalyst onto the light harvester under moderate condition are hardly desired.

In this chapter, Cu-Zn alloy will be nanoparticlized and coated onto the surface of $SrTiO_3$ by using vacuum sealing method, and improved chemical co-reduction and ink method. The properties of the Cu-Zn nanoparticles and Cu-Zn NPs loaded STO will be evaluated. And in-situ FTIR analysis will be operated to clarify why Cu-Zn alloy can selectively catalyze HCOOH generation and how did the reaction pathway proceed on the surface of the Cu-Zn alloy.

5.2 Experimental procedures

5.2.1 Preparation of Cu-Zn nanoparticles using vacuum sealing method.

Pure Cu nanoparticles were first deposited onto the surface of the $SrTiO_3$ powder to obtain Cu nanoparticle-loaded $SrTiO_3$ powder. An aliquot (2 g) of $SrTiO_3$ powder was dispersed in 40 mL of distilled water that contained 5.28 mg of $CuCl_2{\cdot}2H_2O$. This solution was stirred overnight in an Ar atmosphere and cooled in an ice bath. An adequate amount of $NaBH_4$ solution (> 0.61 mL of 1 M solution) was added to this solution to precipitate Cu nanoparticles. The obtained

Cu nanoparticle-loaded $SrTiO_3$ powder was collected by centrifugation and dried under vacuum at 80˚C for 2 hours. The Cu nanoparticle-loaded $SrTiO_3$ powder was then vacuum-sealed in quartz ampoules with pure Zn grains and heated at elevated temperatures for 2 days to yield the desired Cu-Zn nanoparticle-loaded $SrTiO_3$ powder.

5.2.2 Preparation of Cu-Zn nanoparticles ink using chemical co-reduction method. (outline)

Intermetallic Cu-Zn nanoparticles were synthesized by chemical co-reduction of metal precursors using strong reducing agents under anaerobic conditions.[1-3]

5.2.3 Photocatalytic CO_2-reduction performance tests

A 100 mg aliquot of the prepared Cu-Zn nanoparticle-loaded $SrTiO_3$ powder was dispersed in a CO_2-purged 0.1 M $KHCO_3$ solution that was contained in an air-tight glass reactor equipped with a quartz window. The UV light (Hg-Xe lamp (240-300nm), LA-410UV, Hayashi Ltd.) was used as light source. The gaseous products in the headspace such as CH_4, CO, and H_2 were quantified with a gas chromatograph (BID, SHIMADZU). The liquid products in the electrolyte solution such as HCOOH were quantified with an ion chromatograph (SHIMADZU).

5.3 The Cu-Zn NPs synthesized by vacuum sealing method.

5.3.1 Characterization

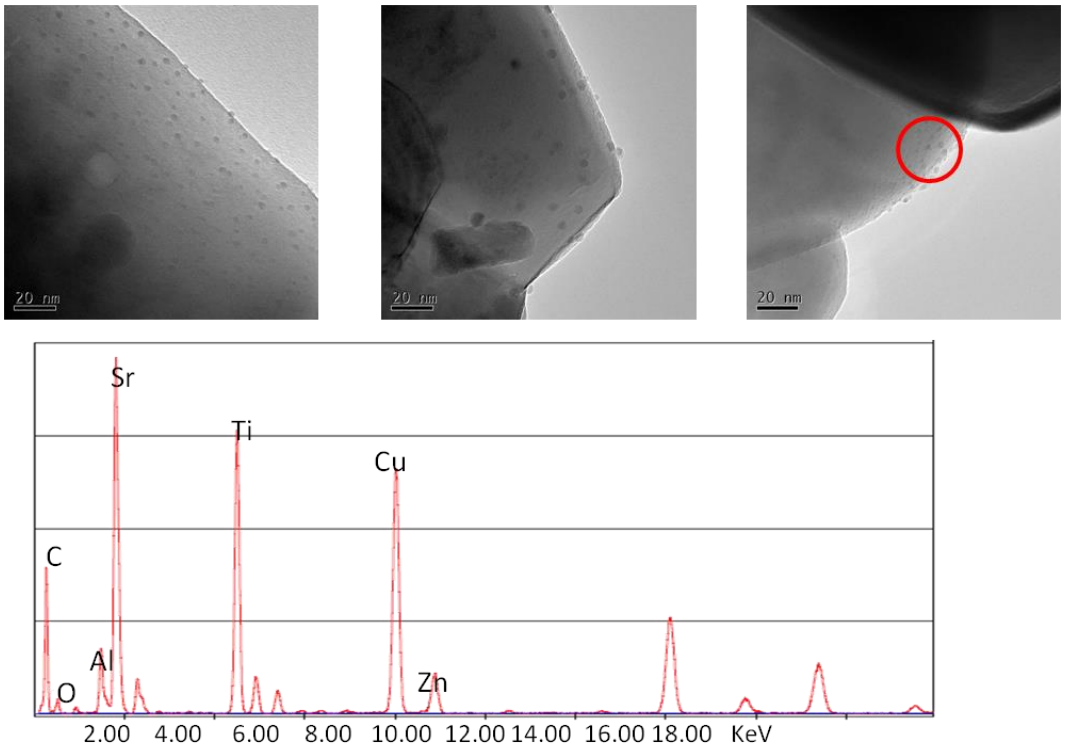

Figure 5.1 *TEM graphs of prepared Cu-Zn nanoparticles loaded $SrTiO_3$ powder and the EDX element analysis was operated inside the red circle.*

As seen in Figure 5.1, we can confirm that Cu-Zn nanoparticles was successfully loaded on the surface $SrTiO_3$ powder from the TEM image and the EDX element analysis. The Cu-Zn nanoparticles were approximately 3~5 nm, uniformly distributed.

XRD pattern and XPS spectra were analyzed to the Cu-Zn NPs loaded $SrTiO_3$ powder. Since the loading amount is very low, we can only find a small peak of Cu_5Zn_8 from the peaks of STO. However, peak of pure Zn also appeared. But the spectra of Cu *2p* and Zn *2p* both shifted from those of pure Cu and pure Zn, indicating that the Cu-Zn NPs was intermetallic.

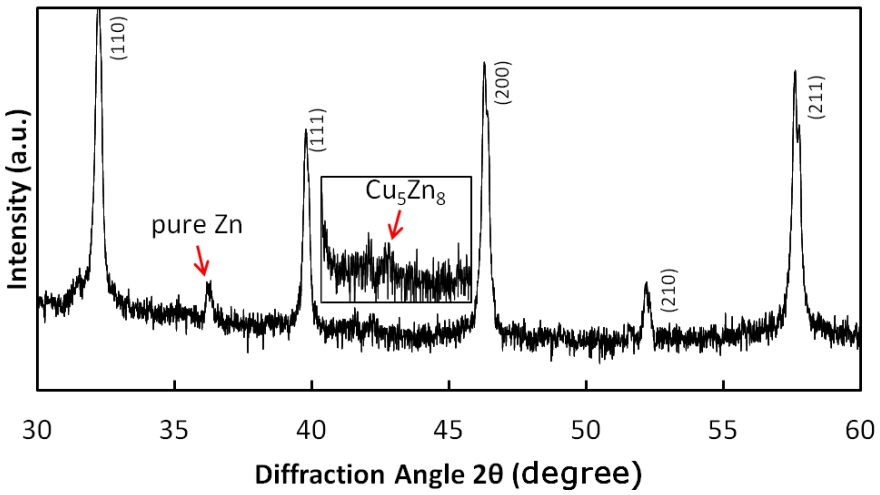

Figure 5.2 *The XRD pattern of the prepared Cu-Zn nanoparticles loaded $SrTiO_3$ powders(5%wt).*

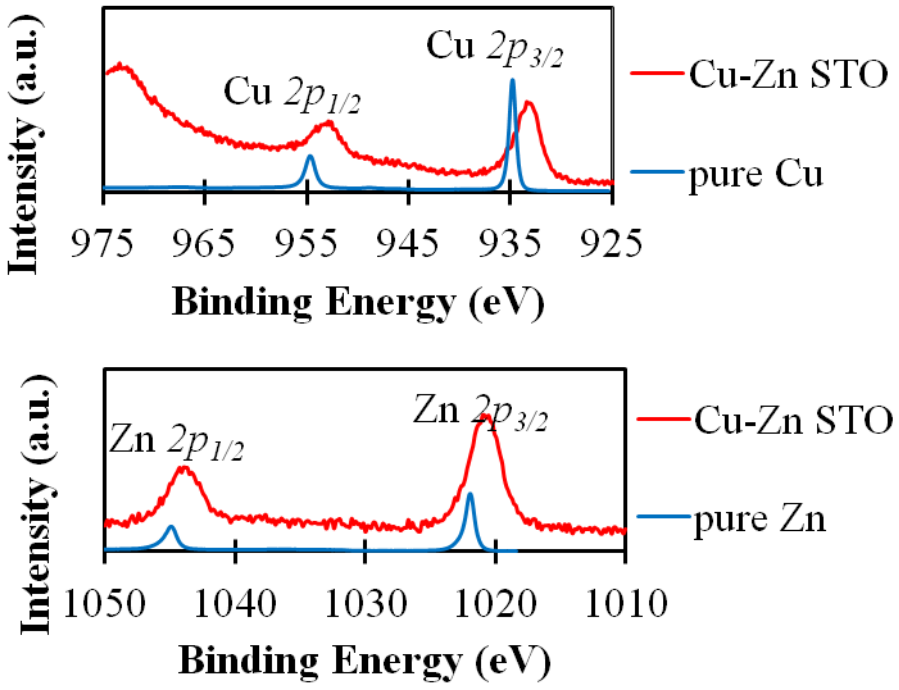

Figure 5.3 *The XPS spectra of Cu2p and Zn2p from the prepared Cu-Zn nanoparticles loaded $SrTiO_3$ powders, pure Cu and pure Zn were used as control groups. Measurement condition: 10 cycles, 3 repetitions, one step = 0.15 eV, 40 ms.*

UV-visible absorption spectra were also analyzed, compared to pure STO, visible light photons were absorbed due to the metallic Plasmon absorptions. However, this part of absorption does not contribute to the CO_2 photoreduction because of the low reductivity. The UV-vis result also proved that the Cu-Zn NPs were successfully loaded to the surface of STO

powders.

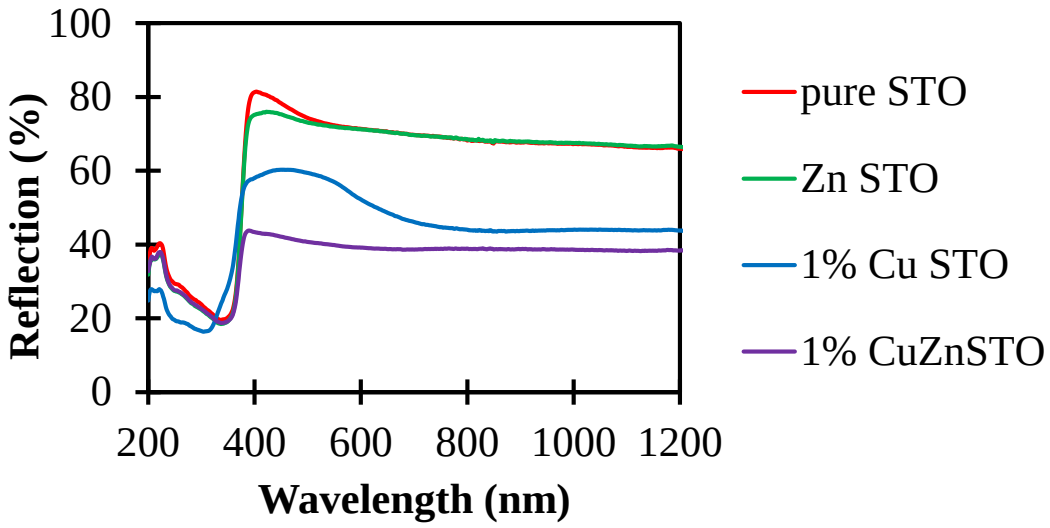

Figure 5.4 *The UV-Visible spectra of pure $SrTiO_3$, Cu nanoparticle-loaded $SrTiO_3$, Zn nanoparticle-loaded $SrTiO_3$, and the Cu-Zn nanoparticles-loaded $SrTiO_3$.*

5.3.2 Photocatalytic evaluation

Under UV irradiation of the Cu-Zn nanoparticle-loaded $SrTiO_3$ powder, CO_2 was mainly converted to HCOOH, whereas CH_4 and CO productions were limited, as shown in Figure 5.5. A negligible amount of hydrogen was detected in the reactor headspace, indicating that the Cu-Zn co-catalyst was highly selective for CO_2 reduction.

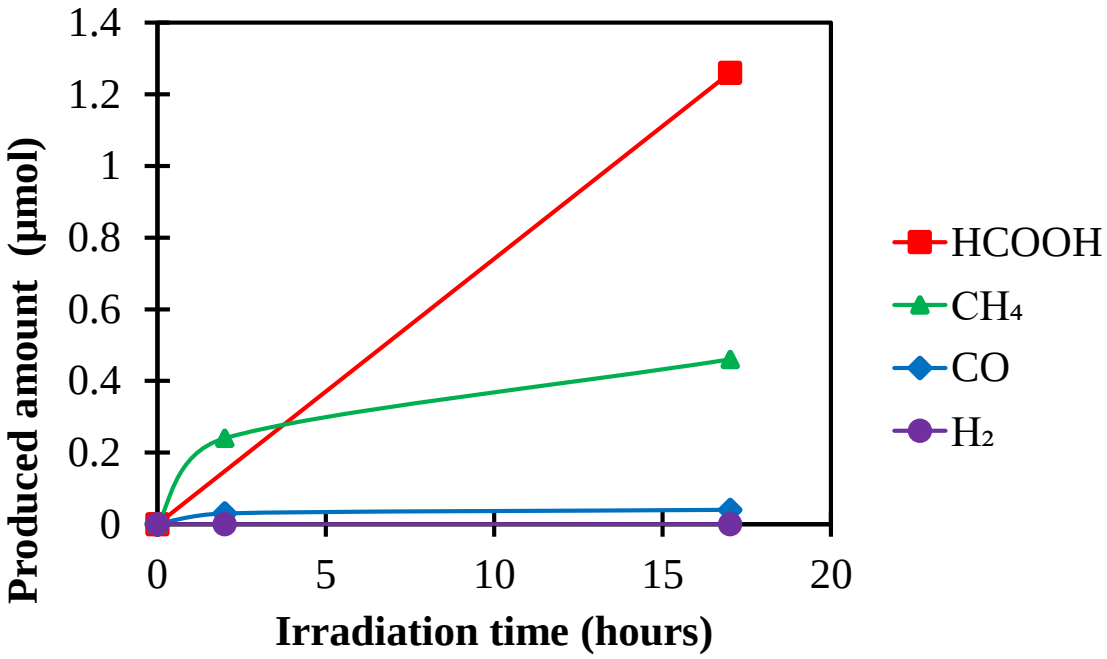

Figure 5.5 *Produced amount from the UV light irradiated Cu-Zn NPs loaded STO powders.*

Oxygen production through water oxidation would proceeded by photogenerated holes in $SrTiO_3$, but oxygen molecules that cannot be ignored already existed in the head space of our reactor and/or were adsorbed on the surface of the photocatalyst powder as H_2O_2 molecules.[4] Therefore, we tried to prove that the water molecule was an electron donor using isotope trace analysis, as shown in Figure 5.6. When $H_2{}^{18}O$ was used as the aqueous electrolyte solution, $^{18}O_2$ (*m/z*=36) generation was detected. This result strongly suggests that water molecules served as the electron donor in our photocatalyst system, which is consistent with photosynthesis in natural plants. We also analysed the gas-phase products in the headspace under $^{13}CO_2$ (*m/z* = 45) isotope bubbling with light irradiation. As a result, gas phase ^{13}CO (*m/z* = 29) was detected, indicating that the extracted electrons from water molecules would be excited into the conduction band of $SrTiO_3$, and these excited electrons react with CO_2 to produce fuel molecules.

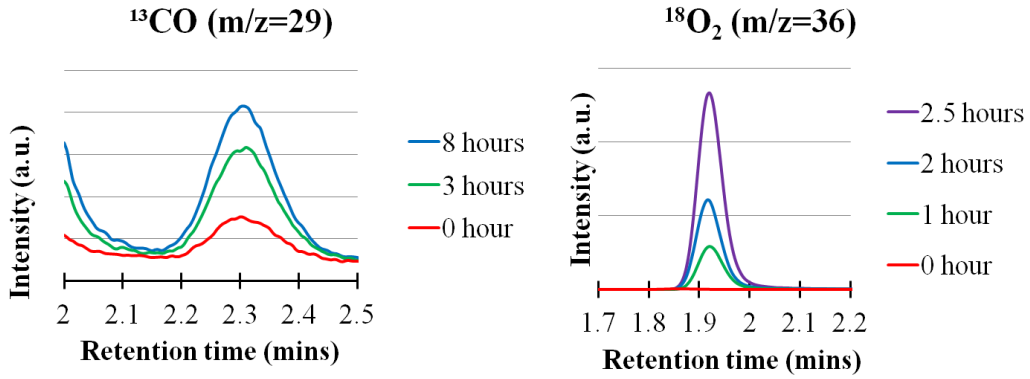

Figure 5.6 *Results of an isotope tracing experiment for the Cu-Zn catalyst decorated $SrTiO_3$, showing that ^{13}CO (m/z=29) and $^{18}O_2$ (m/z=36) were detected among the reactions products under UV irradiation when $^{13}CO_2$ was used as gas source and $H_2{}^{18}O$ was used as water source.*

According to the XPS analysis of the Cu-Zn nanoparticles-loaded $SrTiO_3$ powder collected after the CO_2 reduction (Figure 5.7), there was no valence change of Cu and Zn during the reaction, indicating that our catalyst was stable under photon irradiation in aqueous media and was not oxidized. The TON for the CO_2 reduction of the particulate system was 11.46, which is lower than that of the Cu-Zn thin film electrode system from *Chapter.3* under the same experimental conditions. Even though the two materials were prepared using the same vacuum annealing method, the Zn concentration of the Cu-Zn nanoparticles was higher than that of the Cu-Zn electrode (Table 5.1). The XRD pattern of Cu-Zn nanoparticles loaded $SrTiO_3$ also proved that pure Zn exists (Figure 5.2). As conclusion, we suspected that by using vacuum sealing method, Zn vapour would be directly loaded on the surface of $SrTiO_3$ without reacting with Cu during annealing. The present modification method with Cu-Zn nanoparticles is facile and applicable to various light harvesting materials to enhance their photocatalytic CO_2 reduction activity.

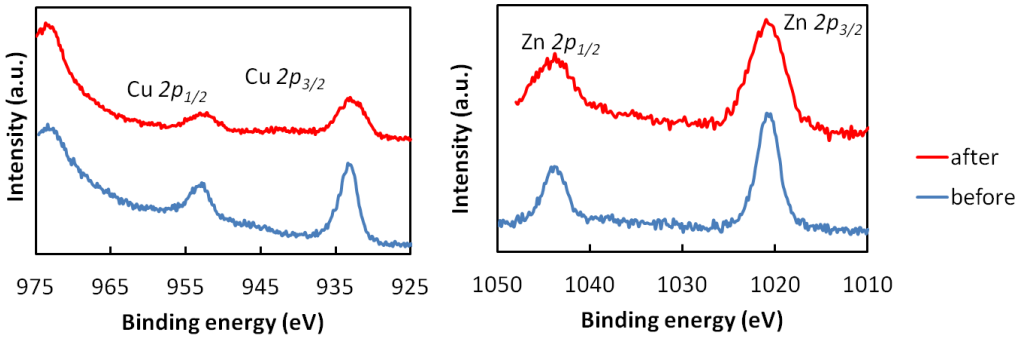

Figure 5.7 *The XPS Cu 2p and Zn 2p spectra of the Cu-Zn nanoparticles loaded $SrTiO_3$, prepared by vacuum sealing method, before and after the CO_2 reduction reaction. Measurement condition: 10 cycles, 3 repetitions, one step=-0.15eV, 40ms.*

Table 5.1 *The XRF and ICP results of the composition analysis of Cu-Zn nanoparticles loaded $SrTiO_3$ prepared by vacuum sealing method.*

Cu	Zn	Ti	Sr
X-ray Fluorescence (mass%)			
0.54	1.54	22.9	75.1

Inductively Coupled Plasma (mg in 1.562mg sample)			
0.0070	0.0174	0.363	0.670

5.4 The Cu-Zn NPs synthesized by chemical co-reduction methods. (outline)

Cu-Zn alloy nanoparticles were also prepared by chemical co-reduction method, which can easily synthesize different kinds of alloy nanoparticles with different compositions. Hard-XPS, XRD, XRF were used for the characterization of the prepared Cu-Zn alloy NPs.

According to electrochemical evaluation and optimization, the prepared Cu_5Zn_8 NPs were proved to behave high selectivity for HCOOH generation. Further, using an ink method, the Cu-Zn NPs can be easily loaded onto the surface of light harvester under moderate conditions. The Cu_5Zn_8 NPs loaded $SrTiO_3$ successfully converted CO_2 into HCOOH as main product under UV irradiation.

5.5 Conclusion

In the present research, we tried to synthesis Cu-Zn nanoparticles and decorated them on the surface of $SrTiO_3$ using 1) vacuum sealing method, 2) chemical co-reduction and ink method.

By using vacuum sealing method, the Cu-Zn alloy nanoparticles was successfully loaded onto the surface of $SrTiO_3$ powder. Under UV irradiation, this system converted CO_2 into HCOOH as main product. However, compared to the Cu-Zn electrode, the TON of the reaction decreased drastically, the element characterization showed that pure Zn nanoparticles also attached to STO during the annealing. Also, it's hard to control the Zn concentration by using vacuum sealing method. Thus, we used chemical co-reduction method as improvement.

Three kinds of Cu-Zn nanoparticles were synthesized by chemical co-reduction, according to the electrochemical evaluation, the Cu_5Zn_8 NPs behaved best CO_2 reduction catalytic property. By making the NPs into a fine dispersed ink, the Cu-Zn NPs were easily loaded on the surface of $SrTiO_3$, even any kinds of light harvesters. Under UV irradiation, HCOOH was selectively generated and the performance was about 10times than that of vacuum sealing prepared Cu-Zn NPs.

References

1. Abe, H.; Matsumoto, F.; Alden, L. R.; Warren, S. C.; Abruña, H. D.; DiSalvo, F. J., Electrocatalytic Performance of Fuel Oxidation by Pt3Ti Nanoparticles. Journal of the American Chemical Society ***2008,*** *130 (16), 5452-5458.*

2. Kodiyath, R.; Ramesh, G. V.; Koudelkova, E.; Tanabe, T.; Ito, M.; Manikandan, M.; Ueda, S.; Fujita, T.; Umezawa, N.; Noguchi, H.; Ariga, K.; Abe, H., Promoted C-C bond cleavage over intermetallic TaPt3 catalyst toward low-temperature energy extraction from ethanol. Energy & Environmental Science ***2015,*** *8 (6), 1685-1689.*

3. Saravanan, G.; Abe, H.; Xu, Y.; Sekido, N.; Hirata, H.; Matsumoto, S.-i.; Yoshikawa, H.; Yamabe-Mitarai, Y., Pt3Ti Nanoparticles: Fine Dispersion on SiO2 Supports, Enhanced Catalytic CO Oxidation, and Chemical Stability at Elevated Temperatures. Langmuir ***2010,*** *26 (13), 11446-11451.*

4. Hirakawa, T.; Kominami, H.; Ohtani, B.; Nosaka, Y., Mechanism of photocatalytic production of active oxygens on highly crystalline TiO2 particles by means of chemiluminescent probing and ESR spectroscopy. The Journal of Physical Chemistry B ***2001,*** *105 (29), 6993-6999.*

Chapter. 6

Visible-light-driven CO_2 photoreduction. (outline)

Even though a Cu-Zn NPs co-catalyst was successfully developed and proved to behave highly activity in the previous chapters, it's still difficult to achieve visible light driven CO_2 reduction because of the cogent requirements for the light harvester system. The light harvester should provide high conduction band position and deep valence band position to catalyze both the CO_2 reduction and water oxidation reactions. Also, it is required to be visible light responsive to expand the range of absorbed solar energy. However, these two requirements are very hard to be satisfied simultaneously because of the trade-off relationship between the high band position and narrow bandgap value.

To solve this problem, a Z-scheme system, which is constructed by visible-light-sensitive $CaFe_2O_4$ (CFO) photocathode and WO_3 nanotree photoanode, has been developed in the present chapter. The CFO powder was prepared by solid state reaction[1-2], highly crystallize CFO electrode was prepared by screen printing and high temperature annealing. The WO_3 nanotree electrode was prepared by hydrothermal synthesis.[3] The CFO photocathode and WO_3 photoanode were connected by an photoelectrochemical cell, as shown in ***Figure 6.1***.

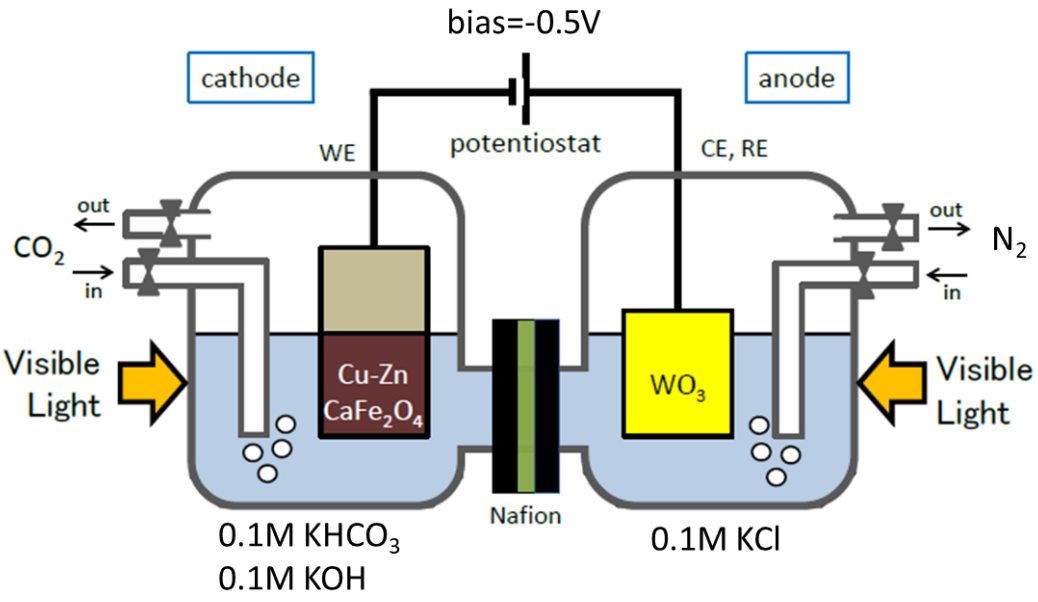

Figure 6.1. *The construction of photoelectrochemical cell, using Cu-Zn NPs loaded CFO electrode and WO_3 nanotree electrode.*

The bandgap of CFO and WO_3 were calculated to be 2.5eV and 2.6 eV, respectively, according to the UV-vis spectra, Current-potential curves of CFO and WO_3 were also analyzed, according to the current threshold, the position of the conduction band and valence band of the CFO photocathode and WO_3 photoanode were calculated. The combination of CFO photocathode and WO_3 photoanode was proposed to be able to catalyze CO_2 reduction, according to the theoretical band model, as shown in ***Figure 6.2***.

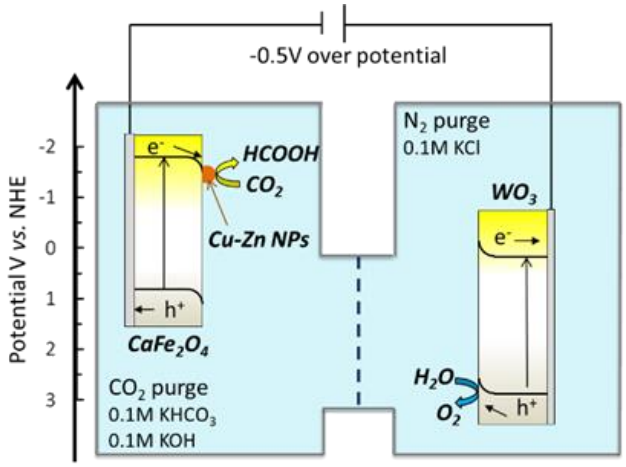

Figure 6.2 *The proposed reaction and band model in H-type photoelectrochemical cell constructed by CFO and WO_3 electrode.*

Under visible light irradiation, H_2 was mainly detected by the Z-Scheme constructed by pure CFO photocathode and WO_3 photoanode with an outer-applied -0.5V over potential. By decorating the surface of CFO using Cu-Zn NPs, the photocatalytic performance for CO_2 reduction increased significantly. HCOOH was generated as main product. The generated amount of O_2 roughly equals to half of the reduction product, indicating that water was the electron donor to produce oxygen.

Compared to the previous researches, this work should be significantly impact in the field of photocatalysis, because of not only achieving visible light photocatalytic CO_2 reduction without sacrificial agents but also showing outstanding selectivity for HCOOH generation. The present study is the first report to achieve more than 50 % selective CO_2 reduction under visible light irradiation through water oxidation. Besides, the light-to-energy conversion efficiency reaches 0.028 %, which is much higher than the previous reports.

References:

1. Matsumoto, Y.; Obata, M.; Hombo, J., Photocatalytic reduction of carbon dioxide on p-type CaFe2O4 powder. The Journal of Physical Chemistry ***1994,*** *98 (11), 2950-2951.*

2. Ida, S.; Yamada, K.; Matsunaga, T.; Hagiwara, H.; Matsumoto, Y.; Ishihara, T., Preparation of p-Type CaFe2O4 Photocathodes for Producing Hydrogen from Water.

Journal of the American Chemical Society **2010,** *132 (49), 17343-17345.*
3. Nukui, Y.; Srinivasan, N.; Shoji, S.; Atarashi, D.; Sakai, E.; Miyauchi, M., Vertically aligned hexagonal WO3 nanotree electrode for photoelectrochemical water oxidation. Chemical Physics Letters **2015,** *635, 306-311.*

Chapter. 7

Design strategy for highly selective catalyst

In the present research, we proved the feasibility of highly selective CO_2 reduction catalyst design by means of tuning the surface adsorption conditions by alloying. Based on comprehensive analyses of the in-situ adsorbed species and the final products, we clarified the reaction pathway of HCOOH generation and successfully developed a Cu_5Zn_8 alloy which can catalyze CO_2 into HCOOH with high selectivity. We synthesized well-defined Cu_5Zn_8 alloy film and nanoparticles, achieved repeatable and reliable performance in electro-and photo-catalytic CO_2 reduction. The present findings can be generally used in various catalytic areas, to stimulate the researchers on wide variety of co-catalysts design and development not only for CO_2 reduction but also other reactions involving multi-electron process.

In this chapter, the contributions of this research will be introduced in details. Based on the scientific findings of the factors for the high selectivity of the developed Cu-Zn alloy, the general design strategy for highly selective catalyst will be presented. The outlook about the future work will also be introduced

7.1 Scientific contribution

7.1.1 the idea of surface adsorption conditions tuning by alloying for highly selective CO_2 reduction catalyst design.

In the previous researches of electrocatalytic CO_2 reduction, a lot of metal co-catalyst was evaluated and the products were detected in a Carpet bombing way.[1] Based on their products, the reaction pathways and the relationship with the metal surface was proposed. Especially in Prof. Hori's work, he comprehensively reviewed the products generated from various kinds of metals and alloys in hydrous or anhydrous electrolyte, and he firstly proposed that the products selectivity was decided by the adsorption strength for the active species such as $\cdot CO_2$.[2-5]

Since the electrocatalytic and photocatalytic CO_2 reduction have gain attention again following with the energy shortage and CO_2 over-emission from the beginning of 21st century, numerous researches have focused on the determination of the reaction mechanism, especially about the products selectivity, both experimentally[6-8] and theoretically[9-14].

The experimental analyses were commonly looking for the volcano plots between the surface

adsorption and the product generation current density. For example, T.F.Jaramillo from Stanford Uni. published his research demonstrating the electrocatalytic conversion of CO_2 to CH_4 or CH_3OH on transition metal surfaces and provided the idea of searching for catalysts with higher products selectivity by means of tuning adsorbate binding energies appropriately, such as in the form of transition-metal alloys.

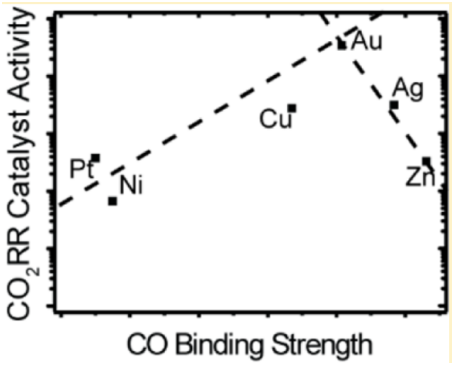

Figure 7.1 the relationship between the catalytic activity for CO_2 reduction and the CO binding strength of several kinds of transition-metals.[8]

In some previous researches about CO and methanol oxidation, the atomic ensemble effect of alloying has been well-proved and documented, however, even though there were a lot of reports using alloy as CO_2 reduction catalyst, the reaction mechanism and design strategy were barely studied. Theoretical researches has operated the DFT calculation of the surface binding or formation energies of the active sites on different kinds of metal or metal alloy, aiming to the design of high selective catalyst[9]. For example, J.Rossmeisl calculated the formation energies of H* and *COOH on various of alloy surfaces, thus found the alloys that can generate HCOOH and prevent H_2 generation.

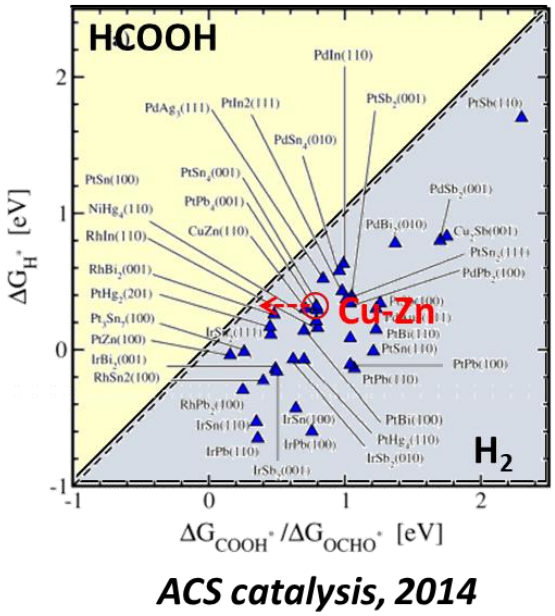

ACS catalysis, 2014

Figure 7.2 the free binding energies of hydrogen against *COOH or *OCHO.

In the yellow area, the ΔG for HCOOH is lower than that of H_2 thus HCOOH generation will proceed in priority, considering the left shift that caused by the inclusion of solvation effect in a practical liquid solvent, the alloys near the diagonal should be positive for HCOOH generation rather than H_2 generation. Cu-Zn was one of them.

In the photocatalytic CO_2 reduction area, compared to the mechanism analyses, the final products amount was paid more attention. While in our research, the high selectivity for HCOOH generation of Cu-Zn alloy was a reason of the comprehensive study and analyses of reaction mechanism, based on the idea of surface adsorption conditions tuning by alloying. Our research provided strong experimental prove for the previous theoretical studies and proved the scientific feasibility of highly selective CO_2 reduction catalyst design by means of tuning the surface adsorption conditions by alloying. We believe that our work can remind the importance of mechanism understanding in the photocatalytic CO_2 reduction area.

7.1.2 the demonstration and experimental prove of the reaction pathway from CO_2 into HCOOH.

Also, our detection of the adsorbed species on the Cu-Zn surface by in-situ FTIR clarified the reaction pathway for HCOOH generation. The formation of HCOOH can be separated into two steps:

$$CO_2(g) + e^- + H^+ \rightarrow COOH(ad) \qquad (1)$$

$$COOH(ad) + e^- + H^+ \rightarrow HCOOH(aq) \qquad (2)$$

However, the reaction (1) may occur as any of the following sequences:

1. $CO_2(g) \rightarrow CO_2(ad)$
   $CO_2(ad) + e^- \rightarrow CO_2^-(ad)$
   $CO_2^-(ad) + H^+ \rightarrow COOH(ad)$
2. $H^+(aq) + e^- \rightarrow H(ad)$
   $H(ad) + CO_2(g) \rightarrow COOH(ad)$
3. $CO_2(g) \rightarrow CO_2(ad)$
   $CO_2(ad) + e^- \rightarrow CO_2^-(ad)$
   $CO_2^-(ad) + H(ad) \rightarrow COOH^-(ad)$
4. $CO_2(g) \rightarrow CO_2(ad)$
   $CO_2(ad) + e^- \rightarrow CO_2^-(ad)$
   $CO_2^-(ad) + H_2O \rightarrow COOH^-(ad) + OH^-$ [15]

In our research, the bidentate surface carbonate specie was detected from the Cu-Zn surface, also, considering that the in-situ FTIR was operated inside of a mixing gas of CO_2 and H_2O vapor, sequences 4 was proved to be the appropriate reaction pathway of the HCOOH formation.

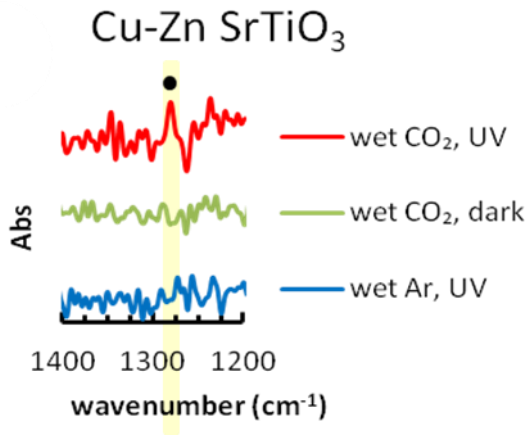

Figure 7.3 the in-situ FTIR spectra of the Cu-Zn loaded $SrTiO_3$, the peaks at 1280cm^{-1} was assigned to bidentate surface carbonate.[16-17]

7.1.3. the Cu-Zn alloy was proved to be the active sites of CO_2 reduction.

A Cu/ZnO alloy oxide material was once used for the hydrogeneration of CO_2 and CO, however the controversy about the active sites during the reaction had continued for years. Many kinds of mechanism model were drawn, because of the different experimental conditions such as temperature and pressure, the different preparation method and composition of the catalyst, even the different reactant (CO_2/H_2, CO/H_2, $CO_2/CO/H_2$). Especially about the effect of the ZnO, there were Cu-Zn alloy model[18-19] and morphology model[20-23], as shown below.

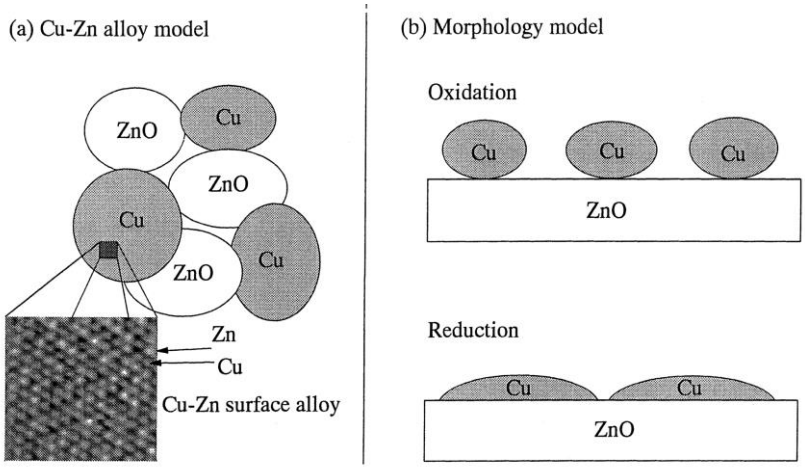

Prof. Nakamura pointed out that Cu-Zn alloy will be generated in the Cu nanoparticles, no matter of the annealing temperature, because of the mixing of Zn and Cu atoms in the metal precursor in the beginning of the preparation. And they advocated that the Cu-Zn alloy was responsible for the CO_2 hydrogeneration to produce methanol. While Prof. Topsøe reported that the morphology changed of the Cu nanoparticles on the ZnO surface and the supported Cu was the key feature of the Cu/ZnO system.

However, in our research, we have proved the activity for CO_2 reduction of a well-defined Cu_5Zn_8 alloy, based on comprehensive evaluation including electrochemical and photocatalytic evaluation. Thus, we could use our results to support Prof. Nakamura's view that the Cu-Zn alloy was the active sites for CO_2 reduction.

7.2 Engineering contribution (outline)

The achievement of the visible light driven highly selected CO_2 photoreduction with water as electron donor, based on robust and economical inorganic component hasn't been done by any groups. Compare to the previous reports, our work showed great advantages, especially in the light-to-energy conversion efficiency and Faradic efficiency. We believe this research will be a big breakthrough of the photocatalytic CO_2 reduction field.

7.3 Industry contribution (outline)

In the present research, a Cu-Zn alloy nanoparticles co-catalyst which can convert CO_2 into HCOOH with high selectivity was developed. By using ink method, the Cu-Zn NPs can be decorated to most kinds of light harvesters under moderate conditions. The general utilization and industry application was expected.

7.4 Outlook (outline)

In the future, the performance of the Cu-Zn NPs and the CFO/WO_3 system will be improved. Deeper analyses about the reaction sites and the atomic ensemble model on the Cu-Zn alloy can be studied theoretically and experimentally.

7.5 General design strategy for highly selective catalyst

The optimization of the surface adsorption condition is important for catalyst design. To change the surface adsorption condition for the active species, several ideas are provided.

1. as the main strategy of the present research, developing intermetallic catalyst by combining two different kinds of metal at atomic level can build the appropriate condition for the selected reaction. Not only for CO_2 reduction, this idea can be used for many kinds of catalytic reaction area. For example, Ni-Ti intermetallic is proposed to be a good catalyst for CO oxidation since the CO can be adsorbed and activated after the strong adsorption from Ni was neutralized by the weak adsorption from Ti.

2. oxidation of the pure metal can change the selectivity, because the local potential of the active metal atom will be changed, thus the adsorption strength and posture of the adsorbed CO_2* and CO* will be different. For example, Cu has been known as a typical catalyst for CH_4 and CH_3OH generation, but the Cu_xO nanocluster mainly converted CO_2 into CO in Chapter 2. As seen below, for pure Cu, it catalyzes route B because the adsorption strength for CO* is strong, but when the Cu atom was surrounding with O atoms, the binding energy of Cu=C will be decreased, thus CO* desorb from Cu and CO was generated.

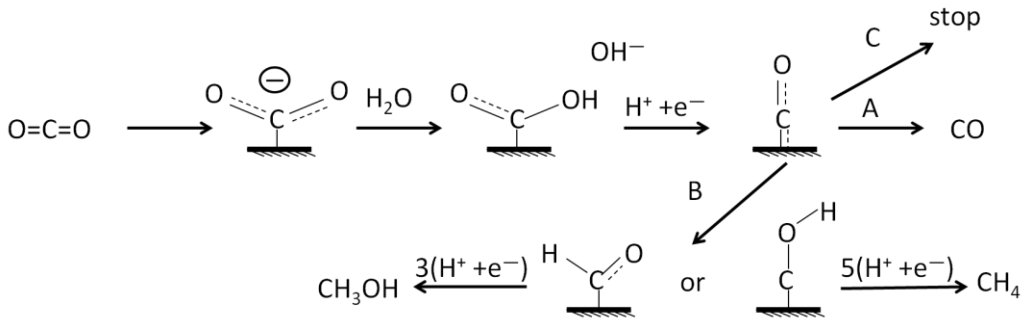

** A. Weak CO radical adsorption strength*
B. Strong CO radical adsorption strength.
C. the CO radical adsorption strength is too strong

Figure 7.4 The pathways of CO, CH_4 and CH_3OH generaion.

Many kinds of catalyst can be inspired by this idea, for example, Ni is not effective for CO_2 reduction because the high CO* adsorption strength poisoned the surface. Through oxidation, the CO* adsorption can be weakened, thus it's possible for NiO to catalyze CO_2 into CO or CH_4. For many kinds of metal that is difficult to be oxidized, such as Au, mixing with other kinds of metal oxide can help them to adjust the adsorption condition for the CO_2* and CO*.

References

1. Azuma, M.; Hashimoto, K.; Hiramoto, M.; Watanabe, M.; Sakata, T., Electrochemical Reduction of Carbon Dioxide on Various Metal Electrodes in Low‐Temperature Aqueous KHCO 3 Media. *Journal of the Electrochemical Society* **1990,** *137* (6), 1772-1778.
2. Hori, Y., Electrochemical CO2 Reduction on Metal Electrodes. In *Modern Aspects of Electrochemistry*, Vayenas, C.; White, R.; Gamboa-Aldeco, M., Eds. Springer New York: 2008; Vol. 42, pp 89-189.
3. Hori, Y., *Modern Aspects of Electrochemistry*. 2008; Vol. 42, p 89.
4. Hori, Y.; Kikuchi, K.; Suzuki, S., Production of CO and CH4 in electrochemical reduction of CO2 at metal electrodes in aqueous hydrogencarbonate solution. *Chemistry Letters* **1985,** (11), 1695-1698.

5. Hori, Y.; Wakebe, H.; Tsukamoto, T.; Koga, O., Electrocatalytic process of CO selectivity in electrochemical reduction of CO2 at metal electrodes in aqueous media. *Electrochimica Acta* **1994,** *39* (11), 1833-1839.
6. Lee, J.; Kwon, Y.; Machunda, R. L.; Lee, H. J., Electrocatalytic Recycling of CO2 and Small Organic Molecules. *Chemistry – An Asian Journal* **2009,** *4* (10), 1516-1523.
7. Koper, M. T., Structure sensitivity and nanoscale effects in electrocatalysis. *Nanoscale* **2011,** *3* (5), 2054-2073.
8. Kuhl, K. P.; Hatsukade, T.; Cave, E. R.; Abram, D. N.; Kibsgaard, J.; Jaramillo, T. F., Electrocatalytic Conversion of Carbon Dioxide to Methane and Methanol on Transition Metal Surfaces. *Journal of the American Chemical Society* **2014**.
9. Norskov, J. K.; Bligaard, T.; Rossmeisl, J.; Christensen, C. H., Towards the computational design of solid catalysts. *Nat Chem* **2009,** *1* (1), 37-46.
10. Peterson, A. A.; Abild-Pedersen, F.; Studt, F.; Rossmeisl, J.; Norskov, J. K., How copper catalyzes the electroreduction of carbon dioxide into hydrocarbon fuels. *Energy & Environmental Science* **2010,** *3* (9), 1311-1315.
11. Hirunsit, P.; Soodsawang, W.; Limtrakul, J., CO2 Electrochemical Reduction to Methane and Methanol on Copper-Based Alloys: Theoretical Insight. *The Journal of Physical Chemistry C* **2015,** *119* (15), 8238-8249.
12. Ma, X.; Li, Z.; Achenie, L. E.; Xin, H., Machine-Learning-Augmented Chemisorption Model for CO2 Electroreduction Catalyst Screening. *The journal of physical chemistry letters* **2015,** *6* (18), 3528-3533.
13. Kim, C.; Jeon, H. S.; Eom, T.; Jee, M. S.; Kim, H.; Friend, C. M.; Min, B. K.; Hwang, Y. J., Achieving Selective and Efficient Electrocatalytic Activity for CO2 Reduction Using Immobilized Silver Nanoparticles. *Journal of the American Chemical Society* **2015,** *137* (43), 13844-13850.
14. Zhang, Y.-J.; Sethuraman, V.; Michalsky, R.; Peterson, A. A., Competition between CO2 Reduction and H2 Evolution on Transition-Metal Electrocatalysts. *ACS Catalysis* **2014,** *4* (10), 3742-3748.
15. Chaplin, R. P. S.; Wragg, A. A., Effects of process conditions and electrode material on reaction pathways for carbon dioxide electroreduction with particular reference to formate formation. *Journal of Applied Electrochemistry* **2003,** *33* (12), 1107-1123.
16. Schild, C.; Wokaun, A.; Baiker, A., On the mechanism of CO and CO2 hydrogenation reactions on zirconia-supported catalysts: a diffuse reflectance FTIR study. *Journal of Molecular Catalysis* **1990,** *63* (2), 243-254.
17. Du, H.; Williams, C. T.; Ebner, A. D.; Ritter, J. A., In situ FTIR spectroscopic analysis of carbonate transformations during adsorption and desorption of CO2 in K-promoted HTlc. *Chemistry of Materials* **2010,** *22* (11), 3519-3526.
18. Nakamura, J.; Choi, Y.; Fujitani, T., On the Issue of the Active Site and the Role of ZnO in Cu/ZnO Methanol Synthesis Catalysts. *Topics in Catalysis* **2003,** *22* (3), 277-285.
19. Nakamura, J.; Uchijima, T.; Kanai, Y.; Fujitani, T., The role of ZnO in Cu/ZnO methanol synthesis catalysts. *Catalysis today* **1996,** *28* (3), 223-230.
20. Chu, S.; Fan, S.; Wang, Y.; Rossouw, D.; Wang, Y.; Botton, G. A.; Mi, Z., Tunable Syngas

Production from CO2 and H2O in an Aqueous Photoelectrochemical Cell. *Angewandte Chemie International Edition* **2016,** *55* (46), 14262-14266.
21. Grunwaldt, J.-D.; Molenbroek, A.; Topsøe, N.-Y.; Topsøe, H.; Clausen, B., In situ investigations of structural changes in Cu/ZnO catalysts. *Journal of Catalysis* **2000,** *194* (2), 452-460.
22. Ovesen, C.; Clausen, B.; Schiøtz, J.; Stoltze, P.; Topsøe, H.; Nørskov, J. K., Kinetic implications of dynamical changes in catalyst morphology during methanol synthesis over Cu/ZnO catalysts. *Journal of Catalysis* **1997,** *168* (2), 133-142.
23. Topsøe, N.-Y.; Topsøe, H., FTIR studies of dynamic surface structural changes in Cu-based methanol synthesis catalysts. *Journal of Molecular Catalysis A: Chemical* **1999,** *141* (1), 95-105.
24. Sahara, G.; Kumagai, H.; Maeda, K.; Kaeffer, N.; Artero, V.; Higashi, M.; Abe, R.; Ishitani, O., Photoelectrochemical Reduction of CO2 Coupled to Water Oxidation Using a Photocathode with a Ru (II)–Re (I) Complex Photocatalyst and a CoO x/TaON Photoanode. *Journal of the American Chemical Society* **2016,** *138* (42), 14152-14158.
25. Chen, S.; Wang, L.-W., Thermodynamic oxidation and reduction potentials of photocatalytic semiconductors in aqueous solution. *Chemistry of Materials* **2012,** *24* (18), 3659-3666.
26. Zhong, D. K.; Gamelin, D. R., Photoelectrochemical Water Oxidation by Cobalt Catalyst ("Co−Pi")/α-Fe2O3 Composite Photoanodes: Oxygen Evolution and Resolution of a Kinetic Bottleneck. *Journal of the American Chemical Society* **2010,** *132* (12), 4202-4207.
27. Carroll, G. M.; Gamelin, D. R., Kinetic analysis of photoelectrochemical water oxidation by mesostructured Co-Pi/α-Fe 2 O 3 photoanodes. *Journal of Materials Chemistry A* **2016,** *4* (8), 2986-2994.
28. Maroun, F.; Ozanam, F.; Magnussen, O.; Behm, R., The role of atomic ensembles in the reactivity of bimetallic electrocatalysts. *Science* **2001,** *293* (5536), 1811-1814.
29. Rodriguez, J. A.; Liu, P.; Stacchiola, D. J.; Senanayake, S. D.; White, M. G.; Chen, J. G., Hydrogenation of CO2 to methanol: Importance of metal–oxide and metal–carbide interfaces in the activation of CO2. *ACS Catalysis* **2015,** *5* (11), 6696-6706.
30. Osako, K.; Matsuzaki, K.; Hosono, H.; Yin, G.; Atarashi, D.; Sakai, E.; Susaki, T.; Miyauchi, M., Examination of interfacial charge transfer in photocatalysis using patterned CuO thin film deposited on TiO2. *APL Materials* **2015,** *3* (10), 104409.

Chapter 8

Summary

The research about photocatalytic CO_2 reduction has been paid more and more attention owing to its advantage of decreasing CO_2 using renewable energies and converting to organic molecules directly. Commonly the photocatalytic CO_2 reduction is achieved by the combination of light harvester and co-catalyst. The light harvester adsorbs solar energy and provide photoexcited electrons and holes, while the co-catalyst provides reaction sites, improves the reaction activity and the product selectivity.

This thesis reports the development of the co-catalyst of photocatalytic CO_2 reduction. Two kinds of co-catalysts, the Cu_xO nanoclusters and the Cu-Zn alloy (electrodes and nanoparticles) were developed. By using Cu-Zn alloy, highly selective HCOOH generation from CO_2 reduction was achieved, following with the discussion on the reaction pathways of CO_2 reduction. Further, by combining the Cu-Zn alloy co-catalyst with a Z-Scheme system, we achieved photocatalytic CO_2 into HCOOH under visible light irradiation, which will be the first report about highly selective CO_2 reduction under visible light without sacrificial agent based on robust and inorganic materials in this area. The content of each chapter is summarized below.

	Chapter 2	Chapter 3 and 5	Chapter 6
Co-catalyst		Higher selectivity and activity →	
	Cu_xO nanoclusters	Cu-Zn alloy electrode and NPs	Cu-Zn alloy NPs
Lighter harvetster		More challenging →	***Goal***
	$Nb_3O_8^-$ nanosheets	$SrTiO_3$ (for photocatalytic evaluation)	$CaFe_2O_4/WO_3$ Z-Scheme
Products	CO	HCOOH	
Publication	*ACS nano, 2014*	*J. Mater. Chem A, 2017*	*To be submitted*
	Evaluation system building	***Chapter 4*** Mechanism	***Chapter 7*** Contribution

Chapter 1 is the introduction about photocatalytic CO_2 reduction. The mechanism was

explained and the difficulties were also introduced based on the introduction of previous researches. The objective and research strategy of this research was clarified, answering to the difficulties. Based on the effect and research status of the co-catalyst and light harvester, I found that the development of co-catalyst is highly needed, thus our research was decided to focus on the development of highly selective and robust co-catalyst.

Chapter 2 describes the development and evaluation of a Cu_xO nanocluster co-catalyst. The Cu_xO nanocluster was successfully prepared by impregnation method and it showed good catalytic properties for CO_2 reduction during electrochemical evaluation. A $Nb_3O_8^-$ nanosheet material was developed as the light harvester during photocatalytic evaluation. The Cu_xO nanocluster grafted $Nb_3O_8^-$ nanosheets converted CO_2 into CO under UV irradiation. To clarify the electron transfer and element sources during the photocatalytic reaction, isotope trace experiments and electron spin resonance (ESR) analyses were operated. The results of isotope experiment confirmed that the produced CO was generated from CO_2 reduction, and in the oxidation side, water was the electron donor and oxidized into O_2. Based on this chapter, the comprehensive evaluation system and experimental setup have been established for subsequent chapters. This research was published in *ACS Nano*, the content can be briefly summarized by Figure 8.1.

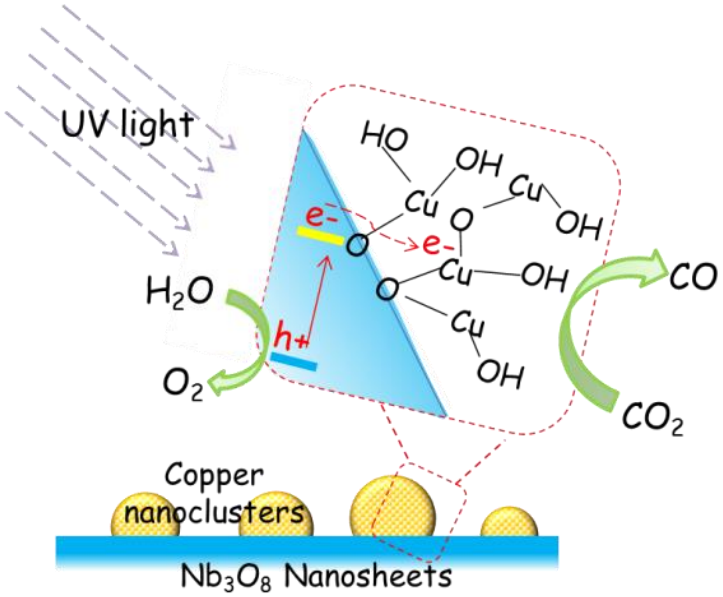

Figure 8.1 *The illustration of the developed Cu_xO nanocluster grafted $Nb_3O_8^-$ nanosheets, converting CO_2 into CO under UV irradiation.*

To improve the activity and selectivity, in ***Chapter 3***, a Cu-Zn alloy electrode has been developed. It was prepared by vacuum sealing method and the composition was characterized as Cu_5Zn_8 intermetallic. The electrochemical evaluation proved that the Cu-Zn electrode could convert CO_2 into HCOOH with Faradic efficiency of 79%. When the Cu-Zn electrode was used as the cathode in a photoelectrochemical cell and $SrTiO_3$ (STO) electrode was used as

photoanode and irradiated by UV light, CO_2 was reduced into HCOOH in the cathodic side without any bias-potential application. The Faradic efficiency for HCOOH generation was over 70% and the turnover number (TON) for CO_2 reduction was as high as 1458. That means high selectivity and activity was owned by Cu-Zn alloy electrode.

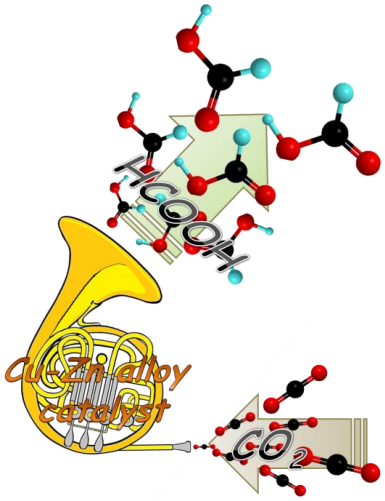

Figure 8.2 *the illustration showing that Cu-Zn alloy catalyst catalyzing CO_2 into HCOOH.*

To understand the reason for the high selectivity of the Cu-Zn alloy, the reaction mechanism was studied in ***Chapter 4***. Literature researches about the reaction pathways and their relationship with the co-catalyst surface condition were reviewed. *In-situ* FTIR analysis was operated to the Cu-Zn NPs loaded STO powder in humid CO_2 atmosphere, by comparing the spectra under humid Ar atmosphere. Consequently, we found the active species of HCOOH generation on the surface of Cu-Zn alloy. In particular, the bidentate carbonate specie was detected on the surface of Cu-Zn/STO, whereas monodentate carbonate was appeared on the surface of Cu/STO sample. These results strongly supported that the CO_2 was reduced to HCOOH through weakly adsorbed bidentate species on the surface of Cu-Zn cocatalyst. In this chapter I presented the strategy to achieve highly selective co-catalyst design, based on tuning the surface adsorption strength for the active species during the reaction pathway. The content of ***Chapter 3*** and ***Chapter 4***, the Cu-Zn NPs prepared by vacuum sealing method and the mechanism analyses in ***Chapter 5*** were published in *Journal of Materials Chemistry A* and chosen to be the front cover with greatest honor.

Chapter 5 describes the nanoparticulation of Cu-Zn alloy and demonstrates its versatility for coating on light harvesting semiconductor. Two methods were tried, *i. e.* vacuum sealing and chemical co-reduction methods. In the case of vacuum sealing, the Cu-Zn alloy NPs were successfully coated onto the surface of STO, but the catalytic performance was decreased by the extra pure Zn NPs which loaded onto the STO surface. Chemical co-reduction method was then managed. This method can easily synthesize different kinds of alloy nanoparticles with different compositions. Cu_5Zn_8 NPs were successfully synthesized and their catalytic properties

were reconfirmed by electrochemical evaluation. Using an ink method, the Cu-Zn NPs can be easily loaded onto the surface of light harvester under moderate conditions, thus the versatility of the Cu-Zn alloy co-catalyst was highly improved. The photocatalytic performance of converting CO_2 into HCOOH with high selectivity was also confirmed.

In ***Chapter 6***, we used the developed Cu-Zn NPs as co-catalyst and achieved photocatalytic CO_2 reduction under visible light irradiation. A Z-Scheme system using $CaFe_2O_4$ (CFO) as photocathode and WO_3 nanotrees as photoanode were enabled. By decorating the surface of CFO using Cu-Zn NPs, the photocatalytic performance for CO_2 reduction increased significantly. HCOOH was generated as main product and water was confirmed to be the electron donor during the reaction.

Compared to the previous researches, this work reveals significant performance for not only achieving visible light photocatalytic CO_2 reduction without sacrificial agents, but also showing outstanding selectivity for HCOOH generation. I would like to emphasize that this work is the first report to achieve more than 50% selective CO_2 reduction under visible light irradiation through water oxidation on the basis of robust inorganic materials. Besides, the light-to-energy conversion efficiency reached 0.028%, which is much higher than the previous outstanding reports (c. f. *J. Am. Chem. Soc.* 138, 14152, 2017).

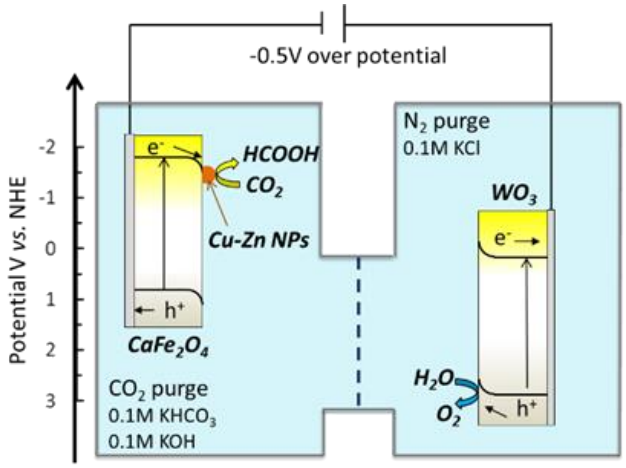

Figure 8.3 *the illustration of the visible-light-driven CO_2 reduction achieved by Cu-Zn NPs decorated CFO/WO_3 system*

Chapter 7 describes the scientific, engineering and industrial contribution of this research to broad readers in the field of chemistry and materials science, also the future works are explained in this chapter.

At last, ***Chapter 8*** summarizes this research.

Acknowledgement

This thesis wouldn't have been finished unless various supporting from the following people.

Firstly, I want to show my appreciation to *Prof. A. Nakajima, Prof. H. Hinode, Prof. S. Matsushita, and Prof. N. Matsushita* for carefully reviewing my thesis and undertaking the investigation of my work.

I would like to give my greatest appreciate and respects to my advisors, *Prof. M. Miyauchi, Prof. E. Sakai, Prof. S. Nakajima* and the Assistant *Prof. D. Atarashi, Prof. A. Yamaguchi* for their benevolent conduction for my research and life during the last five years. They are full of kindness and always leading me to make sensible decisions, encouraging me when I was frustrated. Their serious attitude to research influenced me to keep approaching to perfect. They gave me education much more than what I expected. Especially thanks *Prof. M. Miyauchi* for his kindest guide and concern for me and always showing me wonderful and new area.

I also appreciate the advise from *Prof. H. Abe* from NIMS. He was the most amazing person I ever met and he gave me benevolent conduction for my research, used his wonderful sense of art and humor to inspire and complete my work. I also appreciate *Ms. Y. Nohara* and all the fellows in NIMS for their friendly company and disinterested help.

The laboratory members I cooperated in the past five years are all wonderful people with easygoing and positive hearts, I always feel comfortable and benefited to work and communicate with them. I would give my special appreciate to *Dr. Srinivasan Nagarajan* for his professional direct, the senior members who tutored me since the first day I came to Japan, and *Mr. H.Sako* for his cooperation researches.

It's my honor to get the supporting from *Advanced Catalytic Trasformation program for Carbon utilization (ACT-C)* from Japanese Science and Technology Agency. Also I appreciate the financial supporting from *the Japan Society for the Promotion of Science (JSPS)* and *Japanese Government and Tokyo Institute of Technology from the Japanese Government (Monbukagakusho) Scholarship program*.

There were many other Professors and staffs supported me in this research. I would like to thank *Mr. A. Genseki and Mr. K. Hori* in the Center for advanced materials analysis for the evaluation with TEM, thank *Miss. T. Kanai* for the XPS spectra analysis, thank *Prof. Y. Nosaka,* P*rof. M. Nishikawa,* for the ESR analysis, thank *Dr. S. Ueda* for the analyses in Spring-8.

It's my pleasure to show my grateful and best regards to my parents who are always supporting me and cheering for me. Thank my boyfriend *Mr. Hanli Liu* and my cat *Miss. Paigu* for keeping me positive and full of love. Thank all my friends, they made me a better person and they are always on my prayers.

At last, I would like to offer my best regards to all of those who supported me in any respect during the completion of the research.

Yin Ge 2017/07/13

Appendix

The preparation and evaluation of Zn- and Sn-based alloys.

A1.1 Background.

For electrocatalytic CO_2 reduction, the development of CO_2 electroreduction catalysts is important, they also play an important role in photocatalytic CO_2 reduction as co-catalyst. In the previous researches, various metal electrodes were evaluated for electrocatalytic CO_2 reduction.[1-3] For example, Azuma *et.al*, summarized the distribution of the metal catalysts of electrocatalytic water and CO_2 reduction and their products, as shown in Figure A1.1. As we can see, the metals behaving CO_2 reduction property concentrated in the red area, in which copper, silver and gold behave best performance thus using them as catalysts already became a common sense in this field. The metal nanoparticles which is environmental abundant and easily synthesised such as copper,[4-14] silver,[15-16] gold[17-18] and stannic oxide[19] or tin[20] has already accumulated lots of results in both photocatalytic or electrocatalytic CO_2 reduction application.

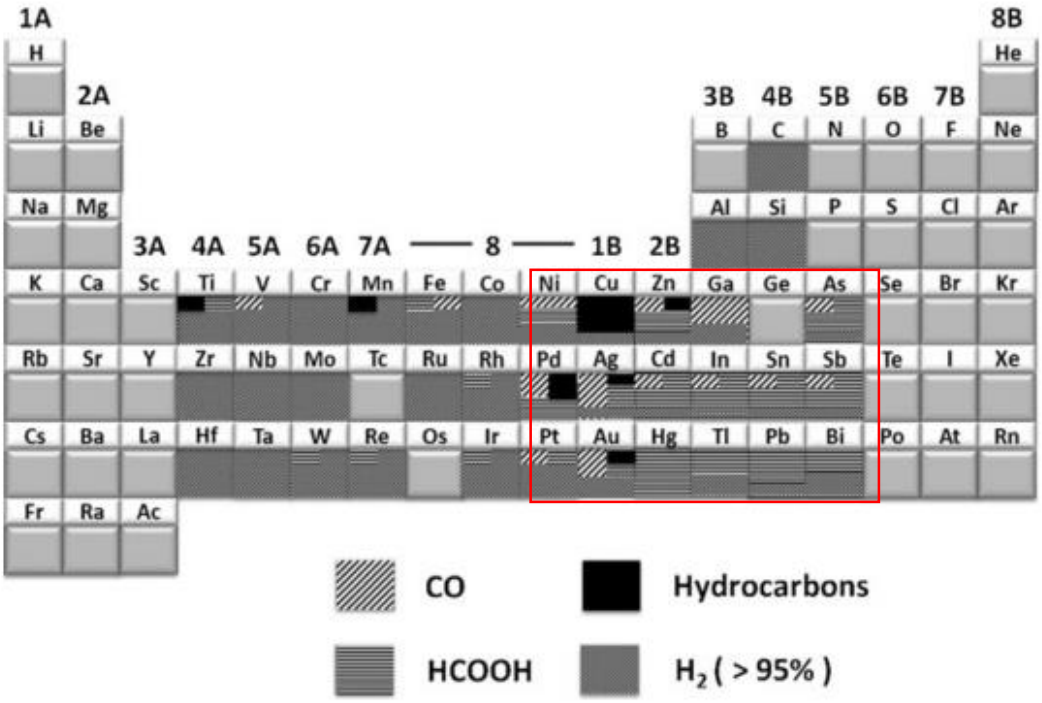

Figure A1.1 *Periodic table showing the electrocatalytic CO_2 reduction products at ambient operation conditions.*

Despite the advances in this field, at present only few studies have exploited the wide range of possibilities that binary combinations of metals offer as cocatalysts in photocatalytic CO_2 reduction. Recently, some kinds of intermetallic material of these metal elements were also developed as the CO_2 reduction catalysts, such as Cu-Au.[21-24] Continuing with this approaching, we were trying to develop more intermetallic materials combining by the already-known metal elements.

During the internship, I was under Professor Hideki Abe's advice. It's great opportunity because Prof. Abe is a specialist in the area of both intermetallic and catalysis. His group already got lots of achievements such as catalytic CO by using Pt_3Ti nanoparticles [25] and photocatalytic water splitting by using Sn_3O_4.[26]

In principle, the metal elements we chose must respect the element strategy, which means they should be environmental friendly and abundant, thus element such as Cd, Hg, As, Ga, In, Tl *et,al* should not be considered as the candidates. Also, to get high originality, most of the combination with copper such as Cu-Au and Cu-Ni should be avoided. At last, to use the experimental procedure which will be introduced in the second session, metal elements with low melting point are needed. According to the above reasons, we chose Zn and Sn combining with Cu, Ni, Ag and Au as the research objects.

A1.2 Experimental and Evaluation

A1.2.1 The synthesis of metal nanoparticles.

To prepare the Zn-X and Sn-X (X=Cu, Ni, Ag, Au) intermetallic electrodes, the X metal nanoparticles grafted electrodes were prepared. Then the further treatments to synthesis intermetallic electrodes were operated by Zn vapour and Sn vapour, which will be introduced in the second part.

Titanium metal sheets were used as the electrode substrate because it's not active for electrocatalytic CO_2 reduction.[31] Ti sheets (0.1×200×200 mm; Nirako Corp.) were cleaned by ultrasonication sequentially in non-phosphate detergent, distilled water (3 times), and ethanol, and were then immediately dried using a nitrogen gas gun.

In the beginning of the internship, Cu metal nanoparticles was synthesized by chemical reduction methods as the first try. Sodium borohydride was used as the reduction agent.[4] $CuCl_2 \cdot 2H_2O$ (170.5mg) was dissolved in 5mL H_2O, and the Ti sheets was put in the solution for one night to get infiltrated. The glass bottle containing the mixture was put in the ice bath to slow the reaction speed before adding a freshly made $NaBH_4$ solution (317.4mg in 3mL H_2O) drop by drop. The Ti sheet was taken out from the bottle till the color of the solution and the surface of the Ti sheet didn't change any more. Then the Ti sheet was washed by distilled water and dried under Ar gas flux.

However, the Cu nanoparticles in the surface of Ti sheets was not uniform and the synthesis

procedure was time-costy. In the later experiments, the X metal nanoparticles were produced by sputtering. The thickness of the coating is about 50nm. The electrodes was shown in Figure A2.1 (a).

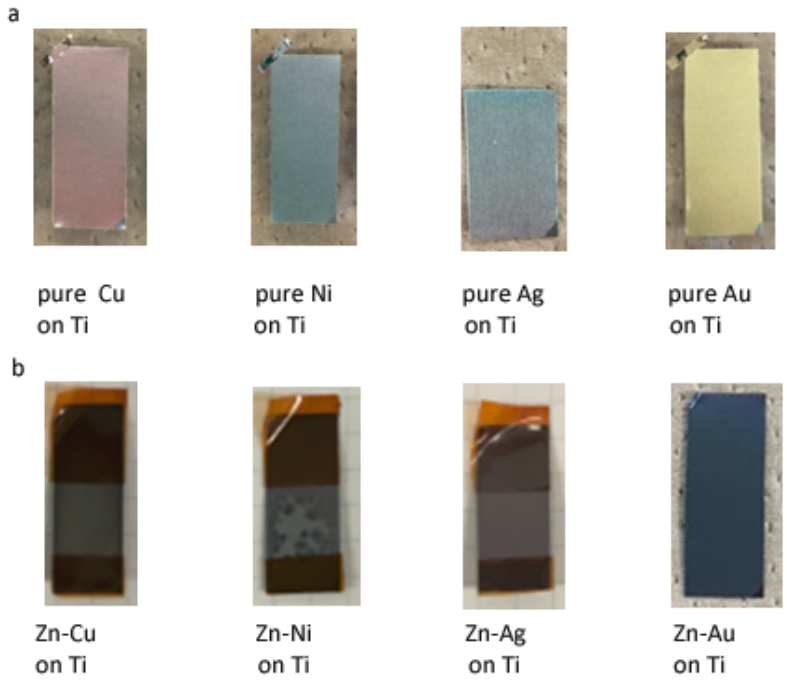

Figure A 2.1 *the prepared electrodes*

A1.2.2 Vacuum sealing.

The Zn or Sn coating of X metal nanoparticles coated Ti sheets in Zn or Sn vapour was achieved by a method called vacuum sealing.

A silica glass tube was heated by hydrogen flame evenly while rotating. The heated part shrunk and shrunk till it was cut. The cut end was heated to get finely rounded and that how we got a silica burette. Then pure Zn metal beads and X metal nanoparticles coated Ti sheets were put into the burette, separated by a silica wool, as the Figure A2.2 shows. Then the open side of this burette was heated until a slim neck with a little hole through and connected to a vacuum pump, vacuuming for 30 minutes. At last the neck was cut by hydrogen flame while vacuuming and a vacuum sealed silica tube with pure Zn and X metal nanoparticles inside was produced. The photo of the electrodes was shown in Figure A2.1(b).

Figure A2.2 *the vacuum sealed silica glass tube with pure Zn beads and Cu/Ti electrodes inside.*

At last the silica tube was put in the oven and heated to 500°C over a 30 minutes period, and was then held at 500°C for 30 minutes.

To get a different composition, silica tubes heated under 400°C were also prepared. The synthesis of Sn-X electrodes was operated in a similar way and the tube was heated under 300°C and 400°C at last.

A1.2.3 Evaluation.

The eletrocatalytic properties of the intermetallic electrodes were evaluated by electrochemical methods. A sealed electrochemical cell was constituted, as shown in Figure 2.3, the evaluated electrodes were used as working electrodes and a platinum sheet was used as counter electrode. The reference was Ag/AgCl electrode and 0.1M $KHCO_3$ solution was used as electrolyte. Ar gas was purged into the electrolyte for 15 minutes to make a non-CO_2 atmosphere and the surface of the electrodes was cleaned by applying a bias-potential (CV, -1.8V~0.1V *vs.* Ag/AgCl, 10 cycles). Then the LSV (-0.1V~-1.8V *vs.* Ag/AgCl, 2 times) curve was measured in Ar atmosphere. CO_2 was purged into the electrolyte for 30 minutes then to produce a CO_2-satisfied environment and the LSV curve was also measured. The electrocatalytic properties of the electrodes was evaluated by comparing the difference between the LSV curves under Ar and CO_2 atmosphere.

The composition of the electrode was detected by Hard X-Ray photoemission spectrum (HX-PES), X-Ray diffraction (XRD) and X-Ray Fluorescence (XRF).

The products in the headspace of the electrochemical cell was also detected by Gas Chromatograph (flame ionization detector (FID) equipped with a methanizer apparatus).

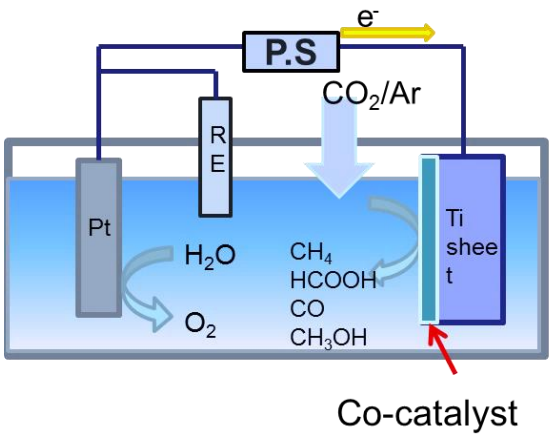

Figure A2.3 *the electrochemical cell used for electrocatalytic evaluation.*

A1.3 Results and Discussion

A1.3.1 Zn-X intermetallic electrodes.

3.1.1 Zn-Cu intermetallic (As introduced in Chapter3 in details, omitted here)

3.1.2 Zn-Ni intermetallic

The LSV curves of the Zn-Ni intermetallic electrodes were shown in Figure A3.5. From those results, we speculate that Ni electrodes behave good electrocatalytic property for water splitting rather than CO_2 reduction, and the adding of Zn improved its ability for both water and CO_2 reduction, however, without products analysis, we cannot confirm which one own higher competitive force. The composition of the Zn-Ni electrodes before and after reaction was listed in Table A3.2.

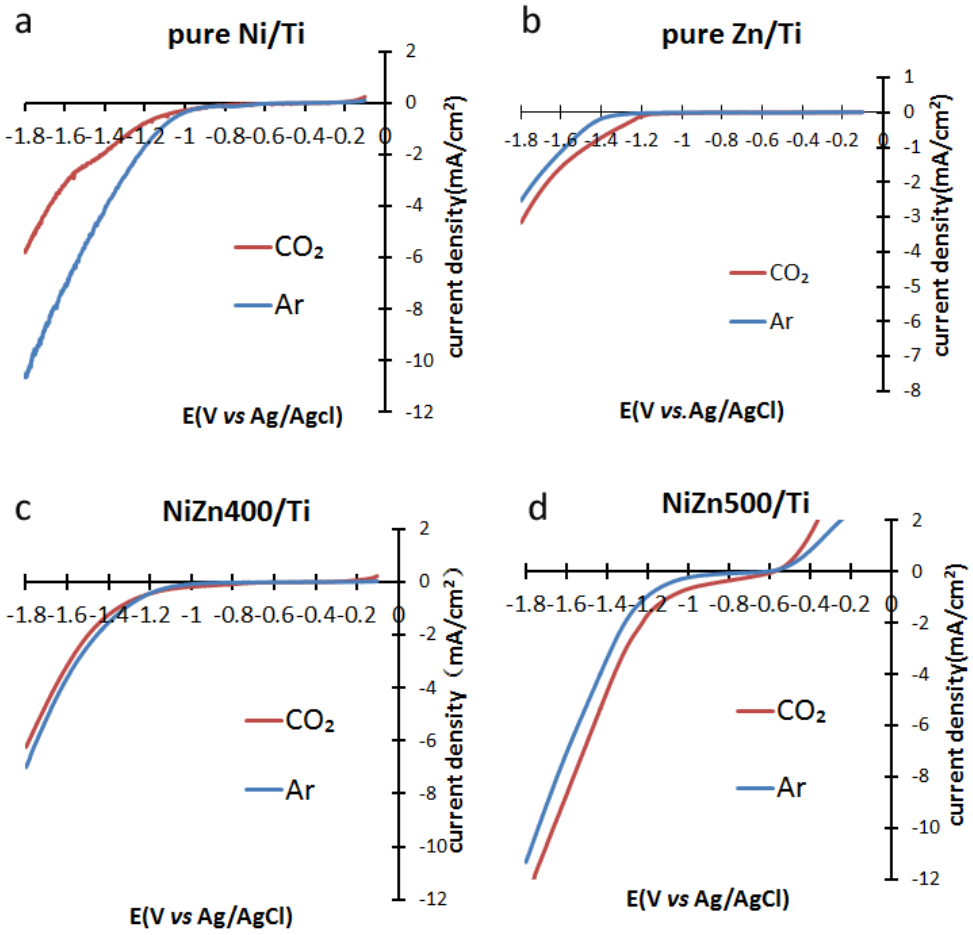

Figure A3.5 *the LSV curves of (a) pure Ni sputtered Ti sheets, (b) pure Zn coated Ti sheets, (c) Zn-Ni intermetallic coated Ti sheets annealed under 400℃, (d) Zn-Ni intermetallic coated Ti sheets annealed under 500℃ in Ar or CO_2 atmosphere, respectively.*

Table A3.2 *The composition of prepared Zn-Ni intermetallic electrodes before and after reaction.*

Zn concentration (wt%)	NiZn 400	NiZn 500
Before	7	88
After	4	86

3.1.3 Zn-Ag and Zn-Au intermetallic

From the results of the electrochemical evaluation, as shown in Figure A3.6, after adding Zn, the onset potential became higher than that of pure Ag. The current difference also didn't show much change, which indicated that the adding of Zn do not lead to any improvement.

Pure Au is a good electrochemical CO_2 reduction catalyst, which is also proved by the electrochemical evaluation results. However, the Zn-Au intermetallic electrodes didn't behave better performance.

The composition of the Zn-Ag electrodes was listed in Table A3.3, the composition detection of Zn-Au failed because in XRF spectra the AuM peak and ZnL peak is too near to separate.

Table 3.3 *The composition of prepared Zn-Ag intermetallic electrodes before and after reaction.*

Zn concentration (wt%)	AgZn 400	AgZn 500
Before	1	40
After	1	40

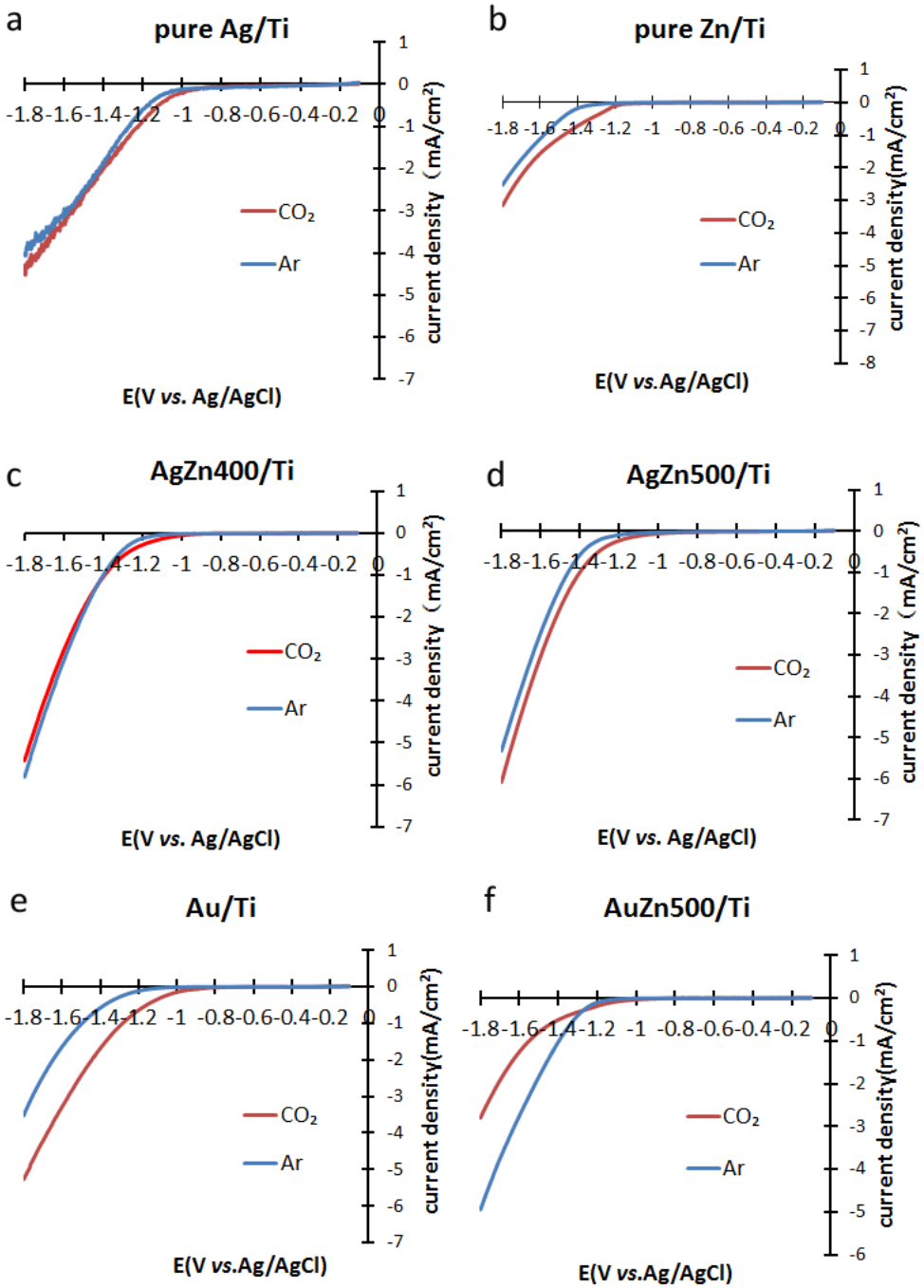

Figure A3.5 *the LSV curves of (a) pure Ag sputtered Ti sheets, (b) pure Zn coated Ti sheets, (c) Zn-Ag intermetallic coated Ti sheets annealed under 400 ℃, (d) Zn-Ag intermetallic coated Ti sheets annealed under 500 ℃, (e) pure Ag sputtered Ti sheets, (f) Zn-Au intermetallic coated Ti sheets annealed under 500 ℃ in Ar or CO_2 atmosphere, respectively.*

3.1.4 Section Summary

According to the electrochemical evaluation, when combining with zinc, the electrocatalytic CO_2 reduction performance of copper and nickel improved, but no significant change for silver and gold. The reason might be explained by the CO binding energy, which is found to be an important factor for the reduction of CO_2 in lots of researches.[7, 27-28] As we can see in Figure A3.6, metals that have strong CO binding strength such as Pt, Ni and Cu are easily poisoned by CO or other intermediates thus hydrogen evolution behave more favorable than CO_2 reduction. On the other hand, metals that have weak CO binding strength such as Zn and Ag produce carbon monoxide during the reaction since CO(g) is easily to desorbed from the surface so the further reduction becomes difficult to happen. Thus gold behave highest current density for CO_2 reduction among these transition metals. This figure can also explain why the combination of Cu-Zn and Ni-Zn behaved better performance while Au-Zn and Ag-Zn didn't. Besides, the selectivity for each kinds of CO_2 reduction products also changes after combination, thus detailed products analyses are needed in the future work.

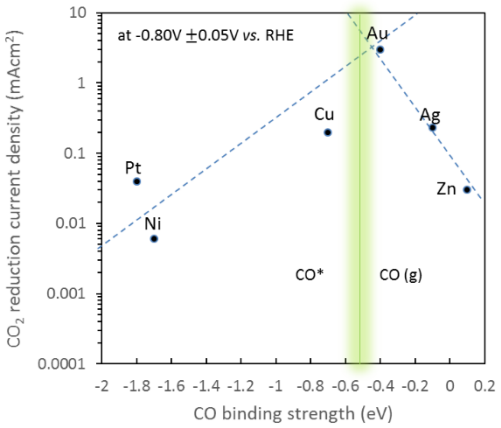

Figure A3.6 *the volcano plots of particle current density for CO_2 reduction at -0.8V (vs. RHE) vs CO binding strength.*

A3.2 Sn-X intermetallic electrodes.

3.1.5 Sn-Cu, Sn-Ni and Sn-Ag intermetallic

According to the electrochemical evaluation results, the performance of pure Sn is not satisfying, but we cannot judge it as an noneffective catalyst for CO_2 reduction without the products detection.

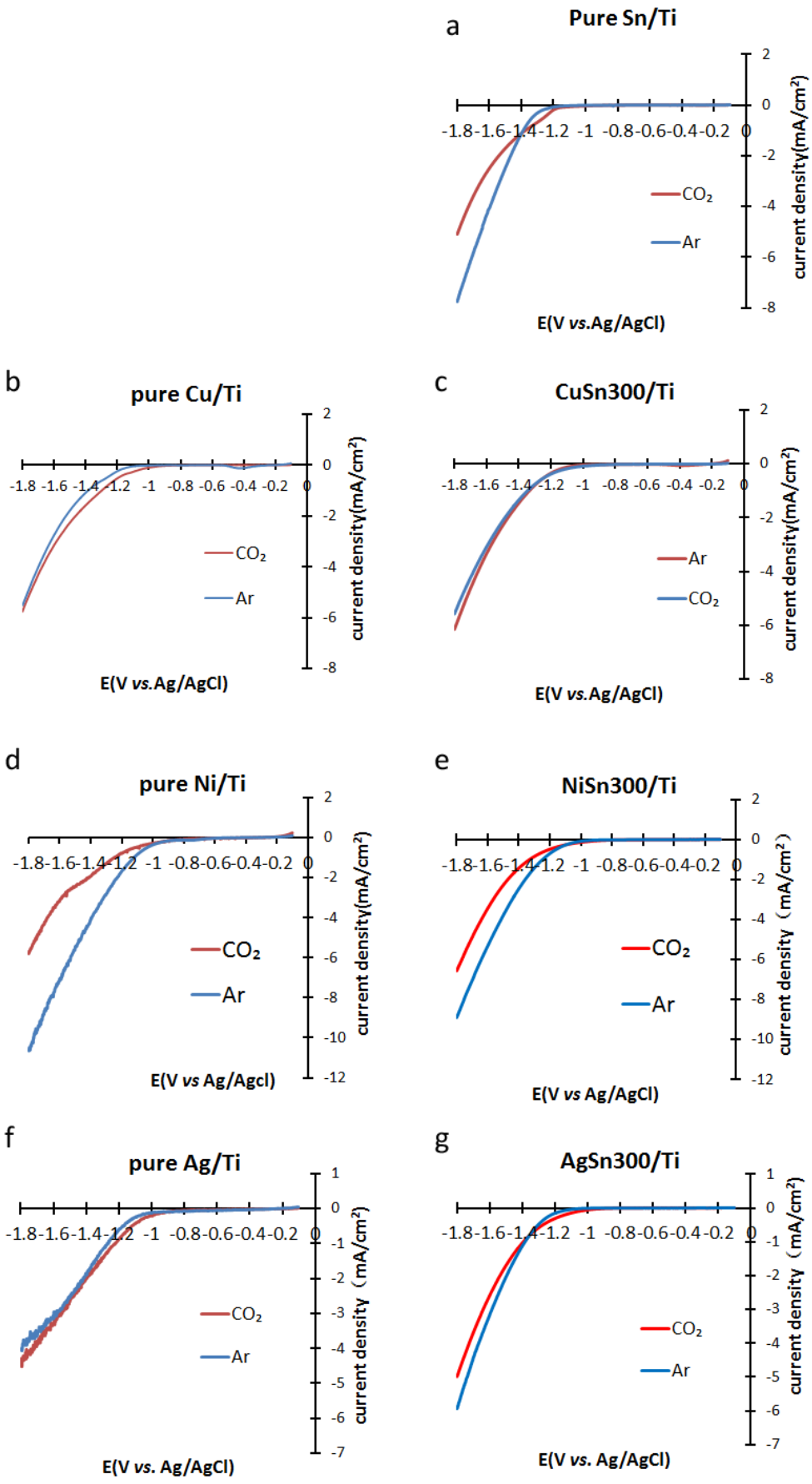
a
Pure Sn/Ti
-1.8 -1.6 -1.4 -1.2 -1 -0.8 -0.6 -0.4 -0.2 0
2 0 -2 -4 -6 -8
current density(mA/cm²)
CO₂
Ar
E(V vs.Ag/AgCl)
b
pure Cu/Ti
-1.8 -1.6 -1.4 -1.2 -1 -0.8 -0.6 -0.4 -0.2 0
2 0 -2 -4 -6 -8
current density(mA/cm²)
CO₂
Ar
E(V vs.Ag/AgCl)
c
CuSn300/Ti
-1.8 -1.6 -1.4 -1.2 -1 -0.8 -0.6 -0.4 -0.2 0
2 0 -2 -4 -6 -8
current density(mA/cm²)
Ar
CO₂
E(V vs.Ag/AgCl)
d
pure Ni/Ti
-1.8 -1.6 -1.4 -1.2 -1 -0.8 -0.6 -0.4 -0.2 0
2 0 -2 -4 -6 -8 -10 -12
current density(mA/cm²)
CO₂
Ar
E(V vs Ag/Agcl)
e
NiSn300/Ti
-1.8 -1.6 -1.4 -1.2 -1 -0.8 -0.6 -0.4 -0.2 0
2 0 -2 -4 -6 -8 -10 -12
current density（mA/cm²）
CO₂
Ar
E(V vs Ag/AgCl)
f
pure Ag/Ti
-1.8 -1.6 -1.4 -1.2 -1 -0.8 -0.6 -0.4 -0.2 0
1 0 -1 -2 -3 -4 -5 -6 -7
current density（mA/cm²）
CO₂
Ar
E(V vs. Ag/AgCl)
g
AgSn300/Ti
-1.8 -1.6 -1.4 -1.2 -1 -0.8 -0.6 -0.4 -0.2 0
1 0 -1 -2 -3 -4 -5 -6 -7
current density（mA/cm²）
CO₂
Ar
E(V vs. Ag/AgCl)

Figure A3.7 *the LSV curves of (a) pure Sn sputtered Ti sheets, (b) pure Cu coated Ti sheets, (c) Sn-Cu intermetallic coated Ti sheets annealed under 300℃, (d) pure Ni coated Ti sheets, (e) Sn-Ni intermetallic coated Ti sheets annealed under 300℃, (f) pure Ag coated Ti sheets, (g) Sn-Ag intermetallic coated Ti sheets annealed under 300℃ in Ar or CO_2 atmosphere, respectively.*

Table A3.4 *the composition of the Sn-Cu, Sn-Ni and Sn-Ag electrodes.*

Sn concentration (wt%)	CuSn 300	NiSn 300	AgSn300
Before	33	86	5
After	22	92	15

Also the intermetallic electrodes of Sn-Cu, Sn-Ni and Sn-Ag (annealing at 300°C) didn't show obvious performance of CO_2 reduction (shown in Figure 3.7). The composition of these electrodes was shown in Table A3.4.

3.1.6 Sn-Au intermetallic

Different with the other Sn-X intermetallic electrodes, the Sn-Au showed outstanding property for electrocatalytic CO_2 reduction. As shown in Figure 3.8. The current density tripled those of pure Au and pure Sn and the onset potential also shifted from -1.0V to -0.8V *vs.* Ag/AgCl. This is the first time that Sn-Au has found to be an effective electrochemical CO_2 redution catalyst, which is worth for deeper research.

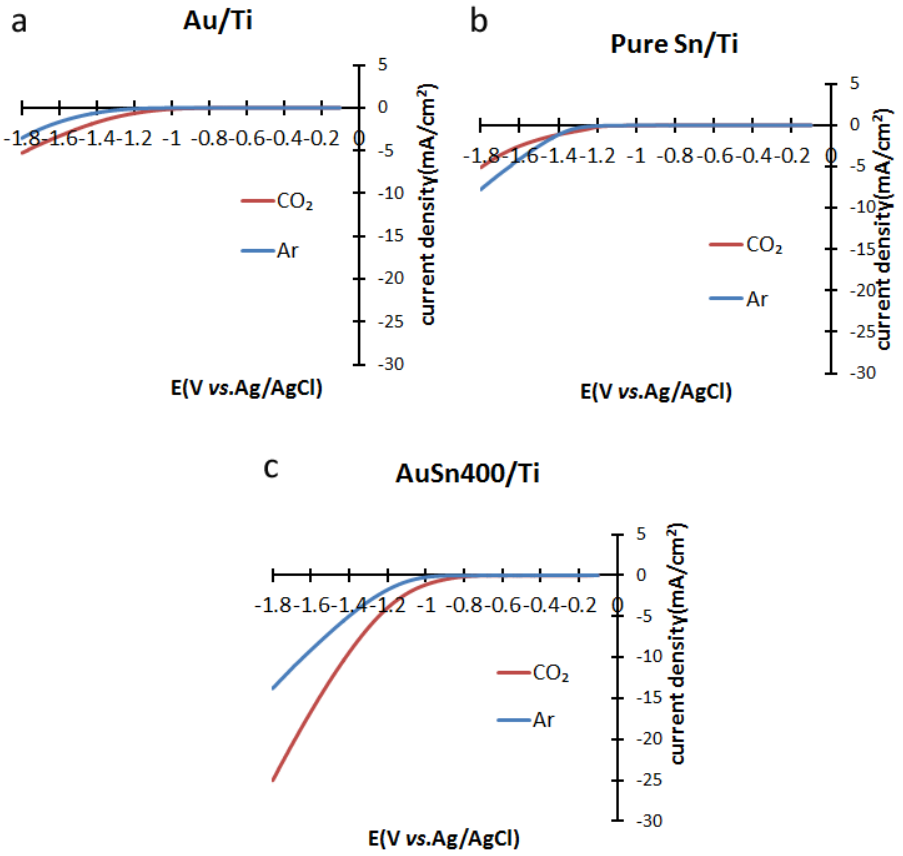

Figure A3.7 *the LSV curves of (a) pure Au sputtered Ti sheets, (b) pure Sn coated Ti sheets, (c) Sn-Au intermetallic coated Ti sheets annealed under 400℃ in Ar or CO_2 atmosphere, respectively.*

3.1.7 Section Summary

I expected to explain the improvement of Au-Sn by the similar theory with Zn-Cu, however, the CO binding energy of Sn was barely researched. However, according to the bonding adsorption strength of intermediate metal-hydrogen (M-H) bond formed during the electrode reaction,[28] the combination of Sn and Au indeed locates in an appropriate area which avoids the evolution of hydrogen and favors the CO_2 reduction. The lack of research also indicated that this result possess high originality.

A1.4 Conclusion

Combining with zinc improved the electrocatalytic properties of copper and nickel, especially the copper-zinc intermetallics behave good CO_2 reduction property, carbon monoxide and methane were detected from the gas phase. But improvement was not observed

on silver and gold.

Intermetallic of tin and gold behave good electrocatalytic CO_2 reduction property, however the other intermetallics of tin with copper, nickel and silver didn't show good performance, but after the composition optimization, they still have potential working as the electrocatalytic CO_2 reduction catalysts.

Both the Zn-Cu and the Sn-Au intermetallic electrodes have high originality as catalyst in the field of electrocatalytic CO_2 redution.

References

1. Hori, Y., Electrochemical CO2 Reduction on Metal Electrodes. In Modern Aspects of Electrochemistry, Vayenas, C.; White, R.; Gamboa-Aldeco, M., Eds. Springer New York: 2008; Vol. 42, pp 89-189.

2. Azuma, M.; Hashimoto, K.; Hiramoto, M.; Watanabe, M.; Sakata, T., Electrochemical Reduction of Carbon Dioxide on Various Metal Electrodes in Low - Temperature Aqueous KHCO 3 Media. Journal of the Electrochemical Society ***1990,*** *137 (6), 1772-1778.*

3. Lee, J.; Kwon, Y.; Machunda, R. L.; Lee, H. J., Electrocatalytic Recycling of CO2 and Small Organic Molecules. Chemistry – An Asian Journal ***2009,*** *4 (10), 1516-1523.*

4. Baturina, O. A.; Lu, Q.; Padilla, M. A.; Xin, L.; Li, W.; Serov, A.; Artyushkova, K.; Atanassov, P.; Xu, F.; Epshteyn, A.; Brintlinger, T.; Schuette, M.; Collins, G. E., CO2 Electroreduction to Hydrocarbons on Carbon-Supported Cu Nanoparticles. ACS Catalysis ***2014,*** *4 (10), 3682-3695.*

5. Calle-Vallejo, F.; Koper, M. T. M., Theoretical Considerations on the Electroreduction of CO to C2 Species on Cu(100) Electrodes. Angewandte Chemie International Edition ***2013,*** *52 (28), 7282-7285.*

6. Durand, W. J.; Peterson, A. A.; Studt, F.; Abild-Pedersen, F.; Nørskov, J. K., Surf. Sci. ***2011,*** *605, 1354.*

7. Gattrell, M.; Gupta, N.; Co, A., A review of the aqueous electrochemical reduction of CO2 to hydrocarbons at copper. Journal of Electroanalytical Chemistry ***2006,*** *594 (1), 1-19.*

8. Manthiram, K.; Beberwyck, B. J.; Alivisatos, A. P., Enhanced Electrochemical Methanation of Carbon Dioxide with a Dispersible Nanoscale Copper Catalyst. Journal of the American Chemical Society ***2014,*** *136 (38), 13319-13325.*

9. Nie, X.; Esopi, M. R.; Janik, M. J.; Asthagiri, A., Selectivity of CO2 Reduction on Copper Electrodes: The Role of the Kinetics of Elementary Steps. Angewandte Chemie International Edition ***2013,*** *52 (9), 2459-2462.*

10. Peterson, A. A.; Abild-Pedersen, F.; Studt, F.; Rossmeisl, J.; Norskov, J. K., How copper catalyzes the electroreduction of carbon dioxide into hydrocarbon fuels. Energy & Environmental Science ***2010,*** *3 (9), 1311-1315.*

11. Reske, R.; Duca, M.; Oezaslan, M.; Schouten, K. J. P.; Koper, M. T. M.; Strasser, P., Controlling Catalytic Selectivities during CO2 Electroreduction on Thin Cu Metal Overlayers. The Journal of Physical Chemistry Letters ***2013,*** *4 (15), 2410-2413.*

12. Reske, R.; Mistry, H.; Behafarid, F.; Roldan Cuenya, B.; Strasser, P., Particle Size Effects in the Catalytic Electroreduction of CO2 on Cu Nanoparticles. Journal of the American Chemical Society ***2014,*** *136 (19), 6978-6986.*

13. Ba, X.; Yan, L.-L.; Huang, S.; Yu, J.; Xia, X.-J.; Yu, Y., New Way for CO2 Reduction under Visible Light by a Combination of a Cu Electrode and Semiconductor Thin Film: Cu2O Conduction Type and Morphology Effect. The Journal of Physical Chemistry C ***2014,*** *118 (42), 24467-24478.*

14. Shown, I.; Hsu, H.-C.; Chang, Y. C.; Lin, C.-H.; Roy, P. K.; Ganguly, A.; Wang, C.-H.; Chang, J. K.; Wu, C.-I.; Chen, L.-C., Highly Efficient Visible Light Photocatalytic Reduction of CO2 to Hydrocarbon Fuels by Cu-NPs Decorated Graphene Oxide. Nano letters ***2014****.*

15. Iizuka, K.; Wato, T.; Miseki, Y.; Saito, K.; Kudo, A., Photocatalytic reduction of carbon dioxide over Ag cocatalyst-loaded ALa4Ti4O15 (A= Ca, Sr, and Ba) using water as a reducing reagent. Journal of the American Chemical Society ***2011,*** *133 (51), 20863-20868.*

16. Lim, H.-K.; Shin, H.; Goddard, W. A.; Hwang, Y. J.; Min, B. K.; Kim, H., Embedding Covalency into Metal Catalysts for Efficient Electrochemical Conversion of CO2. Journal of the American Chemical Society ***2014,*** *136 (32), 11355-11361.*

17. Zhu, W.; Michalsky, R.; Metin, Ö.; Lv, H.; Guo, S.; Wright, C. J.; Sun, X.; Peterson, A. A.; Sun, S., Monodisperse Au Nanoparticles for Selective Electrocatalytic Reduction of CO2 to CO. Journal of the American Chemical Society ***2013,*** *135 (45), 16833-16836.*

18. Kauffman, D. R.; Alfonso, D.; Matranga, C.; Qian, H.; Jin, R., Experimental and Computational Investigation of Au25 Clusters and CO2: A Unique Interaction and Enhanced Electrocatalytic Activity. Journal of the American Chemical Society ***2012,*** *134 (24), 10237-10243.*

19. Magesh, G.; Kim, E. S.; Kang, H. J.; Banu, M.; Kim, J. Y.; Kim, J. H.; Lee, J. S., A versatile photoanode-driven photoelectrochemical system for conversion of CO 2 to fuels with high faradaic efficiencies at low bias potentials. Journal of Materials Chemistry A ***2014,*** *2 (7), 2044-2049.*

20. Zhang, S.; Kang, P.; Meyer, T. J., Nanostructured Tin Catalysts for Selective Electrochemical Reduction of Carbon Dioxide to Formate. Journal of the American Chemical Society ***2014,*** *136 (5), 1734-1737.*

21. Friebel, D.; Mbuga, F.; Rajasekaran, S.; Miller, D. J.; Ogasawara, H.; Alonso-Mori, R.; Sokaras, D.; Nordlund, D.; Weng, T.-C.; Nilsson, A., Structure, Redox Chemistry, and Interfacial Alloy Formation in Monolayer and Multilayer Cu/Au(111) Model Catalysts for CO2 Electroreduction. The Journal of Physical Chemistry C ***2014,*** *118 (15), 7954-7961.*

22. Kang, Q.; Wang, T.; Li, P.; Liu, L.; Chang, K.; Li, M.; Ye, J., Photocatalytic Reduction of Carbon Dioxide by Hydrous Hydrazine over Au–Cu Alloy Nanoparticles Supported on SrTiO3/TiO2 Coaxial Nanotube Arrays. Angewandte Chemie International Edition ***2015,*** *54 (3), 841-845.*

23. Kim, D.; Resasco, J.; Yu, Y.; Asiri, A. M.; Yang, P., Synergistic geometric and electronic effects for electrochemical reduction of carbon dioxide using gold–copper bimetallic nanoparticles. Nat Commun ***2014,*** *5.*

24. Neaţu, Ş.; Maciá-Agulló, J. A.; Concepción, P.; Garcia, H., Gold–Copper Nanoalloys Supported on TiO2 as Photocatalysts for CO2 Reduction by Water. Journal of the American Chemical Society ***2014****.*

25. Saravanan, G.; Abe, H.; Xu, Y.; Sekido, N.; Hirata, H.; Matsumoto, S.-i.; Yoshikawa, H.; Yamabe-Mitarai, Y., Pt3Ti Nanoparticles: Fine Dispersion on SiO2 Supports,

Enhanced Catalytic CO Oxidation, and Chemical Stability at Elevated Temperatures. Langmuir **2010,** *26 (13), 11446-11451.*

26. Manikandan, M.; Tanabe, T.; Li, P.; Ueda, S.; Ramesh, G. V.; Kodiyath, R.; Wang, J.; Hara, T.; Dakshanamoorthy, A.; Ishihara, S.; Ariga, K.; Ye, J.; Umezawa, N.; Abe, H., Photocatalytic Water Splitting under Visible Light by Mixed-Valence Sn3O4. ACS Applied Materials & Interfaces **2014,** *6 (6), 3790-3793.*

27. Kuhl, K. P.; Hatsukade, T.; Cave, E. R.; Abram, D. N.; Kibsgaard, J.; Jaramillo, T. F., Electrocatalytic Conversion of Carbon Dioxide to Methane and Methanol on Transition Metal Surfaces. Journal of the American Chemical Society **2014**.

28. Jaksic, M., Volcano plots along the Periodic table, their causes and consequences on electrocatalysis for hydrogen electrode reactions. Journal of New Materials for Electrochemical Systems **2000,** *3 (2), 153-168.*

Journal Publications

First author:

1. Yin, G., Nishikawa, M., Nosaka, Y., Srinivasan, N., Atarashi, D., Sakai, E., & Miyauchi, M. (2015). Photocatalytic carbon dioxide reduction by copper oxide nanocluster-grafted niobate nanosheets. ***ACS nano***, 9, 2111-2119, 2015. (IF: 13.334, 41 times cited).
2. Yin, G., Abe, H., Kodiyath, R., Ueda, S., Nagarajan, S., Yamaguchi, A., & Miyauchi, M. (2017). Selective electro-or photo-reduction of carbon dioxide to formic acid using Cu-Zn alloy catalyst. ***J. Mater. Chem. A***. 5, 12113-12119, 2017. (IF: 8.262)
3. Yin. G, Sako. H, Gubbala V. Ramesh, Abe. H, Ueda. S, Yamaguchi. A, Miyauchi. M, Visible-Light-Driven Selective CO_2 Reduction into HCOOH without Sacrificial Agents by Z-Scheme Photoelectrodes System. Submitted.

Contributed works:

4. Kondo, A., Yin, G., Srinivasan, N., Atarashi, D., Sakai, E., & Miyauchi, M. (2015). Kelvin probe imaging of photo-injected electrons in metal oxide nanosheets from metal sulfide quantum dots under remote photochromic coloration. ***Nanoscale***, *7*(29), 12510-12515.
5. Osako, K., Matsuzaki, K., Hosono, H., Yin, G., Atarashi, D., Sakai, E., ... & Miyauchi, M. (2015). Examination of interfacial charge transfer in photocatalysis using patterned CuO thin film deposited on TiO_2. ***APL Materials***, *3*(10), 104409.
6. S. Shoji, G. Yin, M. Nishikawa, D. Atarashi, E. Sakai, M. Miyauchi*, Photocatalytic reduction of CO_2 by CuxO nanocluster loaded $SrTiO_3$ thin film; ***Chem. Phys. Lett.***658, 309(2016).
7. K. Osako, K. Matsuzaki, T.Susaki, G. Yin, A.Yamaguchi, H. Hosono, M. Miyauchi1, “Direct observation of interfacial charge transfer between rutile TiO_2 and ultrathin CuO film by visible-light illumination and its application for efficient photocatalysis”, ***Submitted***.

International Conferences

Oral:

1. G. Yin and D. Atarashi, E. Sakai and M. Miyauchi. “Development of Semiconductor based Artifacial Photosynthesis System” 6th *Multidisciplinary International Student Workshop (MISW2014)*, Tokyo Institute of Technology, Tokyo, Japan. August 8th, 2014.
2. G. Yin, D. Atarashi, E. Sakai and M. Miyauchi. “Utilization of $Nb_3O_8^-$ Nanosheets for CO_2 Photoreduction.” *The 15th IUMRS-International Conference in Asia (IUMRS-ICA 2014)*, Fukuoka University, Fukuoka, Japan. August 28th, 2014.
3. G. Yin, D. Atarashi, E. Sakai and M. Miyauchi. “The Development of Photocatalytic CO_2 reduction System Consisted of Copper Ions Nanoclusters and Niobate Nanosheets.” *20th China-Japan Bilateral Symposium on Intelligent Electroohotonic Materials and Molecular Electronics (SIEMME 20th)*, Wangjiang Hotel, Chengdu, China. September 22th, 2014.
4. G. Yin, D. Atarashi, E. Sakai and M. Miyauchi. “Development of Semiconductor based Artificial Photosynthesis System” *Asia-Oceania Top University League on Engineering (AOTULE) 2014 conference*, Melbourne University, Melbourne, Australia. November 27th, 2014.
5. G. Yin, H. Abe, E. Sakai, M. Miyauchi. “A Cu-Zn Intermetallic Catalyst Utilized for Electrochemical, Photoelectrochemical and Photocatalytic CO_2 Reduction”, *Pacific Rim Meeting on Electrochemical and Solid-state Science(PRiME2016)*, Oral, Oct 2nd, 2016.
6. G. Yin, H. Abe, G. V. Ramesh, A. Yamaguchi, M. Miyauchi. “Cu-Zn Intermetallic Nanoparticles Utilized in Catalytic CO_2 Reduction”, *The 22th China-Japan Bilateral Symposium on Intelligent Electrophotonic Materials and Molecular Electronics (SIEMME'22),* Oral, Sep 23th, 2016.

Poster

1. G. Yin, D. Atarashi, E. Sakai and M. Miyauchi. “Photoreduction of CO_2 to Carbon monoxide on $Nb_3O_8^-$ nanosheets with Copper nanoclusters co-catalyst” *The 8th International Conference on the Science and Technology for Advanced Ceramics (STAC8)*, Yokohama, June 25th, 2014.

Domestic Conferences:

Oral:

1. G. Yin, D. Atarashi, E. Sakai and M. Miyauchi. "CO_2 Photoreduction System based on Cu Ion Nanocluster Grafted $Nb_3O_8^-$ Nanosheet" 公益社団法人電気化学会第 81 回大会, Kansai University, Osaka. Match 30th, 2014.

Poster:

1. G. Yin, S. Nagatajan, M, Nishikawa, Y. Nosaka, D. Atarashi, E. Sakai and M. Miyauchi. "Photocatalytic carbon dioxide reduction on the basis of copper oxide nanoclusters grafted niobate nanosheets" 第 21 回シンポジウム光触媒反応の最近の展開, Tokyo University, Tokyo, December 12th, 2014.
2. 2. G. Yin, S. Nagarajan, H. Abe, E. Sakai, M. Miyauchi. " CO2 Reduction Promoted by Cu-Zn Bimetallic Co-catalyst" 第 22 回シンポジウム光触媒反応の最近の展開, Tokyo University, Tokyo, December 4th, 2015.

Awards:

1. Japanese Government (MEXT) Scholarship, 2012.10~2016.03.
2. The Japan Society for the Promotion of Science (JSPS) Research Fellowship for Young Scientist, DC2, 2016.03~2018.03.
3. The Winners of the Award for Encouragement of Research in *The 15th IUMRS-International Conference in Asia (IUMRS-ICA2014)*.
4. The Top 5 Presenters Award in *6th Multidisciplinary International Student Workshop (MISW)*.